Modeling and Simulation of a Hybrid Electric Vessel

by

Tiffany Jaster
B. Eng, University of Victoria, 2006

A Thesis Submitted in Partial Fulfillment
of the Requirements for the Degree of

MASTER OF APPLIED SCIENCE

in the Department of Mechanical Engineering

Supervisory Committee

Modeling and Simulation of a Hybrid Electric Vessel

by

Tiffany Jaster
B.Eng, University of Victoria, 2006

Supervisory Committee

Dr. Zuomin Dong (Department of Mechanical Engineering)
Co-Supervisor

Dr. Andrew Rowe (Department of Mechanical Engineering)
Co-Supervisor

Dr. Curran Crawford (Department of Mechanical Engineering)
Departmental Member

Abstract

Supervisory Committee

Dr. Zuomin Dong (Department of Mechanical Engineering)
Co-Supervisor

Dr. Andrew Rowe (Department of Mechanical Engineering)
Co-Supervisor

Dr. Curran Crawford (Department of Mechanical Engineering)
Departmental Member

A proposed hybrid electric marine vehicle was modeled in MATLAB Simulink and SimPowerSystems. Models for each of the individual propulsion components were developed and incorporated into a complete hybrid electric propulsion model. A vessel resistance model was created to support vessel performance and energy requirement evaluation. The model incorporates data based on the ship principal parameters and hull form. A rule-based supervisory controller for the proposed vessel was constructed. It is an amalgamation of control strategies of three vehicle architectures: electric vehicle, fuel cell electric vehicle, and hybrid electric vehicle (HEV). The complete model of the hybrid electric propulsion, control, and resistance subsystems was simulated on a dSPACE hardware-in-the-loop platform. For each simulation, the energy storage system (ESS) state of charge, station keeping/cruising mode, HEV assist, Beaufort number, current speed, true wind angle, and hotel load were specified. From the simulations, it was demonstrated that using a 30% ESS assisted HEV mode results in reduced emissions and fuel consumption as compared to a conventional HEV mode, supporting the case for plug-in hybrid electric vessels. A larger capacity ESS has the potential to reduce emissions and fuel consumption further, depending on ship usage. The basic rule-based supervisory controller proved functional for facilitating adequate power flows; however, further development is needed to improve efficiency and the mode selection process.

Table of Contents

List of Tables

List of Figures

Nomenclature

Abbreviations

ADVISOR	ADvanced VehIcle SimulatOR
AES	All electric ship
AESD	Advanced Electric Ship Demonstrator
ANL	Argonne National Laboratory
AVR	Automatic voltage regulator
BEV	Battery electric vehicle
BF	Beaufort
BSFC	Brake specific fuel consumption
CD	Charge depleting
COP17	17th Conference of the Parties
CS	Charge sustaining
CVT	Continuously variable transmission
DOD	Depth of discharge
DOE	Department of Energy
DOF	Degrees of freedom
DP	Dynamic positioning
Dymola	Dynamic Modeling Library
EMS	Environmental Management System
ESS	Energy storage system (electricity only)
EV	Electric vehicle
FC	Fuel cell
FCEV	Fuel cell electric vehicle
FLR	Fast load reduction
FS	FreeShip
GHG	Greenhouse gas
HEV	Hybrid electric vehicle
HIL	Hardware-in-the-loop
HPS	Hybrid power system
ICE	Internal combustion engine
IFO	Intermediate Fuel Oil

IMO	International Maritime Organization	
IPS	Integrated power systems	
Ka	Kaplan series	
MARPOL	Marine Pollution	
MBD	Model-based design	
MEA	Membrane electrode assemblies	
MEPC	Marine Environment Protection Committee	
MG	Motor/generator	
MSS	Marine Systems Simulator	
NREL	National Renewable Energy Laboratory	
PEM	Proton exchange membrane or polymer electrolyte membrane	
PHEV	Plug-in hybrid electric vehicle	
PMS	Power management system	
PPP	Power Prediction Program	
PSAT	Powertrain System Analysis Toolkit	
ROPOS	Remotely operated platform for ocean science	
ROV	Remotely operated vehicle	
SOC	State of charge	
SOFC	Solid oxide fuel cell	
SPS	SimPowerSystems	
SS	Sea state	
TEAMS	Total Energy and Emission Analysis for Marine Systems	
THD	Total harmonic distortion	
THS	Toyota Hybrid System	
UC	Ultra capacitor	
UVic	University of Victoria	
VFD	Variable frequency drive	
VTB	Virtual test bed	

Lower Case

a	Engine loading constant	
$b_{e,g}$	Brake specific fuel consumption	[g/kW·h]
f	AC source frequency	[Hz]

f(SOC)	SOC dependent correction factor	
g	Acceleration due to gravity, 9.81	[m/s^2]
h_B	Center of bulb area above keel line	[m]
i_E	Half angle of entrance	[°]
lcb	longitudinal position of centre of buoyancy forward of $0.5L_{pp}$	[% of L_{pp}]
n	Speed	[rps]
t	Thrust deduction factor	
t_{FLR}	Fast load reduction time	[s]
t_{SL}	Safe load time	[s]
w	Wake fraction	
$w_{r,g}$	Ratio of rated generator power	

Upper Case

$\bar{H}^{1/3}$	Significant wave height	[ft/s^2]
A_{BT}	Transverse bulb area	[m^2]
A_E/A_O	Blade area ratio	
A_L	Lateral projected wind area	[m^2]
A_{SS}	Lateral projected area of superstructure	[m^2]
A_T	Transverse projected wind area	[m^2]
A_T	Immersed part of transverse area of transom	[m^2]
B	Breadth (beam) on waterline	[m]
B_N	Beaufort number	
C	Distance from bow of centroid of lateral projected area	[m]
C_A	Correlation allowance coefficient	
C_B	Block coefficient	
C_{BTO}	Bulbous bow cylindrical opening coefficient	
$C_{DC\ bus}$	DC bus capacitance	[F]
$C_{DC,bus}$	DC bus capacitance	[F]
C_{dw}	Wave depth coefficient	
C_F	Frictional resistance coefficient	
C_{LC}	Lateral current force factor	
C_M	Midship section coefficient	

C_p	Prismatic coefficient	
C_R	Friction drag factor	
C_{stern}	Stern shape parameter	
C_{TC}	Transverse current force factor	
C_v	Viscous resistance coefficient	
C_{WP}	Waterplane area coefficient	
C_{XW}	Longitudinal wind force coefficient	
C_{YW}	Lateral wind force coefficient	
D	Propeller diameter	[m]
FC_g	Generator dynamic fuel consumption	[kg]
$F_{L,current}$	Longitudinal current resistance	[kN]
$F_{L,wave}$	Longitudinal wave resistance	[kN]
F_n	Froude number	
F_{ni}	Froude number based on immersion	
$F_{T,current}$	Transverse current resistance	[kN]
$F_{T,wave}$	Transverse wave resistance	[kN]
F_{TC}	Lateral/transverse current force due to pressure	[kN]
F_{TC}'	Lateral/transverse current force due to drag	[kN]
H	Inertial time constant	[s]
J	Advance coefficient	
J_{FC}	Instantaneous fuel consumption cost function	
K_Q	Propeller torque coefficient	
K_T	Propeller thrust coefficient	
K_{TN}	Nozzle/stator thrust coefficient	
L	Load	[% of rated power]
L_{OA}	Overall length	[m]
L_{pp}	Length between perpendiculars/length on waterline	[m]
L_R	Length of run	[m]
M	Number of masts/kingposts in lateral projection	
P	Rated generator power	[kW]
P/D	Nominal pitch over diameter	
P_B	Emergence of bow	[m]
P_D	Delivered propulsive power	[W]

P_E	Effective propulsive power	[W]
P_g	Generator load	[kW]
P_{motor}	Nominal power of motor drive	[W]
$P_{r,g}$	Rated generator power	[kW]
Q	Torque	[Nm]
R_A	Ship-model correlation resistance	[N]
R_{air}	Still air resistance	[N]
R_{app}	Appendage resistance	[N]
R_B	Bulbous bow resistance	[N]
$R_{braking}$	Braking chopper resistance	[Ω]
R_{BT}	Bow thruster resistance	[N]
R_F	Frictional resistance	[N]
R_n	Reynolds number	
R_{TR}	Immersed transom resistance	[N]
R_w	Wave making resistance	[N]
S	Length of perimeter	[m]
S	Wetted area of hull	[m^2]
S_{app}	Wetted area of appendages	[m^2]
SS	Sea state	
T	Thrust	[N]
T	Average molded draught	[m]
T_A	Draught molded on A.P.	[m]
T_F	Draught molded on F.P.	[m]
T_N	Nozzle thrust	[N]
V	Ship velocity	[m/s]
V_a	Speed of advance	[m/s]
$V_{Brake,act}$	Braking chopper activation voltage	[V]
V_{DC}	DC voltage	
V_{DC}	Average DC bus voltage	[V]
V_{LL}	Line-to-line voltage	[V]
V_{pp}	Phase to phase voltage (RMS)	[V]
V_{pp}	Phase to phase voltage, rms	[V]
V_{rw}	Relative wind velocity	[m/s]

V_{tw}	True wind velocity	[m/s]
X_w	Longitudinal wind force	[N]
Y_w	Lateral/transverse wind force	[N]
Z	Number of propeller blades	

Greek/Symbol

∇	Displacement volume molded	[m^3]
η_0	Propeller open water efficiency	
$(1+k_1)$	Hull form factor	
$(1+k_2)$	Appendage resistance factor	
ρ_a	Density of air	[kg/m^3]
α_c	Angle between the longitudinal axis of the ship and the current direction considered from the bow	[°]
α_{rw}	Relative wind angle	[°]
α_w	Wave angle	[°]
α_{tw}	True wind angle	[°]
ρ_w	Density of water, 1025 for saltwater	[kg/m^3]
γ_w	Density of water, 1.034 for saltwater	[t/m^3]
φ_{VSD}	VSD flux	[Wb]
α_{rw}	Relative wind angle	[°]
Δv	Desired voltage ripple	[V]

Chapter 1 Introduction

1.1 Proposed Hybrid Electric Marine Vehicle

A proposed hybrid electric marine vehicle has been designed for the University of Victoria (UVic). The proposed vessel is a converted 26.7m coast guard ship (formerly known as the RV Tsekoa II), which is to be extended with a 9.9m mid-body insert. Details of the original ship are given in Appendix A. The operational requirements of the proposed vessel include:

- ROV platform (ROPOS);
- endurance of 15 days;
- range of 8000 nm (15,000 km) at optimal transit speeds;
- speed of 10 knots sustainable for sea state (SS) 1-4, and 7 knots in SS 5;
- sea keeping capability in SS 1-4, with greater than 50 % operation in SS 5; and
- station keeping capability up through SS 4 with maximum deviation from fixed location ±5m.

Motivations for development of hybrid electric vessels and an overview of the hybrid propulsion system of the proposed vessel are presented in this section.

1.2 Ship Powertrain Hybridization Motivations

In 2007, the transportation sector accounted for 14.5% (7733 Mt) of CO_2 emissions due to fossil fuel consumption worldwide [1]. This sector strongly relies on fossil fuels which account for 98% of the energy source. Specifically for Canada, in 2007, 29% of the CO_2 emissions were produced by the transportation industry. Of this percentage, 76% of the contribution was due to road transport while international marine made up 1% [2].

Even though the marine transportation industry contribution to global CO_2 emissions is small compared to land transportation, the industry discharges other pollutants of note. The diesel engines used on-board ships utilize heavy fuel oil, marine diesel oil or marine gas oil. Similar to automotive engines, marine engines produce CO_2; however, they also yield SO_2, NO_X, and particles of soot among various other pollutants in smaller quantities.

Many countries are under increased pressure to reduce their collective green house gas emissions (GHGs) due to environmental concerns. However, another key forethought is achieving greater autonomy through reducing and/or eliminating a country's dependence on foreign oil. With respect to the transportation industry, there is an increased interest in hybrid propulsion and, in time, fully electric propulsion as a potential solution to these concerns. However, considerable obstacles hinder the departure from a fossil fuel based transportation industry to vehicles powered by renewable sources. Aside from climate change concerns, economic growth, safety, infrastructure, technology and policy must be addressed in order for widespread implementation and acceptance of ship hybrid propulsion.

1.2.1 Shipping Industry/Government Participation

The shipping industry, like the automotive industry, has a governing body which sets regulatory requirements. In 1948, the International Maritime Organization (IMO) (previously known as the Inter-Governmental Maritime Consultative Organization) was formed; it is a specialized agency of the United Nations. At the Marine Pollution (MARPOL) Convention in 1973, the IMO passed the International Convention for the Prevention of Pollution from Ships. The original MARPOL convention did not come into force due to lack of ratifications. A combination of the 1973 MARPOL Convention and 1978 MARPOL Protocol represent the current convention, which entered into force October 1983. The convention required all participating parties to implement marine environmental protection regulations in all vessels operating under their sovereignty. Specifically, the subject of air pollution produced by ships is regulated through Annex VI, which came into effect May 19, 2005 (later amended in April 2008). Emission limits were set for nitrogen oxides, sulphur dioxide and volatile organic compounds; substances which cause harm to the ozone layer were regulated. However, Annex VI fell short in providing a comprehensive set of emission limits as CO_2 emissions were not included [3]. The limitation/reduction of GHGs produced by marine fuels as outlined by the IMO is included in the Kyoto Protocol (1997); article 2.2 of Kyoto requires all signatory countries of MARPOL Annex I to pursue emission limits set by the IMO.

At the Marine Environment Protection Committee (MEPC) 62 in July 2011, mandatory measures to reduce GHGs from international shipping were adopted. This is the first time the international industry sector has adopted a compulsory global CO_2 reduction regime. Amendments made to MARPOL Annex VI include regulations regarding energy efficiency for ships – new ships must adhere to the Energy Efficiency Design Index, and all ships must abide by the Ship Energy Efficiency Management Plan. These regulations apply to ships of 400 gross tonnage and above, and came into effect internationally in January 2013 [4].

As of July 2011, the IMO committed to reducing CO_2 emissions 20% by 2020, with further reductions to follow (as outlined in Figure 1). The IMO has asked for clear market based measures outlining CO_2 emission reduction to be mandated by the United Nations Climate Change Conference. However, this was not addressed at the 17th Conference of the Parties (COP17) in Durban, South Africa in November 2011.

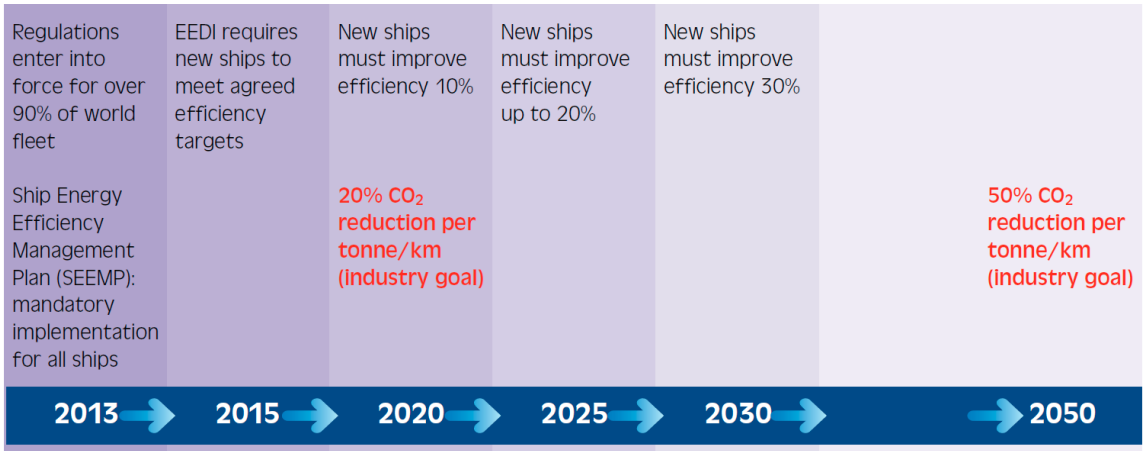

Figure 1: IMO Agreement on Technical Regulations to Reduce Ships` CO_2 Emissions

Many countries have established economic incentives to encourage the development of cleaner ships. Some examples include the Green Award, Bonus/Malus System, U.S. Coast Guard Qualship 21, Blue Angel, environmental class notations, and the Green Passport of the IMO [5].

Aside from government and shipping industry regulators encouraging the shift towards greener shipping, a group of tanker industry representatives have also stepped up to the challenge [5][6]. At an INTERTANKO event in Athens in April 2005, a selection of tank owners and tanker industry representatives initiated the “Poseidon Challenge” with the

aims of achieving zero fatalities, zero pollution and zero detentions within the next five years. They sought to encourage and inspire other major players in the oil transportation sector to reach/accept the same goals. The INTERTANKO event resulted in the first Poseidon Challenge gathering in Singapore, April 2006. It included representatives from shipping agents, to insurance agencies, ship builders, ship owners and training providers to name a few. An annual award was created to recognize an association, company, society, link, individual or team who has done the most to meet the Poseidon Challenge in the past year.

1.2.2 Hybrid Electric Ship Versus Conventional Ship Emissions

A graphical representation of the power system for the proposed UVic hybrid electric marine vehicle, including propulsion devices, is given in Figure 2. Loads and other buses are not shown. The pertinent energy source information is given in Table 1.

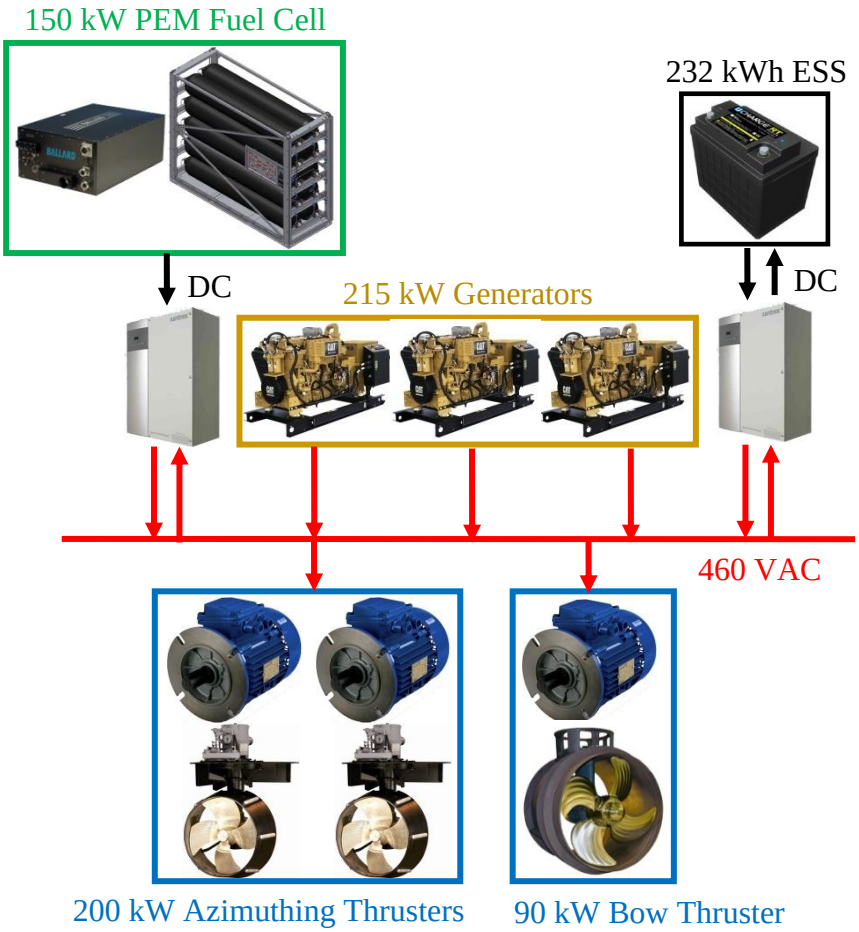

Figure 2: Vessel Propulsion System Overview

Table 1: Hybrid Vessel Energy Sources

Component	Power/Energy Content Rating	Fuel Source
Diesel Generator (3)	215 kW	Marine Diesel
ESS	232 kWh	Electricity
PEM Fuel Cell	150 kW	Hydrogen

Rough GHG emissions and marine diesel fuel consumption were calculated for three mission cycles for both the hybrid vessel specified above and a conventional ship using only diesel generators (the same as selected for the hybrid vessel). The main GHGs thought to contribute to global warming are carbon dioxide, methane and nitrogen oxides; they were the only diesel emissions taken into account. The marine diesel fuel rates based on load for both the hybrid and conventional ship are given in Table 2 [7]. For the conventional vessel, the fuel rate selected was based on whether the load was propulsive or electric; for hotel load, generator power rating was used, and likewise, engine power was used for propulsive loads. Table 3 lists the production and combustion emission factors applied to the marine diesel fuel consumption [8].

Table 2: Generator Performance Data

Generator [ekW]	Engine Power [BkW]	Percent Load [%]	Fuel Rate [LPH]
21.5	24.3	10	10.9
43	48	20	16.4
53.8	59.6	25	19.2
64.5	71.1	30	21.9
86	93.6	40	27.3
107.5	115.6	50	32.7
129	138.4	60	38.4
150.5	161.4	70	44.3
161.3	173	75	47.3
172	184.6	80	50.4
193.5	208.1	90	56.9
215	232	100	63.5

Table 3: Marine Diesel Emission Factors

Emission Factor	Fuel Combustion [g/mmBtu]	Fuel Production [g/mmBtu]
CO_2	10181	77260
CH_4	8.1	4.6
N_2O	0.16	2.0
Energy Conversion Factor: 0.0359 GJ/L		

In calculating power consumption for the hybrid powertrain, it is assumed that once the ESS has been depleted, it is not recharged. The emission contribution of electricity used to charge the batteries is 25 tCO_2e/GWh [9]. The amount of hydrogen available for the fuel cell is enough to provide maximum power for a period of 9 hours. As there are no emissions produced during consumption of the hydrogen, only production emissions are taken into account. Hydrogen is produced at 0.0117 kg/kWh with the only contributing input being electricity as the hydrogen is a collected waste stream (this is explained in more detail in Section 1.1.1). Lastly, there is no limit to the amount of marine diesel fuel on-board.

Comparison of the estimated GHG emissions and fuel consumption of select mission cycles as completed by the hybrid ship and the conventional ship is given in **Error! Not a valid bookmark self-reference.**.

Table 4: Rough Estimate of Fuel Consumption & GHG Emissions for Select Mission Profiles

Mission	Load	Hybrid Electric	Diesel Only	Savings
Cruising, 2 hours	200 kW Thrusters + 110 kW Hotel	GHGs: 0.45 tCO2e Diesel: 149 L	GHGs: 0.86 tCO2e Diesel: 286 L	GHGs: 0.41 tCO2e Diesel: 137 L
ROPOS Operations, 8 hours*	200 kW Thrusters + 110 kW Hotel + 30 kW Hydraulic Power Pack + 50 kW Bow Thruster + 35 kW ROPOS	GHGs: 0.92 tCO2e Diesel: 303 L	GHGs: 2.90 tCO2e Diesel: 965 L	GHGs: 1.98 tCO2e Diesel: 662 L
Anchored, 8 hours	110 kW Hotel	GHGs: 0.01 tCO2e Diesel: 0 L	GHGs: 0.80 tCO2e Diesel: 268 L	GHGs: 0.79 tCO2e Diesel: 268 L

*ROPOS requires half an hour to both deploy and recover. For this mission profile, the bow thruster and ROPOS are only in operation for 7 hours. The hydraulic power pack is in operation for one hour total (ROPOS deployment/recovery).

1.3 Research Objectives

The model-based design (MBD) process provides a common framework for communication throughout the design process while adhering to the development cycle. An example of a controls development V-diagram is shown in Figure 3. It supports the design, analysis and optimization of complex powertrain systems which are tested under various driving/load cycles, providing practical insight to vehicle performance and powertrain efficiency. The MBD process moves design tasks from the lab/field to the desktop, enabling faster, more cost-effective design development. MBD is commonly used in automotive applications to support the development of battery electric vehicle (BEV), fuel cell electric vehicle (FCEV), hybrid electric vehicle (HEV) and plug-in hybrid electric vehicle (PHEV).

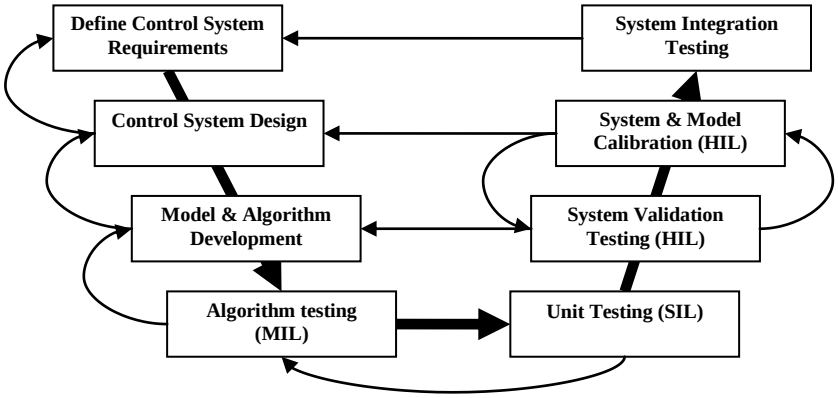

Figure 3: Controls Development V-Diagram

This research utilizes the design of a proposed hybrid electric research vessel as a test case to explore the feasibility and capability of MBD applied to the propulsion system design of hybrid electric marine vehicles. The simplified MBD process used to model this system is as follows:

1. Define the system
2. Identify system components
3. Model the system with equations
4. Construct the Simulink/SimPowerSystems (SPS) block diagram

5. Run the simulation (MIL, HIL)

6. Validate the simulation results

For the proposed hybrid vessel, system definition and component specification has been prepared by third parties. In creating the system model, equations will be utilized to define components where no previously created Simulink/SPS blocks are available. Where used, SPS blocks will be parameterized to reflect the actual component, however, the equations defining the specific component model will not be presented (they can be found in the SPS block definitions). The size and hull shape of the proposed vessel, along with the selected thrusters and power/energy devices will be modeled using real component data wherever available. Other devices with limited information provided will be modeled using data from comparable components. Those components deemed overly complex will be replaced with a simplified model where possible to facilitate ease of simulation.

Model simulation will occur in the Simulink environment during initial system design and debugging. When the subsystems are linked together, the simulation will be moved to a HIL platform to enable faster simulation. It should be noted that simulation on a HIL platform is generally used for control development where real-time CAN communication and control methods can be accurately replicated and tested. In this case, the HIL is specifically utilized to speed up system simulation as the model has a small time step. Validating the entire system model, the last step of the simplified MBD process, is not possible. No measured propulsion or power system data exist at present.

This research is aimed at introducing the models of the propulsion system, powertrain components, ship drag and load cycles, and integration of these modules. This model may be used to evaluate an initial hybrid power system design with respect to power/energy source selection and sizing, operation, as well as assessing and improving power system performance through modifications of the supervisory control strategy. Various mission cycles, utilizing different combinations of power/energy sources, can be implemented to better understand powertrain limitations during a given mission, ensuring safety of operations (blackout prevention).

The key objectives of this thesis are:

- create a Simulink/SPS model of the hybrid electric propulsion system of the proposed UVic research vessel;
- create a vessel resistance model using data available from industry generated reports and industry accepted calculation methods;
- implement a rule-based energy control strategy for high-speed and low-speed cruising modes, utilizing selected combinations of power/energy sources; and
- perform simulation and evaluation of propulsion system performance during low speed cruising and station keeping mission cycles.

1.4 Organization of the Thesis

Chapter 2 provides an overview of electric/hybrid electric powertrain configurations, basic PEM fuel cell operation, and a summary of ship demonstrations, simulation software and hybrid ship modeling research.

Chapter 3 details the vessel's overall hybrid propulsion system, including selected components and fuel analysis. The Simulink/SPS models of the components are also presented.

The vessel resistance model which includes open water, wind, wave and current resistance components, along with their Simulink implementation, is given in Chapter 4.

Chapter 5 discusses the mode specific control strategies and ESS partitioning, while Chapter 6 presents simulation results for different mission cycles. The last chapter provides a summary of this thesis and recommendations for future work.

Chapter 2 Background

2.1 Electric/Hybrid Electric Powertrain

2.1.1 Configuration of Electric Vehicles

BEV

In a BEV, power flows from an on-board ESS through a DC/DC converter to an inverter and finally through an electric motor to the final drive (Figure 4). The ESS is charged through an external source as well as by regenerative braking. A main drawback of the BEV is the limited travel range (before recharging) due to technology limitations of the ESS.

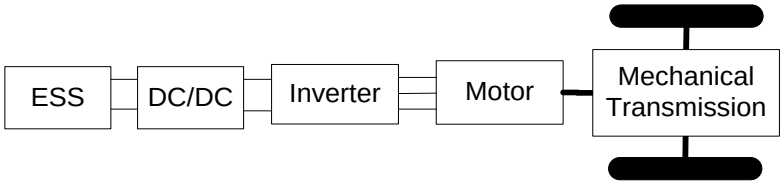

Figure 4: BEV Architecture

FCEV

FCEVs consist of a fuel cell stack, some type of on-board fuel, and an ESS and/or ultra-capacitors (UC) (Figure 5). For PEM FCs, often neat hydrogen gas is stored in on-board high pressure gas cylinders. PEM FCs are the most researched and developed FC for small vehicle applications due to their lower operating temperature as compared to other types of FCs.

The most commonly selected electrical energy sources to be paired with a FC are UCs and batteries. As with HEVs, with the additional energy source(s), the primary power source can be downsized, reducing fuel cell stack size and associated costs and allowing for the FC to be operated in a high efficiency region. For the FC-UC-ESS hybrid vehicle, often the UC is sized to optimally capture the regenerative braking energy, while the ESS acts as a fuel cell power assist to maintain vehicle transient performance.

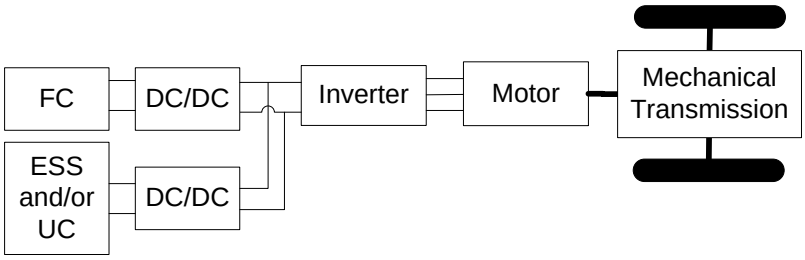

Figure 5: FCEV Architecture

2.1.2 Configuration of Hybrid Electric Vehicles

An HEV combines a conventional engine (ICE) with an electric propulsion system. They can be classified according to how power is supplied to the drivetrain, either series, parallel or powersplit.

Series Hybrid

For series hybrid vehicles, energy flows in a series path from the engine to an electric generator, to an on-board ESS, to an electric motor and ultimately to the final drive (Figure 6)**.** Simply put, it is an electric vehicle with an on-board battery charger. For this type of HEV, the electric motor must be relatively large and, consequently, heavy as it alone propels the vehicle. Due to this mass requirement, series HEVs are usually reserved for large vehicle applications such as buses, submarines, and diesel-electric locomotives. One benefit of series hybrids is that the engine can be continuously operated in a region of high efficiency as the engine has no mechanical link to the transmission.

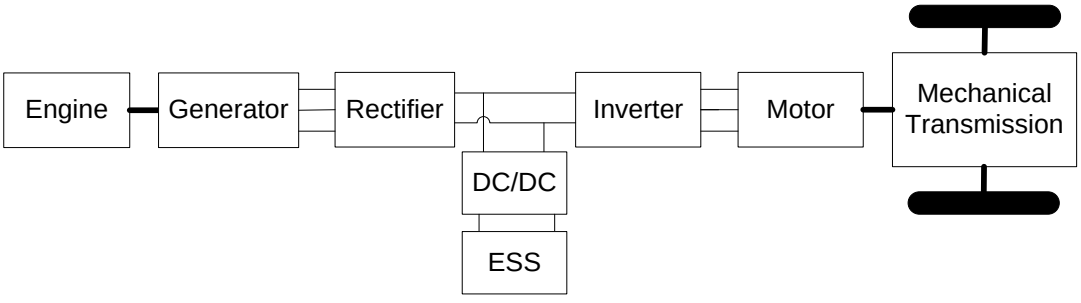

Figure 6: Series HEV Architecture

Parallel Hybrid

Parallel hybrids allow for energy flows in parallel paths. Adding in an ESS and an electric motor/generator (MG) at any spot on the drivetrain of the series design previously mentioned will result in a parallel configuration (Figure 7). The vehicle is

propelled by the engine, or the MG, or both simultaneously. For this configuration, typically the MG provides all propulsive power at low speeds and the engine propels the vehicle at higher speeds, along with recharging the ESS. Replacing the fixed step transmission with a continuously variable transmission (CVT) allows for continuous shifting of the most efficient operating points of the engine at a given torque demand. The CVT design can lower fuel consumption due to more efficient fuel use. Overall, there is greater flexibility in the configuration, component sizing, and control of parallel hybrids as compared to the series arrangement.

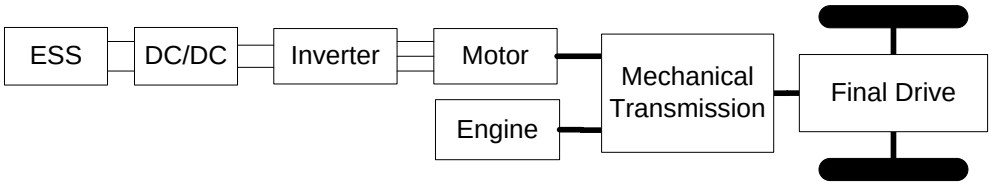

Figure 7: Parallel HEV Architecture

Powersplit Hybrid

Powersplit hybrids are HEVs in which power output from a MG and an engine are joined, typically at or within a transmission; this arrangement incorporates both series and parallel power paths (Figure 8). Powersplit hybrids can be further defined as input-, output- or compound-split. The mode selection device can be as simple as using clutches to select which shaft is connected to the engine. Another option is to utilize a planetary gear train. Hybrid vehicles which have a single continuously variable gear ratio range within the electric variable transmission represent one-mode designs. Likewise, a two-mode HEV would contain two continuously variable gear ratio ranges.

The Toyota Hybrid System (THS), part of the Toyota Prius, is a commercially available power-split HEV first offered in 1997, with an improved THS system (THS II) introduced in 2004.

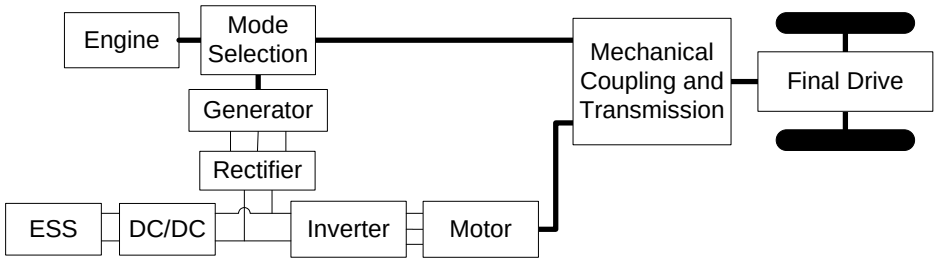

Figure 8: Series-Parallel HEV Architecture

2.1.3 Plug-in HEV

More recently, PHEVs are being introduced to the market. PHEVs are HEVs with rechargeable batteries which can be restored to full capacity through connecting the battery pack to an external electric power source.

With PHEVs, three modes of operation are possible: charge sustaining (CS), electric vehicle (EV), and charge depleting (CD). The selected mode is based on the SOC of the ESS and driver torque demand.

In CS mode, the engine, MG(s), or combination of both provide propulsive power with the objective of maintaining the ESS SOC within a predefined window. When operating in EV mode, the vehicle is propelled using only electric power. The engine may turn on during this mode if the MG cannot meet the driver torque demand or if the ESS SOC becomes insufficient. Lastly, in CD mode the vehicle is powered by either the engine, MG(s) or both, with a net decrease in ESS SOC. When the ESS becomes sufficiently depleted, the vehicle switches to CS mode.

Three distinct categories can be used to describe PHEVs based on the algorithm which selects the use of CS, EV or CD modes: all electric + conventional, all electric + hybrid, and blended [10]. The first category of PHEVs operate initially as EVs until the ESS SOC has been sufficiently depleted. At this point, they switch to full engine propulsive power, operating as a conventional non-hybrid vehicle. The all electric + hybrid vehicle first functions in EV or CD mode until the predefined SOC has been attained. Following this, the vehicle operates as an HEV in CS mode. Finally, vehicles which follow a blended strategy make use of both the MG(s) and engine for propulsion throughout the trip. With this approach, the strategy could result as a toggle between CD and CS modes.

2.1.4 Degree of Hybridization

Hybrid vehicles can be further classified by their degree of hybridization, namely micro, mild or strong (full) hybrid. Micro hybrids possess a small secondary power source and cannot provide electric only propulsion. They afford the capability of regenerative breaking and start/stop assist. Mild hybrids offer the same features in combination with modest levels of engine assistance. Examples of mild hybrids include the hybrid Honda Civic, Accord and Insight which all utilize a parallel hybrid powertrain

- the Integrated Motor Assist. Vehicles classified as strong hybrids can run on engine only, ESS only, or a combination of the two. There is a growing trend in the automotive industry to explore greater degrees of hybridization of vehicles.

2.2 Proton Exchange Membrane Fuel Cell

The FC is an electrochemical device - it directly converts chemical energy stored in the bonds between atoms into electrical energy. In a conventional engine, a purely chemical combustion of fuel and oxidizer is used to generate heat. This heat is then converted into motion using a piston and into electrical power through a generator if electricity is the final desired product. Each of the reactions, electrochemical or chemical, with the same fuel and oxidizer begin with the same chemical energy stored in the reactants; the same chemical energy per mole of reactant is released during either reaction. The significant difference between the two energy conversion paths is that the chemical reaction, producing heat, is limited in its thermal efficiency by the Carnot cycle, whereas the electrochemical reaction is not. However, it should be strongly noted that this does not imply that an electrochemical reaction is without efficiency limitations, nor can it be assumed to always have a greater thermodynamic efficiency than its chemical counterpart. In actuality, operating conditions can significantly affect an electrochemical reaction, and may in turn cause it to be less efficient than a chemical based reaction.

Each FC is comprised of multiple membrane electrode assemblies (MEA), also referred to as cells, connected in series using bipolar plates. For a PEM FC, the MEA consists of a solid polymer electrolyte, often Nafion, sandwiched between two electrodes as shown in Figure 9. The polymer electrolyte is designed to allow for the propagation of mobile H^+ ions through it while hindering electron transport.

The two reactant gases supplied to the PEM FC are oxygen, in the form of air, and hydrogen. Hydrogen is supplied at the anode where it is ionized, releasing electrons and forming H^+ ions, as given by Equation 1.

$$H_2 \rightarrow 2H^+ + 2e^- \quad (1)$$

The electrons flow through the external circuit and the H^+ ions migrate through the electrolyte toward the cathode. At the cathode, oxygen reacts with the electrons and H^+

ions, forming water (Equation 2). For every two hydrogen molecules, one oxygen molecule is needed to keep the system in balance. The overall reaction is given by Equation 3.

$$O_2 + 4H^+ + 4e^- \rightarrow 2H_2O \quad (2)$$

$$H_2 + \frac{1}{2}O_2 \rightarrow H_2O \quad (3)$$

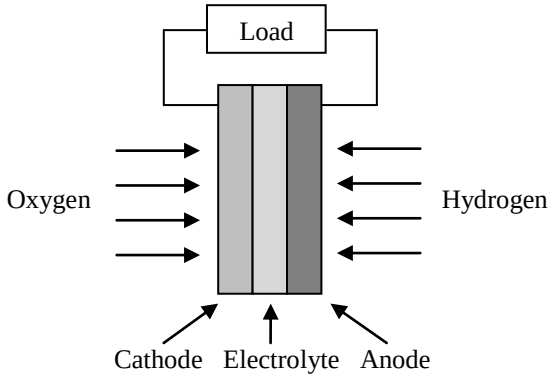

Figure 9: Basic Cathode-Electrolyte-Anode Cell Construction

2.3 Ship Hybrid Power System Demonstrations

Hybrid Powertrain	Details
Elding I (2008)	
• 10 kW PEM FC to provide hotel power	• 120 ton, Icelandic whale watching ship [11] • FC added to remove the noise caused by auxiliary diesel generators which are kept running (main engines were turned off) when whales are in sight • Part of the SMART-H2 project (Sustainable Marine and Road Transport, Hydrogen in Iceland)
San Francisco Hornblower Hybrid (2008)	
• One 1.2 kW photovoltaic solar array, two 1.2 kW 10 ft Savonius wind turbines, two 320 kW diesel generators	• First U.S. hybrid ferry [12] • 64 foot ferry, operates in the San Francisco Bay transporting passengers to Alcatraz • Recycled catamaran, originally built for commercial diving
Carolyn Dorothy (2009)	
• Two Cummins QSK50 engines, two Cummins QSM11 1800 Hp generators, 126 SES 12V gel batteries (340 kWh)	• Considered world's first true hybrid tug, serving ports of Long Beach and Los Angeles

	• Dolphin series tug designed by Robert Allen Ltd • XeroPoint hybrid power system jointly adapted to the tug by Aspen Kemp and Associates (AKA) and Foss Maritime • Auxiliary generators with ESS supplement main engines as sources of propulsion power
Viking Lady (2009)	
• 320 kW molten carbonate fuel cell, HotModule by MTU On Site Energy (Munich, Germany), operates on liquefied natural gas • On-board 220 cubic meter tank, holds approximately 90 metric tons of liquefied natural gas • Four 2010 kW Wärtsilä 6R32DF dual-fuel engines, four 1950 kW Alconza NIR 6391 A-10LW generators • Emergency generator: Volvo Penta D9-MG-RC • Propulsion: two Rolls Royce AZP 100FP propeller systems	• World's first commercial ship to utilize a fuel cell adapted for marine use [13] • 5900 metric ton, 92.2m offshore supply vessel • FC does not assist in driving any of the four electric engines or propellers; it provides auxiliary power • Operates in the North Sea and requires refueling roughly once per week
FCS Alsterwasser (2009)	
• Two Proton Motor 48 kW PEM fuel cell systems (PM Basic A50) • 560V, 360 Ah lead-gel buffer battery • 12 hydrogen tanks, 350 bar, 50 kg H_2 total • Propulsion: 100 kW propulsion motor, 20 kW bow thruster	• First ZemShip (Zero Emission Ship) [14] • 25.46m Alster excursion ship, world's first fuel cell driven passenger ship • Operates on tourist routes on Alster lake and the River Elbe in the area of the Port of Hamburg, Germany • 50 kg of gaseous hydrogen sufficient fuel for three days' use
Makin Island (LHD-8) (2012)	
• Gas-turbine-electric and diesel-electric hybrid drive • Cruising (70% of the time): six 4000 kW Fairbanks Morse diesel generators • Fast transport: two 35,000 hp GE-LM 2500+ gas turbines	• Navy's first hybrid drive warship [15] • On average, consumes 15,000 gallons of fuel per day • Ship is capable of 17,600 km range at 20 knots
New York Hornblower Hybrid (2012)	
• 32 kW PEM FC by Hydrogenics • Two diesel engines which power two Baldor Reliance 700 hp generators, 192 Odyssey AGM batteries, a 20 kW SunPower Corp. solar panel, and two 5 kW Helix Wind vertical axis wind turbines	• 168 ft hybrid ferry • Operates in New York carrying passengers from Battery Park to the Statue of Liberty • To date, the installation of the fuel cell system has been delayed due to the certification process; no hydrogen

	propulsion systems have been used in commercial vessels thus far in the U.S. • ESS is used to augment the diesel generators during periods of high loads • ESS can be charged using shore side electric power • Wind and solar power are cited to power navigation equipment, lights and televisions
E-KOTUG (2012)	
• Main power: three Caterpillar 3512 C-HD engines, three Westinghouse MGs • Auxiliary engines: two 250 kW Caterpillar C9, one 36 kW Caterpillar C4.4 • Corvus Energy lithium-ion ESS	• Europe's first hybrid tug, converted RT Adriaan tug [16] • XeroPoint Hybrid Propulsion System designed by AKA
Undine	
• One 20 kW Wärtsilä WFC20 solid oxide fuel cell (SOFC), fuelled with methanol	• 228m cargo ship [17] • FC unit provides auxiliary power

2.4 Simulation Software

The use of simulation software is critical for the optimization of vehicle component sizing, as well as implementation and verification of various control strategies ahead of in-vehicle application.

Two methods used for vehicle simulation are forwards facing and backwards facing modeling. With a backwards facing model, the vehicle speed is known and the required power throughout the system is calculated; it is a wheel-to-engine approach. This approach is not optimal for ensuring vehicle drivability. It is possible for the optimum solution to jump significantly between two solution points between time increments. This implies non-smooth transitions during vehicle operation, resulting in unwanted behaviour. Simulation programs using the standard drive cycles as inputs are backwards facing. The forward facing method is more representative of real world situations. The model input is a driver command which produces a resultant vehicle performance; the flow of calculation is in the same direction as power flow. Drive cycles can still be incorporated into this type of simulation through the creation of a driver model. This technique is practical to evaluate the performance of real-time controllers.

Commercial Vehicle Simulation Software

A commercial vehicle simulator, the ADvanced VehIcle SimulatOR (ADVISOR), was developed in 1994 by U.S. Department of Energy's (DOE) National Renewable Energy Laboratory (NREL) and is now offered for public use through AVL [18]. The program is written in the MATLAB Simulink environment and employs a combination of forward and backwards facing simulation attributes. It is capable of simulating commercial, electric, hybrid and fuel cell vehicles, allowing for the assessment of the vehicle performance, fuel economy and exhaust emissions. A drawback to the program is its dependency on old versions of MATLAB Simulink - R13 and R14.

Argonne National Laboratory (ANL) and the U.S. DOE developed the Powertrain System Analysis Toolkit (PSAT) in 1999 [19]. The program employs a forward looking model which can be used to evaluate fuel economy, engine performance, drive cycle studies, parametric modeling and controller design. PSAT is written in MATLAB Simulink and Stateflow and covers a range of vehicle configurations - conventional, electric, fuel cell, series hybrid, parallel hybrid, and powersplit hybrid.

In 2007, ANL partnered with General Motors to develop Autonomie, the next generation of automotive simulation tool [20]. The tool capitalizes on using a plug-and-play architecture which facilitates rapid and easy integration of models. Autonomie uses a forward looking model and is capable of incorporating models from CarSim, AMESim and GT-Power.

The MATLAB Simulink package offers additional libraries including SPS and SimDriveline. SPS provides tools for modeling and simulation of generation, transmission, distribution and consumption of electrical power. Component models are available for three phase electrical machines, electric drives, FACTS devices, etc. As well, the toolbox offers automated system analysis of harmonics and load flow. The SimDriveline toolbox offers component libraries for modeling one dimensional mechanical systems. Models from either package can be converted into C code to be executed on a real-time platform.

Modelica is an object orientated and equation based open source modeling language used for modeling complex physical systems. Dynamic Modeling Library (Dymola) developed by Dassault Systèmes/Dynasim provides a modeling environment that is able

to utilize Modelica models. Dymola also allows for the compilation of the model into simulation code to be simulated on HIL systems such as xPC or dSpace. Effectively, Dymola Modelica is comparable to MATLAB Simulink in the functionality provided. The Mathworks SimDriveline contains all Dymola functions.

Other commercially available simulation packages include AVL CRUISE by AVL and GT-Drive by Gamma Technologies.

Ship Performance Prediction/Simulation Software

There are a limited number of programs now available which offer a comprehensive package for predicting ship performance. Standard modeling modules include open water hull resistance, and propeller performance and efficiency. Effects of environment interaction are also available such as hull fouling, sea state, and wind.

Many commercial ship power prediction software exist, however, they are specifically used to evaluate preliminary ship design. With these programs, ship architecture can be assessed and adjusted, ensuring the ship will be capable of reaching the desired planning speed. These programs often have a multiple document interface setup, similar to spreadsheets with corresponding graphs. Many are also capable of modeling the ship's hull or importing ship codes created in another program.

A review of accepted methods and university/industry models for calculation of preliminary ship power requirements were examined for their suitability to be executed as computer programs [21]. The most favourable methods were then combined to form the Power Prediction Program (written in Pascal). Features evaluated include: hull resistance, appendage resistance, fouling resistance, propellers, propulsion coefficients, and weather effects.

NavCad by HydroComp is a software tool designed for prediction and analysis of vessel speed and power performance [22]. It includes resistance prediction, steady state propulsion analysis, vessel acceleration analysis and propulsion component sizing. Other HydroComp software includes PropExpert and SwiftTrial which are tools for sizing and analysis of propellers, and management and analysis of sea trials, respectively.

MARIN has developed DESP, a propulsive performance prediction software for early ship design [23]. Other programs developed for preliminary ship design include SeaPower.

Accurate ship motion prediction is significant as it directly relates to the design, control and economic operation of the ship. Ship motion prediction software is also strongly prominent as a teaching/training resource. The SEAWAY program is capable of simulating 6 degrees of freedom (DOF) ship motions, incorporating wave induced loads, motions, added resistance, and internal loads in regular and irregular waves [24]. MANSIM is a surface ship manoeuvring, station keeping, and seakeeping simulator [25]. Written in Fortran, it is utilized for scenario training purposes, and includes a graphical representation of the simulation during run-time. DYNASIM by DYNAFLOW INC. is an interactive, physics based, real-time, PC-based, ship manoeuvring simulator.

The Marine Systems Simulator (MSS) by Marine Control is a marine systems library and simulator written in MATLAB Simulink [26]. MSS includes GNC and Hydro toolboxes. The GNC library contains blocks and functions for guidance, navigation and control including vessel models, autopilots, dynamic positioning (DP) control systems, guidance systems, etc. Many of the models are written in editable .m files or Simulink models. The MSS Hydro toolbox accepts data files generated by hydrodynamic programs and processes the information for use in MATLAB Simulink. Models built in ShipX (Veres) by Marintek or Wamit by Wamit can be directly imported into the Simulink environment. The ship codes can be used to simulate vessels in 6 DOF. This feature removes the burden of describing the vessel geometry directly in MATLAB Simulink and takes advantage of existing graphical programs designed for this purpose.

Tools for simulating shipboard electric power systems include the Alternative Transient Program (ATP), PSpice and Saber [27]. ATP is capable of modeling both electromagnetic and electrochemical phenomena in complex networks. Together with detailed component modeling, the program can also be used to simulate fault disturbances and implement control systems. Microsim Corporation developed PSpice which uses linear, discrete, passive and active electrical elements, etc, for network simulation. Finally, Saber, similar to PSpice, is a circuit simulation tool. The program uses the analog hardware description language MAST to model physical systems. The

system can be drawn as a circuit schematic or described in a text editor. All of these programs are limited in the capability of their GUIs, which are not particularly user friendly for building complex shipboard power systems, establishing monitoring points, or processing output data.

PSCAD/EMTDC, created by the Manitoba HVDC Research Centre, is a power systems modeling tool capable of electromagnetic time domain transient simulation. It has been commercially available since 1993, but has been in development since 1988. The program provides an advanced GUI which allows for dynamic control of events and input data during simulation. Models developed in C, Fortran, and MATLAB can be interfaced with PSCAD.

2.5 Ship Power Performance Modeling Research

Shipboard integrated power systems supply both propulsion and hotel loads through a common electrical platform. Electric drives offer advantages over mechanical drives in terms of meeting the increasing on-board power demand, as well as improving cost effectiveness and survivability (avoiding blackouts).

More recently, there has been a surge of interest in predicting/understanding the shipboard power system during operation, particularly during load transients, rather than just ensuring the power requirements are satisfied during the design phase. Models with this focus can be used for power system analysis, fault insertion and system reconfiguration/restoration, fuel consumption and emissions estimation, novel power system evaluation, and control system development. The following are examples of ship power system simulation research.

A 6 DOF time domain hydrodynamic ship simulator was used to model an all-electric ship (AES) [28]. The model is capable of predicting prime mover fuel consumption for a ship in random seas, and power bus fluctuation during execution of a low radius turn. The AES model has a time domain hull model which combines nonlinear manoeuvring equations, seakeeping equations, and second order wave forces. The value of this model is the ability to predict propeller elevation and velocity in random seas; propeller load fluctuations can impart large electrical transients on-board. The knowledge from these simulations can be applied during the AES design stage. Another AES, based on the

Visby-class corvette was modeled with the aim of better understanding the issues arising with voltage stability in a shipboard DC power system [29]. Similarly, an AES model to investigate DC-link voltage regulation and propeller control strategies was created by [30].

In [31], the basic structure and component elements of a ship's electrical system are presented in conjunction with a controllable pitch propeller model. The aim of the study was to examine transient response during prevalent system disturbances, namely the switching of mechanical/electrical loads.

A selection of PEM fuel cells coupled with batteries was assessed for their feasibility for use in the Advanced Electric Ship Demonstrator (AESD); the power system hybridization factor was evaluated [32]. The AESD is a one-quarter scale prototype destroyer operated by the U.S. Navy. From the results of the simulation, the authors recommended the HD6 FC module over the other PEM FCs to be the prime shipboard power source. However, the secondary energy source needed for appropriate power conditioning due to slow dynamic FC response to fast load changes was not addressed.

A hybrid power system for an AES was developed in the virtual test bed (VTB) simulation environment [33]. System power is provided by two sets of SOFC/gas turbine hybrid engine systems. The FC is represented as a physics based one dimensional model. As well, ship, propeller and motor models are also included. Behavior of the hybrid power system during transients, specifically step changes in the ship drag coefficient and ship service load, were evaluated.

A large combat ship with an electric power system consisting of two 36.5 MW propulsion motors with variable speed drives, two 36 MW generators with gas turbines, and two 4 MW auxiliary generators was modeled in PSCAD [34]. The study examined the dynamic response of the electrical system over a wide frequency range, as well as during fault and load scenarios.

In [35], a reduced order dynamic hybrid power system (HPS) model was developed to address real-time power management schemes along with effective power converter control for use in military applications. Two versions of the hybrid system were developed, each with a different purpose. One model was created for control and optimization development of the HPS for shipboard integrated power systems (IPS) and

auxiliary power units. The second was used as a simulation orientated IPS model; it was used for real-time simulation and analysis of the IPS. The system is comprised of a gas turbine generating set, a reformer and fuel cell system, and a lithium-ion ESS complete with the associated power converters and propulsion system. A real-time hierarchical controller for normal mode HPS was implemented, as well, a failure mode power management strategy was addressed.

A ship power system was modeled by [36] with the aim of developing a power management system to handle major power system faults, improve system robustness against blackouts, minimize operational costs, and maintain power system equipment within safe operational limits.

Capilano Maritime Ltd. presented a paper on the design of a hydrogen powered hybrid electric tug which included hybrid propulsion system modes and when/how long the tug could be operated in each mode [37].

2.5.1 Summation

The above modeling contributions are evaluated for their inclusion of the following:

- simulation environment,
- propeller model,
- resistance/environment model or power load profile based on recorded/testbed data,
- real-time simulation/drive cycles, and
- influence of the power management strategy.

Simulation Environment

Of the aforementioned ship power systems models, the majority utilized MATLAB Simulink [31][36], in combination with either Fortran [28][30], SPS [29][35], or other programs [32][33]. Other ship electrical system simulation studies using MATLAB Simulink in conjunction with other programs have been carried out by [38][39].

Propeller Model

Propeller models/loads were included in [28][29][31][33]. In [31] only a very simple mathematical model of the propeller was used. The propeller load in [29] was modeled as

a function of torque versus speed which was derived from data collected of the water jet operating on the Visby-class corvette; propulsion data utilized is directly obtained from the testbed. The propeller of the AES modeled in [28] used data from the Waginingen B-class propeller series, as well as thrust and torque equations commonly accepted by industry; this propeller data and method are incorporated into many ship performance prediction software. The model in [33] used a similar approach.

Resistance/Environment

Only a handful of models created take into account the ship environment and the resulting resistance. Ship resistance for the AES model [28][33] was described by a simplified equation; necessary empirical parameters were derived experimentally or approximated. Using this resistance along with thrust produced by the propellers, the ship's surge velocity was calculated. The model presented in [35] utilized a ship dynamic model which includes added mass, and hydrodynamic forces and moments acting on the ship. Unfortunately, details of the exact ship model have been left out - only an extensive reference is given. To obtain a desired ship speed, the desired motor speed and torque are calculated in the ship dynamics model and input to the propulsion motor control unit.

Real-Time Simulation/Drive Cycles

In [28], the AES time domain model is executed on an end-to-end AES simulator which is run in real-time on a Dell M1530 laptop using Simulink's Rapid Accelerator mode. An OpalRT real-time simulator was used by [35]. The VTB used by [33] has a real-time extension, the VTB-RT.

The tug model in [37] is derived using the typical approach of equipment selection based on loads/usage rather than simulation. However, it is noted here because a duty profile of similar sized tugs, the Seaspan Hawk and the Seaspan Falcon, was documented over a 30 day period, the results of which formed a baseline power duty profile for the tug design. This duty profile relays the percentage of engine load to be expected over a 30 day period, information which is valuable in formulating a control strategy. As well, although the authors chose to present the information as a percentage of engine load versus percentage of engine hours, the raw data can be instead plotted as power required over time for a captured time frame - similar to a vehicle drive cycle. Of course, this data

would only be applicable to a similar sized vessel operated in a similar manner, but this can serve as a baseline for creating tug drive cycles to be used for real-time performance evaluation simulations.

Power Management Strategy

In [35], power management strategies applied to hybrid systems in land-based hybrid vehicles, shipboard power systems, and portable electronic devices were reviewed to assist with creating a real-time feasible optimization algorithm. The author remarked that application of power management strategies for commercial land-based vehicles would not be practical for application in military shipboard power systems. Investigation into fuel consumption minimization for the model in [36] used land-based power generation and marine vessel power generation strategies for system comparison and development of an optimized power management strategy.

Chapter 3 Hybrid Propulsion System

3.1 Vessel Propulsion System

The main powertrain system of the proposed hybrid electric vessel, including propulsion devices, is given in Figure 2. The power sources include a Ballard HD6 PEM fuel cell, an ESS consisting of 165 Valence U24-12XP battery modules, and three diesel generators. One bidirectional DC/AC converter facilitates power flow between the ESS to the 460 VAC bus, while the FC system utilizes one unidirectional DC/AC converter. The vessel propulsion is provided by two ZF Marine HRP Z-drives. For slow speed manoeuvring or station keeping, the azimuthing thrusters are used in conjunction with a ZF Marine HRP bow thruster.

3.2 Vessel Fuels: Well-to-Pump Emissions

Three main fuel sources selected for the proposed hybrid electric vessel are marine diesel, hydrogen, and electricity.

3.2.1 Marine Diesel

Marine diesel is a standard fuel for combustion in diesel engines/generators on-board ships. In the marine industry, diesel fuel can be classified by fuel type: distillate, intermediate, and residual (Table 5) [40]. As a note, the term ‘diesel’ is not always included in the industry name for marine diesel fuels.

Table 5: Diesel Fuel Types for Marine Use

Fuel Type	Fuel Grades	Common Industry Name
Distillate	DMX, DMA, DMB	Gas Oil, Marine Gas Oil
Intermediate	IFO-180, IFO-380	Marine Diesel Fuel, Intermediate Fuel Oil (IFO)
Residual	RMA-RML	Fuel Oil, Residual Fuel Oil

In order to determine the fuel type required, the data sheets for the generators selected in Section 3.4.6 were consulted; it is assumed that the same fuel type would be used across the industry for the size/type of generator required. The data sheets for the CAT

C9 generator list fuel consumption rates for a specified fuel. The fuel type is not listed, only particular fuel properties are given (Table 6) [7].

Table 6: Generator Fuel Information

Fuel Specifications	Generator Data Sheet
Lower heating value [kJ/kg] ([btu/lb]) @ 29˚C	42780 (18390)
Density [g/L] ([lbs/US gal])	838.9 (7.0)
Calculated Values	
Energy Content [BTU/US gal]	128748
Density [g/US gal]	3176

Emission factors could not be found for the production of distillate or intermediate type fuels, only residual oil and conventional diesel emission factors were available. (Bunker fuel for ocean tankers was included in GREET, however, the details listed are the same as those for residual oil [41].) Consequently, conventional diesel fuel specifications in the Total Energy and Emissions Analysis for Marine Systems (TEAMS) excel program were altered to reflect the fuel properties given on the CAT C9 generator data sheet. One other variable changed was the sulphur level which was set to 100 ppm or 0.01% by weight [42], typical of distillate marine diesel fuel.

To confirm the fuel properties and corresponding production emission factors would be suitable, the combustion emissions for carbon dioxide and sulphur oxides calculated in TEAMS were compared to auxiliary engine combustion calculations given in Equations 27 and 30 (used for pump-to-propeller emission calculations). This is a reasonable comparison as CO_2 and SO_2 emissions are fuel dependent, while NO_x, CO, and *VOC* emissions are dependent on the combustion process (engine type). The results of the emission calculations are outlined in Table 7. Both emission stream calculations are aptly comparable, consequently, the resulting conventional diesel production emissions calculated in TEAMS will be utilized (Table 8).

Table 7: TEAMS Combustion Emission Comparison

Fuel Specifications	Conventional Diesel (TEAMS)	Generator Combustion Calculations
Energy Content [BTU/US gal]	128748	-
Density [g/US gal]	3176	-
CO_2 [kg per 1000 kg fuel combusted]	3132	3200
SO_x [kg per 1000 kg fuel combusted]	0.2	0.2

Table 8: Marine Diesel Production Emissions

Emission	Emission Factor [g/mmBtu]
VOC	1.260
CO	2.966
NO_x	14.428
PM_{10}	2.071
SO_x	14.207
CH_4	8.106
N_2O	0.155
CO_2	10181

3.2.2 Electricity (British Columbia)

The electricity ‘well-to-pump’ emissions encompass the production of electricity from a stationary source used to charge the ESS while it is in port (utilizing its plug-in capability). It is assumed that the ship will be primarily operated within BC, and hence the BC Hydro emission factor of 25 tCO_2e/GWh will be used [9].

3.2.3 Hydrogen

The gaseous hydrogen fuel sourced for use in the proposed vessel is a recovered by-product from the manufacture of sodium chlorate. Typically, the off-gases of production are approximately 97.5% hydrogen, 2% oxygen, and 0.5% chlorine [43]. To remove the chlorine from the hydrogen stream, the gases are sent through a caustic scrubber. The

sodium chlorate is manufactured by the electrolysis of sodium chloride solution in electrochemical cells without diaphragms. The overall chemical reaction is:

$$NaCl + 3H_2O = NaClO_3 + 3H_2 \quad (4)$$

This process requires approximately 5 kWh of energy to produce one kilogram of sodium chlorate [43] and, roughly, 56.8 g of hydrogen. Using this information, approximately 0.0117 kg of hydrogen is produced per kWh. The BC Hydro emission factor will be used to derive the GHG emissions generated due to the production of hydrogen.

3.3 Ship Powertrain Components & Propulsion Devices

An overview of the major power sources, power converters and propulsion devices specified for the proposed hybrid vessel is given below.

Fuel Cell

PEM fuel cells were primarily considered for this project due to their history of use in transportation applications along with their low operating temperature. The fuel cell selected for this project is the Ballard FCvelocity-HD6. This heavy duty PEM FC was designed for automotive applications, specifically to be utilized on transit buses. It is the same FC used by New Flyer Industries in their hydrogen bus fleet which was put into service during the 2010 Winter Olympics. The power rating of the pack, coupled with its size and history of use made it an ideal candidate. The pack details include [44]:

- DC voltage: 550-800V
- Maximum current: 300A
- Weight: <400 kg
- Length x width x height: 1270 x 870 x 505 mm
- Fuel: gaseous hydrogen, commercial grade per SAE J2719
- Oxidant: air
- Coolant: 50/50 pure ethylene glycol and water
- Temperature (nominal): 63˚C
- Fuel pressure (minimum): 12 barg

- Air pressure (nominal): 1.2 barg
- Control interface: CANbus

Hydrogen Storage

Hydrogen is not a typical fuel utilized on-board ships and, presently, no regulations exist with respect to on-board hydrogen storage; ships are evaluated on a per case basis. For the proposed hybrid vessel, a custom built hydrogen PowerCube manufactured by Sacre-Davey was selected. The PowerCube consists of ten 450 bar Dynetek cylinders, providing a hydrogen capacity of 86 kg, and is equipped with integrated safety features and controls.

PowerCube details include [45]:

- 450 bar (6500 Psi) compressed hydrogen distribution system
- Transport Canada approved aluminum lined, carbon-fibre reinforced cylinders
- Ten cylinders mounted in a structural steel framework form a PowerCube module
- Nominal capacity (15˚C): 86.4 kg of hydrogen gas
- Nominal weight (empty): 3360 kg
- Dimensions (length x width x height): 3265 x 1200 x 2613 mm

Energy Storage System

A large ESS is desired so as to increase the amount of electric power available which is advantageous when quiet/clean operation is required for long periods. Valence U24-12XP battery modules were selected for this application due to their capacity, reliability, and complete battery bank management option available. The Valance module chemistry is lithium iron magnesium phosphate and its specifications include:

- Voltage (nominal): 12.8V DC
- Nominal capacity (C/5, 23˚C): 110 Ah
- Weight: 15.8 kg
- Max continuous load current: 150 A
- Dimensions: (length x width x height): 260 x 172 x 225 mm

Given 165 Valence modules in a 55 series, 3 parallel configuration, the system specifications are given in Table 9 [46].

Table 9: ESS Specifications

System Discharge Voltage	V	704.0
System Charge Voltage (Max)*	V	803.0
System Charge Voltage (Min)*	V	759.0
System Discharge Voltage Cutoff (Min)	V	550.0
System Discharge Current Max Continuous	A	450
System Discharge Current Max Peak (30s)	A	900
Total ESS Capacity*	Ah	330
Total System Energy*	kWh	232.3

*Energy calculations use 5 hr rate capacities (C/5)

DC/AC Converters

One bidirectional DC/AC converter, 354 kVA, was selected to link the ESS to the 460 VAC bus. A second unidirectional 177 kVA DC/AC converter facilitates power flow from the FC to the 460 VAC bus. The bidirectional converter would also serve the connection point for the shore power plug-in.

Azimuth Propulsion Thrusters

The thrusters specified are two HRP 2111 WM, made by ZF Marine HRP. Each Z-drive is driven by its own electrical motor (ABB M3BP series), controlled by a variable frequency drive (VFD). These fixed pitched thrusters are appealing in their ability to provide 360˚ steering, affording better manoeuvrability especially during station keeping and slow speed propulsion. Z-drive details include:

- Continuous power rating: 200 kW
- Voltage: 460V, 3ϕ, 60 Hz
- Input speed: 1800 rpm
- Propeller: 750 mm diameter in nozzle

Bow Thruster

The bow thruster selected is an HRP 1000 series, type 1001TT. Similar to the Z-drives, a VFD will be used to control the vertical electric motor. Technical specifications of the fixed pitch tunnel thruster include:

- Power: 90 kW
- Voltage: 415V, 3ϕ, 50 Hz
- Input speed: 1500 rpm
- Propeller diameter: 630 mm
- Tunnel: 680 x 15 mm, length 1000 mm

Diesel Generator

Three identically sized diesel generators were stipulated in the proposed design. Their basic specifications include:

- Power: 215 kW, 0.8 pf
- Voltage: 460 VAC, 3ϕ, 60 Hz

The generators were sized so as to be capable of providing all power for propulsive and hotel loads during normal operation in the absence of fuel cell or ESS assistance.

3.4 Simulink/SPS Model

The hybrid electric ship model of the proposed vessel was implemented in MATLAB Simulink and utilized blocks from the SPS toolbox.

3.4.1 Fuel Cell Module & Hydrogen Storage

A comprehensive PEM FC module has already been created for the SPS library [47]. This model was parameterized to suitably reflect the operation of the Ballard HD6 unit in terms of its operating conditions and subsequent voltage output over a wide operating range. Operating parameters of the stack are assumed to be constant; these are listed in Table 10. The HD6 polarization curve is given in Figure 10 [48]. Approximately 20 kW is consumed by the auxiliary fuel cell devices [46]. Taking into account the FC module auxiliary loss, overall, the maximum power available is 130 kW.

The maximum hydrogen capacity of the PowerCube subsystem is 86.4 kg. The FC stack block calculates the instantaneous stack fuel consumption, which is subtracted from

the total hydrogen remaining. The PowerCube subsystem also calculates the GHG emissions due to the production of hydrogen (as discussed in Section 1.1.1). This is a fixed value based on the initial PowerCube hydrogen capacity.

Table 10: Fuel Cell Model Parameters

Operating temperature [˚C]	70
Nominal fuel supply pressure [bar]	17
Nominal air supply pressure [bar]	2
Nominal air flow rate [lpm]	3450
Nominal stack efficiency [%]	55
Maximum continuous fuel flow [g/s]	2.5

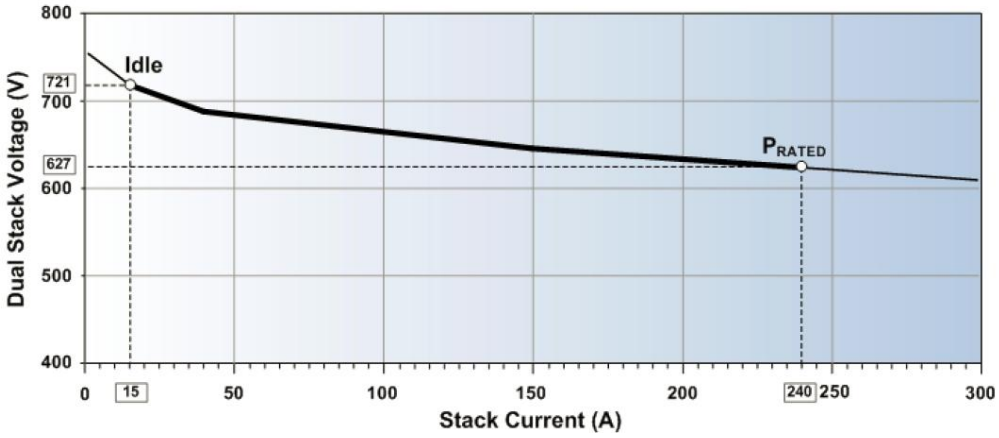

Figure 10: HD6 Polarization Curve

3.4.2 Valence ESS

The proposed ship's ESS consists of 165 Valence modules arranged in 55 series, 3 parallel strings. This 230 kWh configuration operates at a nominal DC voltage of 704V and has a 330 Ah capacity. The SPS lithium-ion battery block was parameterized to reflect a single Valence module. The C/5 rate was modeled as that is the standard for battery data sheet information; the parameters used are given in Table 11 [49], and the resulting nominal discharge curve for C/5 rate is shown in Figure 11.

Table 11: Battery Mask Parameters

Nominal Voltage [V]	12.8
Rated Capacity [Ah]	110

Maximum Capacity [Ah]	110
Fully Charged Voltage [V]	13.25
Nominal Discharge Current [A]	22
Internal Resistance [Ω]	0.006
Capacity [Ah] @ Nominal Voltage	86.9
Exponential Zone [Voltage [V], Capacity [Ah]]	[13, 55]

The Valance voltage profiles for different charge C-rates in terms of capacity are given in Figure 12 [49], with the Simulink module C/5 rate overlaid for comparison. The voltage profiles for the same C-rates versus time for a single Valance Simulink module are shown in Figure 13.

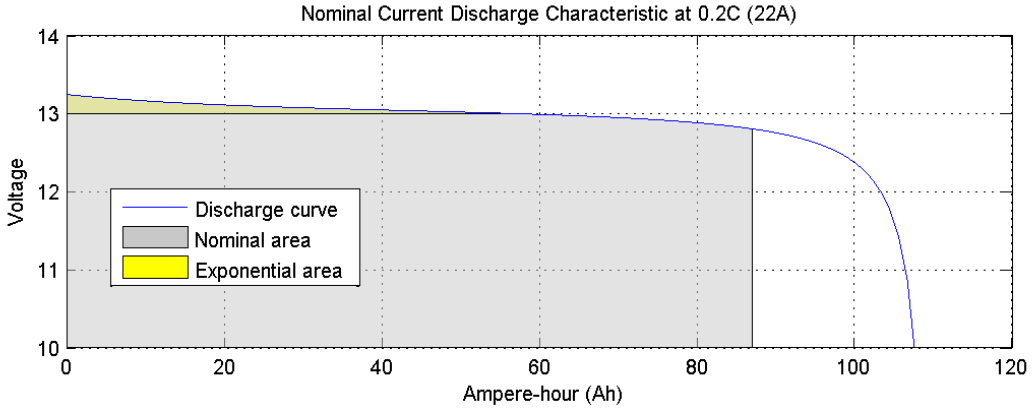

Figure 11: C/5 Discharge Rate for Valence U12-24XP Simulink Module

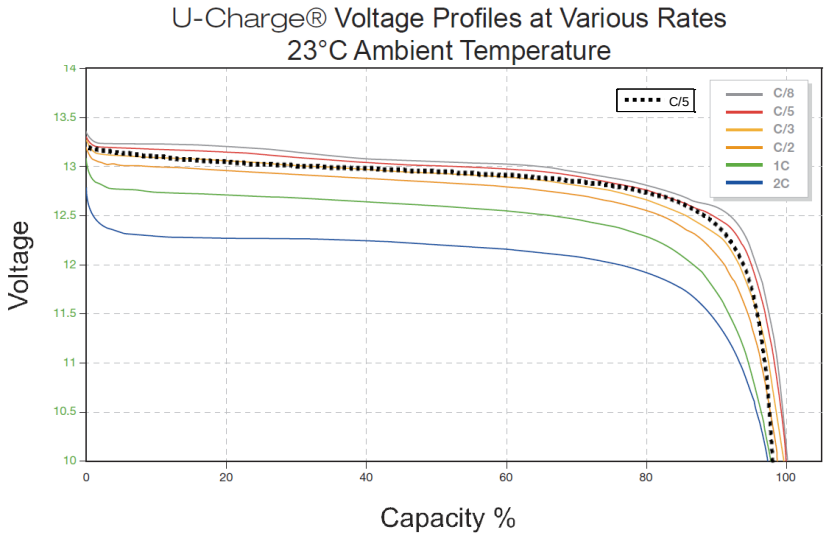

Figure 12: Voltage Profile of Valence U24-12XP

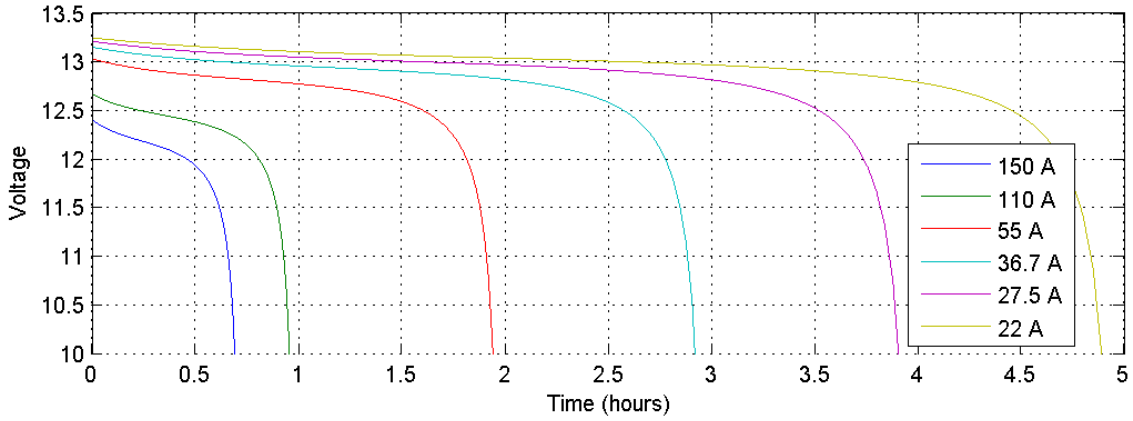

Figure 13: Voltage Profile of Valance U24-12XP Simulink Module

In order to reduce the number of modules required (165), the mask of the battery module was altered so each block would represent one series string of modules. With this representation, only three battery modules in parallel are used to represent the complete ESS. It should be noted that this configuration does not allow for battery modules to have different SOC and thus cannot be used for battery bank module balancing simulations.

3.4.3 Power Converters

For the proposed hybrid vessel, the power converters were not specified. Consequently, a three phase PWM IGBT converter with simple PI control was used.

The ESS converter is bidirectional, capable of facilitating a continuous power flow of 354 kVA or 500A discharging, and 177 kVA or 250A charging. In ESS or FC mode, the bidirectional converter operates as a grid forming inverter and utilizes voltage regulation. The converter maintains system frequency within ±2 Hz. During HEV mode, the bidirectional converter acts as a grid feeding converter and uses PQ regulation. The FC converter is limited to 177 kVA or 250A and operates under PQ regulation (grid feeding).

Each IGBT power converter is modeled using an SPS universal bridge with the average-model based VSC option selected. This option makes use of an average-model type of voltage source converter to represent the power electronic switches. Reference signals characterizing the average voltages generated at the ABC terminals are used to simulate the firing pulses. The average-model does not represent harmonics and can also be readily used with larger sample times without diminishing the average voltage dynamics, both of which are desirable attributes.

Direct DC to AC power conversion from either of the DC sources to the 460 VAC bus using the selected IGBT converter is not possible given the voltage levels of the DC sources. For the ESS bidirectional converter, a 430V/460V transformer is employed. A 350V/460V transformer is utilized for the FC converter. The transformer voltage values were chosen by ensuring the equality given in Equation 5 was satisfied.

$$V_{DC} \geq \frac{2\sqrt{2}}{\sqrt{3}} V_{LL} \tag{5}$$

3.4.4 Propeller VFDs

A field oriented control induction motor drive was used to control both the azimuth and bow thrusters. SPS's AC3 induction motor drive block was used for this application. For the main thrusters, the motor parameters are taken from Blue Max performance data sheet for 460V constant torque motors - 300 HP, 1788 rpm (Appendix F). Likewise, for the bow thruster, the BlueMax 125 HP, 1788 rpm motor data was used. The DC bus capacitance, braking chopper resistance and machine flux values needed for the SPS motor drive block are calculated using Equations 6, 7 and 8, respectively. The average DC bus voltage V_{DC} is equal to $1.35V_{PP}$, the desired ripple voltage is set to 50V, and the braking chopper activation voltage is set to 700V. AC3 mask parameters are given in Table 12.

$$C_{DC\ bus} = \frac{P_{motor}}{12 f \Delta v V_{DC}} \tag{6}$$

$$R_{braking} = \frac{V_{Brake,act}^2}{P_{motor}} \tag{7}$$

$$\varphi_{VSD} = \frac{V_{pp}}{2\sqrt{3} \cdot \pi f} \tag{8}$$

Table 12: AC3 Mask Parameters

Asynchronous Machine		**Azimuthing Thruster**	**Bow Thruster**
Nominal values	Power [VA]	250e3	115e3
	Voltage [V_{rms}]	460	460
	Frequency [Hz]	60	60
Rotor values	Inertia [kg·m^2]	4.0455	1.833
	Friction [N·m·s]	0.08	0.08
	Pole pairs	2	2

Equivalent circuit values	Stator: resistance [Ω]	0.007	0.024
	Stator: leakage inductance [H]	0.000204352	5.3582e-4
	Rotor: resistance [Ω]	0.006	0.010
	Rotor: leakage inductance [H]	0.000167197	3.3953e-4
	Mutual inductance [H]	0.007407113	0.0144
Converters and DC bus			
Rectifier	Resistance [Ω], capacitance [F]	10e3, 20e-9	10e3, 20e-9
DC bus	Capacitance [F]	0.0112	0.0051
Braking chopper	Resistance [Ω]	1.96	4.2609
	Chopper frequency [Hz]	4000	4000
	Activation voltage [V]	700	700
	Shutdown voltage [V]	660	660
Controller			
Speed Controller	Speed ramps: acceleration/deceleration [rpm/s]	±900	±1500
	PI regulator: proportional gain, integral gain	10,100	10,100
	Speed cutoff frequency [Hz]	500	500
	Torque output limits [N·m]	±2473	±1175
Machine flux	Initial [Wb]	0.705	0.705
	Nominal [Wb]	0.705	0.705
Field orientated control	Flux controller: proportional gain, integral gain	100,90	100,90
	Flux output limits [Wb]	1.0575	±1.0575
	Lowpass filter cutoff frequency [Hz]	500	500

From the VFD subsystem, the motor shaft speed is output to the propeller subsystem, which returns the corresponding propulsor torque.

3.4.5 Propellers

The proposed ship's main propellers are podded Z-drives, thus, a ducted propeller series was used to model the generated thrust. The Ka 5-75 propeller in a 19A nozzle was selected. The 19A nozzle is a commonly used flow accelerating duct. The propeller designation is given as: series screw type, number of blades, and expanded blade area

ratio. The Kaplan series is designated with Ka. The Kaplan blade type, with its wider blade tips, is preferred over the B-series screw type as it is less susceptible to cavitation at the blade tips when used within a duct. The Ka 5-75 is the only Kaplan 5 blade fixed pitch propeller which was tested within the 19A nozzle [50].

Podded propeller thrust is a combination of propeller thrust, and nozzle and stator thrust. The propeller thrust coefficient K_T, and nozzle/stator thrust coefficient K_{TN} are given in Equation 9 and Equation 10, respectively [50]. The torque coefficient K_Q is similarly expressed in Equation 11. Appendix E contains data and calculations performed by Industry for the propeller noted in Section 3.3. Nominal propeller pitch P over diameter D is given as 1.06.

$$K_T = 0.033 - 0.153463J - 0.398491J^3 - 0.435515J\left(\frac{P}{D}\right) + 0.664045\left(\frac{P}{D}\right)^2 + 0.283225J^2\left(\frac{P}{D}\right)^2 - 0.162764\left(\frac{P}{D}\right)^3 \quad (9)$$

$$K_{TN} = -0.000813 + 0.034885J - 0.276187J^3 - 0.626198J\left(\frac{P}{D}\right) + 0.450379J^2\left(\frac{P}{D}\right) + 0.359718\left(\frac{P}{D}\right)^2 - 0.087289\left(\frac{P}{D}\right)^3 - 0.003751J^2\left(\frac{P}{D}\right)^6 \quad (10)$$

$$K_Q = 0.007210 - 0.01467J^2 - 0.006398J^4 - 0.03138J^2\left(\frac{P}{D}\right) + 0.010386J^2\left(\frac{P}{D}\right)^2 + 0.053169\left(\frac{P}{D}\right)^3 - 0.014731\left(\frac{P}{D}\right)^4 \quad (11)$$

The advance coefficient J is calculated using Equations 12 through 15. It is a non-dimensional measurement of propeller performance. It represents the ratio between the speed of advance of the propeller V_a [m/s] and the propeller rotational speed n [rps] and diameter D [m]. The speed of advance is the ship speed V [m/s] less the wake fraction coefficient w. The wake fraction is the percentage of the ship velocity seen at the propeller. The propeller operates in the wake of a ship, therefore the 'freestream' velocity as seen by the propeller is lower than the ship speed. Calculation of w for twin-screw ships is given in Equation 14. It is calculated using the viscous resistance coefficient C_V, the block coefficient C_B, the ship breadth on waterline B [m], and the average molded draught T [m]. The viscous resistance is comprised of form resistance, naked hull skin friction and appendage resistance. Equation 15 represents a formula to estimate these resistance contributions. It includes the hull form factor $1+k_1$, the frictional resistance

coefficient C_F, and the correlation allowance coefficient C_A, which are all described in Section 4.1.1.

$$J = \frac{V_a}{nD} \tag{12}$$

$$V_a = V(1 - w) \tag{13}$$

$$w = 0.3095C_B + 10C_V C_B - 0.23\frac{D}{\sqrt{BT}} \tag{14}$$

$$C_V = (1 + k_1)C_F + C_A \tag{15}$$

Using the thrust and torque coefficients, the thrust T [N] delivered by the propulsor and the torque Q [Nm] delivered to the propulsor are given by Equations 16 and 17, respectively. The thrust is made up of the propeller thrust T_P and the nozzle/stator thrust T_N. Both equations include their respective coefficients, the water density, and the propeller diameter and rotational speed. The salt water density ρ_w is 1025 kg/m^3.

$$T = T_p + T_N = (K_T + K_{NT})\rho_w D^4 n^2 \tag{16}$$

$$Q = K_Q \rho_w D^5 n^2 \tag{17}$$

Effective power delivered by the propulsor and power delivered to the propulsor is given in Equations 18 and 19, respectively [51]. Their ratio P_E/P_D is equal to the propeller open water efficiency η_0.

$$P_E = TV_a \tag{18}$$

$$P_D = 2\pi n Q \tag{19}$$

A similar approach was used for the bow thruster propeller model. Information on the bow thruster is limited; it has 4 blades and it is contained within a cylindrical duct. For this reason, the Kaplan series Ka 4-70 propeller was selected (the 4 bladed series with the largest expanded blade area ratio). However, the nozzle/stator thrust coefficient was not included. The corresponding thrust and torque coefficients are given in Equations 20 and 21, respectively.

$$\begin{aligned} K_T = {} & 0.030550 - 0.148687J - 0.391137J^3 - 0.432612J\left(\frac{P}{D}\right) \\ & + 0.667657\left(\frac{P}{D}\right)^2 - 0.172529\left(\frac{P}{D}\right)^3 - 0.017293J\left(\frac{P}{D}\right)^6 \end{aligned} \tag{20}$$

$$\begin{aligned} K_Q = {} & 0.006735 - 0.016306J^2 - 0.007244J^4 - 0.024012J^2\left(\frac{P}{D}\right) \\ & + 0.005193J^2\left(\frac{P}{D}\right)^2 + 0.046605\left(\frac{P}{D}\right)^3 - 0.007366\left(\frac{P}{D}\right)^4 \\ & - 0.001730\left(\frac{P}{D}\right)^6 - 0.000337J\left(\frac{P}{D}\right)^6 + 0.000861J^2\left(\frac{P}{D}\right)^6 \end{aligned} \tag{21}$$

The Simulink model does not take into account ship movement in three dimensions. For this reason, there is no advance speed in the direction of sway. This assumption is suitable when simulating the ship's station keeping ability. When simulating the ship as holding station, the thrust produced by the L-drive (with advance coefficient *J* set to zero) should be equal to the lateral resistance forces experienced by the ship. If the L-drive thrust should overcome the lateral resistance (overcorrect), the effect of advance speed generated is ignored.

The azimuthing propeller model implements Equations 9 through 17. The resulting thrust calculation is doubled to account for twin propellers. For a single propeller, the torque, thrust and open water efficiency calculated by two industry sources is compared to the Simulink model in Figure 14 (Industry sources as given in Appendix D and Appendix E). The figure represents the propeller curve - the thrust and torque coefficients, and the open water efficiency displayed over the advance coefficient. The curves are useful for propeller optimization and determining the operation point (rpm, thrust, torque, power) of the ship. Presenting propeller information in this form is common practice. From the figure, it can be noted that the Simulink propeller model more readily agrees with the industry values when the nozzle thrust is not included. As a result, it was removed from the model to allow for better comparison with the industry prepared data.

Similarly, the bow thruster model uses the thrust and torque coefficients as given in Equations 20 and 21, respectively. There is no industry provided data specific to the bow thruster.

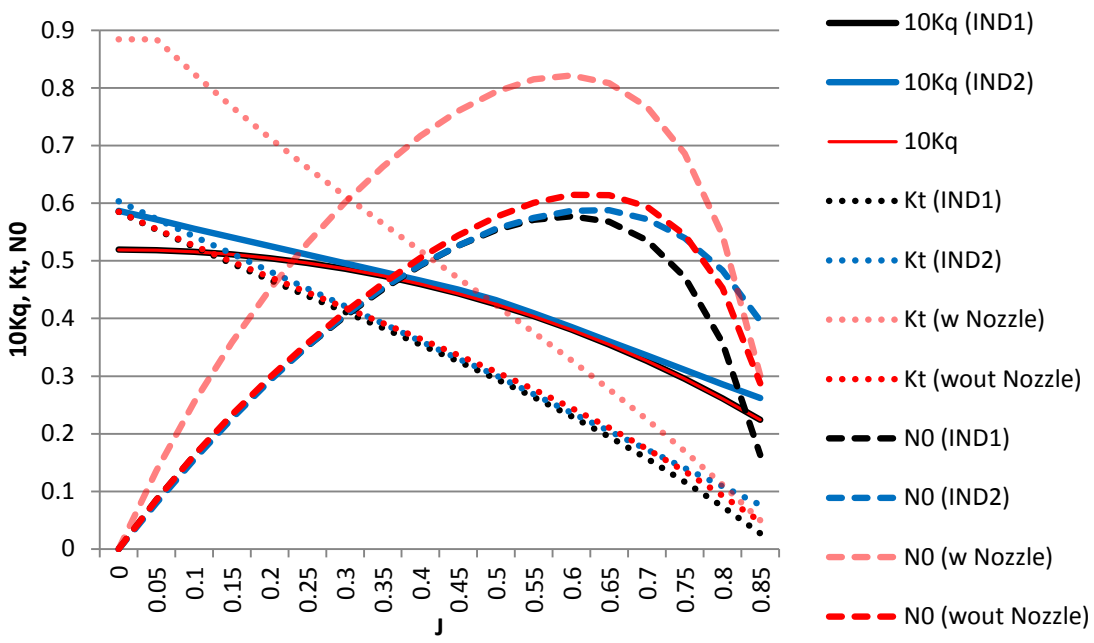

Figure 14: Ka 5-75 Screw Series in Nozzle 19A

3.4.6 Diesel Generator

The diesel generator is modeled as a diesel engine shaft rpm input to a synchronous generator sized as described in section 3.2. The generator electrical output is controlled by varying the shaft speed; the greater the mechanical input to the generator, the greater the rotor angle leading and the greater the electrical output. The generator control unit regulates the voltage of the generator to 460V phase to phase, and synchronizes the output with the bus frequency before connection to the bus. The generator is modeled using an SPS three phase simplified synchronous machine. The mask parameters are given in Table 13.

Table 13: Simplified Synchronous Machine Mask Parameters

Nominal Power [VA]	269e3
Line-to-line Voltage [V_{rms}]	460
Frequency [Hz]	60
Inertia [kg·m^2]	1.89
Damping Factor	21
Pairs of Poles	2
Internal Impedance [Ω, H]	[0.021, 0.00055]

3.4.6.1 Fuel Rate/Emissions

The generator model is based on the Caterpillar Marine C9 Generator set. The dynamic fuel consumption FC_g per unit time of the generator is calculated using Equation 22 [36]. The dynamic brake specific fuel consumption (BSFC) is given in Equation 23, and the static BSFC is derived from generator operating data (Equation 24). The specific fuel consumption and brake power over the range of generator operating power is taken from the CAT C9 performance data sheets [7]; details are given in Table 14.

$$FC_g(P_g) = b_{e,g}(P_g)P_g \tag{22}$$

$$b_{e,g} = b^s_{e,g}(P_g) + b^s_{e,g}(P_g)\frac{7\cdot 10^{-4}}{3600}\left(\frac{d}{dt}P_g\right)^2 \tag{23}$$

$$\begin{aligned} b^s_{e,g}(P_g) = 606.27 - 3461.7\frac{P_g}{P_{r,g}} + 14503\left(\frac{P_g}{P_{r,g}}\right)^2 - 32933\left(\frac{P_g}{P_{r,g}}\right)^3 \\ + 41304\left(\frac{P_g}{P_{r,g}}\right)^4 - 26823\left(\frac{P_g}{P_{r,g}}\right)^5 + 7034.9\left(\frac{P_g}{P_{r,g}}\right)^6 \end{aligned} \tag{24}$$

Table 14: Caterpillar C9 Generator Set Performance Data

Generator [ekW]	Percent Load	Engine Power [B·kW]	Fuel Rate [g/B·kWh]
21.5	10	24.3	376.2
43	20	48	287.6
53.8	25	59.6	270.3
64.5	30	71.1	258.9
86	40	93.6	245.1
107.5	50	115.6	237.4
129	60	138.4	232.7
150.5	70	161.4	230.2
161.3	75	173	229.5
172	80	184.6	229.1
193.5	90	208.1	229.3
215	100	232	229.5

The breakdown of the exhaust emissions for an auxiliary engine, operating on marine diesel, is given by Equations 25 through 30 [42]. Emission factors are in units of kg/tonne fuel. The rated power of the generator P is 215 kW. The load L is in percent of rated power. Finally, s is the sulphur content of the marine diesel fuel (1% sulphur) [42].

$$NO_x = 108.5 - 2.47P + 0.0136P^2 - 0.000018P^3 + 0.000684PL \quad (25)$$

$$CO = 20.72 - 0.218L - 0.0231P + 0.000345PL \quad (26)$$

$$CO_2 = 3200 \quad (27)$$

$$VOC = 3.27 - 2.16P - 0.0144P^2 + 0.0000203P^3 - 0.719L + 0.00476L^2 \quad (28)$$

$$PM = 1.1 \quad (29)$$

$$SO_x = 20s \quad (30)$$

The emissions equations for an auxiliary engine do not include methane or nitrous oxide. For these substances, emission values for marine diesel combustion were extracted from TEAMS and are given in Table 15. Emissions due to production of the marine diesel fuel consumed are given in Table 8. All of these emissions are included in the fuel consumption and emissions subsystem.

Table 15: Marine Diesel Combustion Emissions

Emission	Emission Factor [g/mmBtu]
CH_4	4.58
N_2O	2.00

3.4.7 ROPOS

ROPOS is an additional device which does not constitute part of the powertrain, but is an important load during station keeping mission simulations. The maximum power of ROPOS is 46 kW (100A at 460V). In order to simulate a changing ROPOS load, a random generated number, limited between 0-1, is multiplied with the maximum ROPOS power. This demand is fed into a three phase dynamic load block. For simplicity, the reactive power demand is set to zero. The sampling time of the power demand is set to 30s.

Chapter 4 Vessel Environment Model

The proposed hybrid electric ship Simulink model can be used as a platform for testing supervisory power management strategies and how they affect the ship's performance in terms of efficiency, performance response, and emissions. The focus is on the ship's powertrain. With this in mind, the vessel dynamics model need not be complex. An important factor is how much power is required to overcome drag forces and propel the vessel at a desired speed or how much power is required to perform station keeping in specified environmental conditions.

In general, the ship's propulsion power requirement is influenced by the following ship and environment attributes:

- hull resistance,
- appendage resistance,
- effect of hull roughness,
- effect of hull fouling,
- propulsion factors,
- propellers,
- wind resistance, and
- influence of sea state.

4.1 Vessel Resistance Calculations

The resistance experienced by the vessel is divided into calm water resistance and resistance due to environmental factors. Calm water resistance is comprised of all drag experienced by the vessel during Beaufort (BF) sea state zero: negligible wind, waves and current. Likewise, resistance due to environmental factors incorporates the presence of wind, waves and current at higher Beaufort numbers.

The selected ship resistance method is Holtrop and Mennen [52], and Holtrop [53]. This approach utilizes regression analysis of random model and full scale test data from the Netherlands Ship Model Basin. This method was considered the most suitable as no

model scale test data is required. As well, it is applicable to the size and speed of the proposed hybrid vessel.

4.1.1 Open Water Resistance

The components of calm water resistance are shown in Figure 15. The total ship resistance at a given speed in calm water is given by:

$$R_T = R_F(1 + k_1) + R_W + R_{app} + R_B + R_{TR} + R_A + R_{air} \quad (31)$$

where: R_F = frictional resistance [N],

$(1 + k_1)$ = hull form factor coefficient,

R_{app} = appendage resistance [N],

R_B = resistance due to the bulbous bow [N],

R_w = wave making resistance [N],

R_{TR} = resistance due immersed transom [N],

R_A = ship-model correlation resistance [N], and

R_{air} = still air resistance [N].

Each component of resistance, save the still air resistance, is discussed in this section; still air resistance is presented as part of wind resistance in the following section.

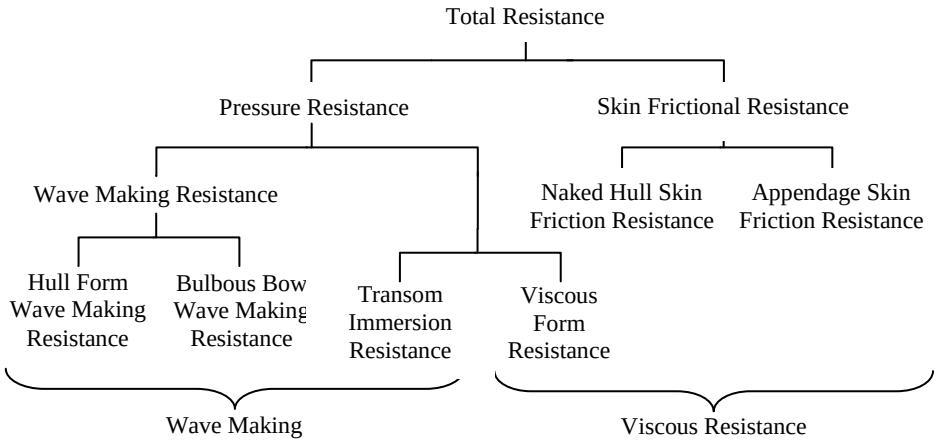

Figure 15: Ship Open Water Resistance Components

The frictional resistance is caused by the motion of the ship's hull through a viscous fluid. The frictional resistance is calculated according to the 1957 ITTC friction line (Equation 32) [54]. The formula includes the wetted surface area of the hull S [m^2], water density ρ_w [kg/m^3], the ship's velocity V [m/s] and the frictional resistance coefficient C_F.

The density of saltwater is 1025 kg/m^3. The frictional resistance coefficient formula is given by Equation 33 and is based on Reynolds number R_n.

$$R_F = 0.5\rho_w S V^2 C_F \tag{32}$$

$$C_F = \frac{0.075}{(\log_{10} R_n - 2)^2} \tag{33}$$

The hull form factor coefficient $1+k_1$ is a function of afterbody form, breadth B [m], length along the waterline L_{pp} [m], length of run L_R [m], ship displacement ∇ [m^3] and the prismatic coefficient C_P. It is calculated according to Equation 34. The length of run formula is based on the waterline length, prismatic coefficient and the longitudinal center of buoyancy *lcb* [% of L_{pp}]. C_{stern} is set to zero to correspond with a normal afterbody form.

$$(1 + k_1) = 0.93 + 0.487118 c_{14} \left(\frac{B}{L_{pp}}\right)^{1.06806} \left(\frac{T}{L_{pp}}\right)^{0.46106} \left(\frac{L_{pp}}{L_R}\right)^{0.121563} \left(\frac{L_{pp}{}^3}{\nabla}\right)^{0.36486} (1 - C_P)^{-0.604247} \tag{34}$$

$$L_R = L_{pp}\left(\frac{1 - C_P + 0.06 C_P lcb}{4C_P - 1}\right) \tag{35}$$

$$c_{14} = 1 + 0.011 C_{stern} \tag{36}$$

Wave making resistance R_w is the result of waves emanating from the bow and stern of a ship as it moves through undisturbed water. Of the generated transverse and divergent waves created by the ship, the transverse waves make up the majority of the wave making resistance. This resistance is calculated using Equations 37 through 48 for Froude numbers F_n less than 0.4 (slow speed vessels). The Froude number is a non-dimensional measurement of a body's inertia to gravitational forces. It is used to determine resistance of a partially submerged object moving through water. The greater the Froude number, the greater the resistance. The half angle of entrance i_E is the angle of the waterline at the bow to the center plane, neglecting the local shape at the stern.

$$R_W = c_1 c_2 c_5 \nabla p_w g exp[m_1 F_n^d + m_4 \cos(\lambda F_n^{-2})] \tag{37}$$

$$c_1 = 2223105 c_7^{3.78613} \left(\frac{T}{B}\right)^{1.07961} (90 - i_E)^{-1.37565} \tag{38}$$

$$c_7 = \frac{B}{L_{pp}} \quad for\ 0.11 < \left(\frac{B}{L_{pp}}\right) < 0.25 \tag{39}$$

$$c_2 = exp\left(-1.89\sqrt{c_3}\right) \tag{40}$$

$$c_3 = \frac{0.56A_{BT}^{1.5}}{BT\left(0.31\sqrt{A_{BT}} + T_F - h_B\right)} \tag{41}$$

$$c_5 = \frac{1 - 0.8A_T}{BTC_M} \tag{42}$$

$$\lambda = 1.466C_P - 0.03\frac{L_{pp}}{B} \quad for\ \frac{L_{pp}}{B} < 12 \tag{43}$$

$$d = -0.9 \tag{44}$$

$$m_1 = 0.0140407\frac{L_{pp}}{T} - 1.75254\frac{\nabla^{\frac{1}{3}}}{L_{pp}} - 4.79323\frac{B}{L_{pp}} - c_{16} \tag{45}$$

$$c_{16} = 8.07981C_P - 13.8673C_P^2 + 6.984388C_P^3 \quad for\ C_P < 0.8 \tag{46}$$

$$m_4 = c_{15}0.4exp(-0.034F_n^{-3.29}) \tag{47}$$

$$c_{15} = -1.69385 \quad for\ \frac{{L_{pp}}^3}{\nabla} < 512 \tag{48}$$

where: R_w = wave making resistance [N],

F_n = Froude number,

g = acceleration due to gravity [m/s^2],

T = average molded draught [m],

B = breadth on waterline [m],

L_{pp} = length on waterline [m],

ρ_w = saltwater density [kg/m^3],

i_E = half angle of entrance [°],

A_{BT} = transverse bulb area [m^2],

∇ = ship displacement [m^3],

A_T = immersed part of transverse area of transom [m^2],

T_F = forward draught [m],

h_B = center of bulb area above keel line [m],

C_P = prismatic coefficient, and

C_M = midship section coefficient.

Appendages are defined as any item which protrudes from the hull of the ship or causes a deviation of the natural flow of the hull lines. This includes shafts, rudders, gondolas and bow thrusters. Their added resistance can be attributed mostly to friction. Appendage resistance R_{app} is calculated in Equation 49 and accounts for the gondola and bow thruster

resistance contributions. The appendage resistance factor $(1+k_2)$ accounts for the dome and is approximated to be a value of 2.7 [52]. A value of 0.003 was selected for the coefficient C_{BTO} which corresponds to the bow thruster opening located in the cylindrical part of the bulbous bow [52]. Additional variables included are the wetted area of the appendages S_{app} [m^2], the frictional resistance coefficient C_F, and the bow thruster resistance R_{BT} [N].

$$R_{app} = 0.5\rho_w V^2 S_{app}(1+k_2)_{eq} C_F + R_{BT} \tag{49}$$

$$R_{BT} = \rho_w V^2 \pi d_{BT}^2 C_{BTO} \tag{50}$$

$$C_{BTO} = 0.003 \tag{51}$$

Bulbous bow resistance R_B is given in Equation 52. The equation includes the emergence of bow P_B [m], and the Froude number based on the immersion F_{ni}.

$$R_B = \frac{0.11exp(-3P_B^{-2})F_{ni}^3 A_{BT}^{1.5}\rho_w g}{1+F_{ni}^2} \tag{52}$$

$$P_B = \frac{0.56\sqrt{A_{BT}}}{T_F - 1.5h_B} \tag{53}$$

$$F_{ni} = \frac{V}{\sqrt{g\left(T_F - h_B - 0.25\sqrt{A_{BT}}\right) + 0.15V^2}} \tag{54}$$

The vessel has a portion of the transom which is immersed. This type of stern gives way to vorticity occurring behind the transom, which leads to a pressure loss behind the hull. The resulting resistance R_{TR} [N] is calculated using Equations 55 and 56. C_{WP} is the waterplane area coefficient.

$$R_{TR} = 0.5\rho_w V^2 A_T c_6 \tag{55}$$

$$F_{nT} = \frac{V}{\sqrt{\frac{2gA_T}{B+BC_{WP}}}} \tag{56}$$

Ship-model correlation resistance R_A [N] is calculated by Equations 57 through 60. It describes the effect of the hull roughness and the still air resistance. The equation includes the block coefficient C_B, and the correlation allowance coefficient C_A.

$$R_A = 0.5\rho_w V^2 S C_A \tag{57}$$

$$C_A = 0.006\left(L_{pp}+100\right)^{-0.16} - 0.00205 + 0.003\sqrt{\frac{L_{pp}}{7.5}}C_B^4 c_2 (0.04 - c_4) \tag{58}$$

$$c_6 = \begin{cases} 0.2(1-0.2F_{nT}) & for\ F_{nT} < 5 \\ 0 & for\ F_{nT} \geq 5 \end{cases} \tag{59}$$

$$c_4 = 0.04 \quad for \ \frac{T_F}{L_{pp}} > 0.04 \tag{60}$$

Fouling refers to the growth/collection of seaweed, barnacles, etc on the submerged part of the hull. The level of fouling will affect the frictional resistance. Fouling can be difficult to measure as the rate of growth on the underwater hull surface is not uniform, as well, the antifouling paint can suffer mechanical damage during operation. The standard accepted hull roughness is 150 microns and is automatically included in the ship-model correlation equation [52].

4.1.2 Wind Resistance

The longitudinal and lateral wind forces are calculated using Equations 61 and 62, respectively [51]. The longitudinal wind force X_w [N] is included in total ship resistance which the azimuthing propellers must overcome to achieve a desired ship speed. The lateral wind force Y_w [N] will be used when determining power required for station keeping missions. The thrust produced by the bow thruster must overcome the lateral wind force and any lateral current and wave forces for DP. A_T and A_L [m^2] are the transverse and lateral projected wind area above the water line, respectively. Other variables included in the equations are the density of air ρ_a [kg/m^3], wind resistance coefficients C_{XW}/C_{YW}, and the real wind angle α_{rw} [°]. The latter two are explained in further detail in this section.

$$X_w = 0.5\rho_a V_{rw}^2 C_{XW}(\alpha_{rw}) A_T \tag{61}$$

$$Y_w = 0.5\rho_a V_{rw}^2 C_{YW}(\alpha_{rw}) A_L \tag{62}$$

The true wind speed V_{tw} [m/s] will coincide with the selection of the sea state; wind speed and wave heights are correlated as per the Beaufort scale given in Table 16. For simplicity, it will be assumed that wind and waves originate from the same direction. Equation 63 is used to estimate the wind speed at 10m above the waterline given the Beaufort number. This wind speed is then converted to correspond to a height of 3m above the waterline (approximate centroid height of transverse projected wind area given a 2m waterline) using Equation 64.

$$V_{tw,10} = 0.863BN^{1.5} \tag{63}$$

$$V_{tw} = V_{tw,x} = V_{tw,10}\left(\frac{x}{10}\right)^{0.11} \tag{64}$$

Table 16: Beaufort Scale

#	Wind [kts]	Description	Sea State	Wave Height [ft]	Effects at Sea
0	< 1	Calm	0	0	Sea like a mirror
1	1-3	Light air			Ripple with appearance of scales; no foam crests
2	4-6	Light breeze	1	< 0.3	Small wavelets: glassy crests, no breaking
3	7-10	Gentle breeze	2	0.3-1.6	Large wavelets: crests begin to break, scattered whitecaps
4	11-16	Moderate breeze	3	1.6-4	Small waves, becoming longer; numerous whitecaps
5	17-21	Fresh breeze	4	4-8	Moderate waves, taking longer form; many whitecaps; some spray
6	22-27	Strong breeze	5	8-13	Larger waves forming; whitecaps everywhere; more spray
7	28-33	Near gale	6	13-20	Sea heaps up; white foam from breaking waves begins to be blown in streaks
8	34-40	Gale			Moderately high waves of greater length; edges of crest break into spindrift; foam is blown in well marked streaks
9	41-47	Strong gale			High waves; sea begins to roll; dens streaks of foam; spray may reduce visibility
10	48-55	Storm	7	20-30	Very high waves with overhanging crests; sea surfaces takes white appearance as foam blown in very dense steaks; rolling is heavy and visibility reduced
11	56-63	Violent storm	8	30-46	Exceptionally high waves; sea covered with white foam patches; visibility seriously affected
12	> 63	Hurricane/typhoon	9	> 46	Air filled with foam; sea completely white with driving spray; visibility greatly reduced

The relative wind velocity V_{rw} [m/s] and relative wind direction α_{rw} [°], calculated from the true wind velocity V_{tw} [m/s] and true wind direction α_{tw} [°], are given in Equations 65 and 66. For a head wind, the wind direction is equal to zero.

$$V_{rw} = \sqrt{V^2 + V_{tw}^2 + 2V \cdot V_{tw}} \tag{65}$$

$$\alpha_{rw} = arctan\left(\frac{V_{tw} sin\alpha_{tw}}{V + V_{tw} cos\alpha_{tw}}\right) \tag{66}$$

Finally, the wind resistance coefficients are calculated using [55]:

$$C_{XW} = A_0 + A_1 \frac{2A_L}{L_{OA}^2} + A_2 \frac{2A_T}{B^2} + A_3 \frac{L_{OA}}{B} + A_4 \frac{S}{L_{OA}} + A_5 \frac{C}{L_{OA}} + A_6 M \tag{67}$$

$$C_{YW} = B_0 + B_1 \frac{2A_L}{L_{OA}^2} + B_2 \frac{2A_T}{B^2} + B_3 \frac{L_{OA}}{B} + B_4 \frac{S}{L_{OA}} + B_5 \frac{C}{L_{OA}} + B_6 \frac{A_{SS}}{A_L} \tag{68}$$

in which: L_{OA} = overall length [m],

B = beam on waterline [m]

C = distance from bow of centroid of lateral projected area [m],

S = length of perimeter of lateral projection excluding water line and slender bodies (masts, ventilators) [m],

A_L = lateral projected wind area [m^2],

A_T = transverse projected wind area [m^2],

A_{SS} = lateral projected area of superstructure [m^2], and

M = number of distinct groups of masts or kingposts seen in lateral projection.

The coefficients A_x and B_x can be found in Table 23 and Table 24, respectively [55]. The value for M was set to zero as there are no masts/kingposts on the vessel. The A-frame on the stern was not included as part of the perimeter of lateral projection S nor did it contribute to the M value; it was disregarded. It should be noted that the S value will change when the fuel cell unit and other equipment is included on a voyage, however, only the ship itself is considered in calculating wind resistance for the given model. The transverse and lateral resistance coefficients have been calculated for a given wind direction of zero through 180° and are given in Table 18.

Table 17: Wind Resistance Variables

L_{OA}	B	C	S
38.5 m	7.0 m	13.7 m	49.3 m
A_L	A_T	A_{SS}	M
105.1 m^2	28.5 m^2	22.8 m^2	0

Table 18: Wind Resistance Coefficients

α_{rw} [°]	C_{XW}	C_{YW}
0	0.822	-
10	0.744	0.127
20	0.713	0.277
30	0.717	0.445
40	0.724	0.615
50	0.511	0.837
60	0.293	0.877
70	0.116	0.841
80	0.041	0.826
90	0.039	0.816
100	0.156	0.785
110	0.088	0.779
120	-0.034	0.779
130	-0.272	0.729
140	-0.458	0.605
150	-0.533	0.432
160	-0.887	0.254
170	-1.011	0.113
180	-0.943	-

4.1.3 Current and Wave Resistance

4.1.3.1 Surge Resistance

A seakeeping standard series for cruiser-stern ships is used to calculate wave and current resistance during non-station keeping operations [56]. The seakeeping tables are applicable for calculating added resistance in head seas only. (There exists a report which presents seakeeping standard series tables for calculation of added resistance in head to following seas [57]. However, the author was unable to obtain a copy of this report.)

The seakeeping tables are selected based on 5 parameters. This includes three ship principle values: B/T, L_{pp}/B, and the block coefficient C_B. The two additional parameters are the Froude number and non dimensional sea state. The validity range for each

parameter used to select the correct seakeeping table is listed in Table 19. Non dimensional sea state is given by Equation 69. The significant wave height $\bar{H}^{1/3}$ [m] is the average of the 1/3 highest wave heights. It is related to the wind speed at 19.5m as given in Equation 70.

Table 19: Seakeeping Table Parameter Validity Ranges

$2.0 \leq B/T \leq 4.0$
$5.5 \leq L_{pp}/B \leq 8.5$
$0.55 \leq C_B \leq 0.9$
$0.1 \leq F_n \leq 0.3$
$0.015 \leq S \leq 0.1$

$$SS = \frac{\bar{H}^{1/3}}{L_{pp}} \tag{69}$$

$$\bar{H}^{1/3} = \frac{0.5968 V_w^2}{32.174} \tag{70}$$

4.1.3.2 Station Keeping Resistance

The current resistance is calculated using the Standard Spanish ROM 0.2-90 method [58]. The lateral/transverse current resistance $F_{T,current}$ [kN], given by Equation 71, is comprised of components F_{TC} and F_{TC}' which result due to pressure and drag, respectively. The current resistance is also dependent on the velocity of the current V_c [m/s] and ship parameters, including the ship length between perpendiculars L_{pp} [m], draught T [m] and beam B [m]. The wave angle α_w [°] is measured between the longitudinal axis of the ship, considered from the bow to the stern, and the direction of the wave. The specific gravity of seawater γ_w is 1.034 t/m^3. The C_{TC} factor is set as 1.0 for deep water, and the friction drag factor C_R is 0.004 for a ship in service.

$$F_{T,current} = F_{TC} + F'_{TC} \tag{71}$$

$$F_{TC} = 10 C_{TC} \gamma_w A_{LC} \sin \alpha_w \frac{V_C^2}{2g} \tag{72}$$

$$F'_{TC} = 10 C_R \gamma_w A'_{TC} (\sin \alpha_w)^2 \frac{V_C^2}{2g} \tag{73}$$

$$A'_{TC} = (L_{pp} + 2T)B \tag{74}$$

$$A_{LC} = L_{pp} T \tag{75}$$

The longitudinal current force on a ship is given by Equation 76. The components due to pressure and drag are given by Equations 77 and 78, respectively. The C_{LC} factor is 0.6 for conventional bows (bulb).

$$F_{L,current} = F_{LC} + F'_{LC} \tag{76}$$

$$F_{LC} = 10 C_{LC} \gamma_w A_{TC} \frac{V_C^2}{2g} \tag{77}$$

$$F'_{LC} = 10 C_R \gamma_w A'_{LC} (cos\, \alpha_w)^2 \frac{V_C^2}{2g} \tag{78}$$

$$A'_{LC} = (B + 2D) L_{pp} \tag{79}$$

$$A_{TC} = B \cdot D \tag{80}$$

The wave resistance is also calculated using the Standard Spanish ROM 0.2-90 method. The lateral/transverse wave resistance $F_{T,wave}$ [kN] is given by Equation 81, while the longitudinal wave resistance $F_{L,wave}$ [kN] is given by Equation 82. The depth coefficient C_{dw} is set to 1.0 for deep water. To determine C_{fw}, if $(2\pi/L_w)\cdot D$ is greater than 1.4, C_{fw} = 0.064, and if it is less than 0.2, C_{fw} is set to 0.

$$F_{T,wave} = 10 C_{fw} C_{dw} \gamma_w \left(\bar{H}^{1/3}\right)^2 D' (\sin \alpha_w)^2 \tag{81}$$

$$F_{L,wave} = 10 C_{fw} C_{dw} \gamma_w \left(\bar{H}^{1/3}\right)^2 D' \cos \alpha_w \tag{82}$$

$$D' = L_{pp} \sin \alpha_w + B \cos \alpha_w \tag{83}$$

4.2 Simulink Vessel Resistance Model

Open water surge resistance represents the forward resistance experienced by the ship in calm water. The environmental disturbances subsystem includes wind, wave and current resistance models. The surge resistance factors combined with propeller generated thrust are used to determine the ship surge speed. This is the same method as used by [28]. As well, the combination of lateral resistance and bow thruster thrust verifies if the vessel is holding station. It should be noted that if station keeping is not of interest during simulation, the lateral resistance is ignored.

The bare displacement of the vessel is 338.35 m^2. The vessel resistance mask is shown in Figure 16, and the underlying Simulink model is shown in Figure 17.

Figure 16: Vessel Resistance Mask

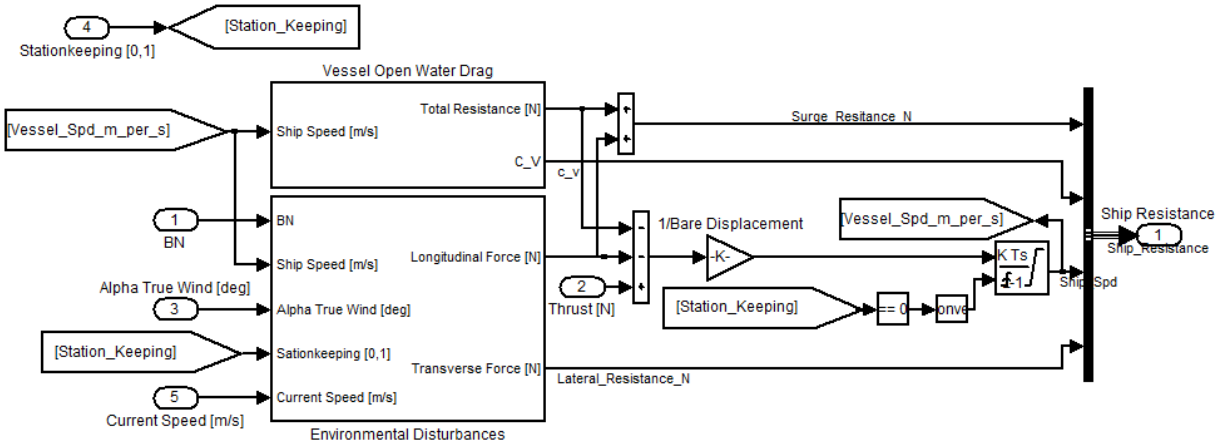

Figure 17: Vessel Resistance Subsystem

4.2.1 Vessel Resistance Model

Vessel static parameters are considered to be any constants related to or calculated values based on ship dimensions. Basic principal particulars can be acquired from the ship lines plan. To get a reasonable estimation of all static parameters, FreeShip (FS) was utilized. The vessel lines plan was imported as a background image into the FS model, scaled to actual size, and traced. The resulting lines plan generated in FS is shown in Figure 18. The superstructure information is included in the vessel resistance calculations but not in the lines plan.

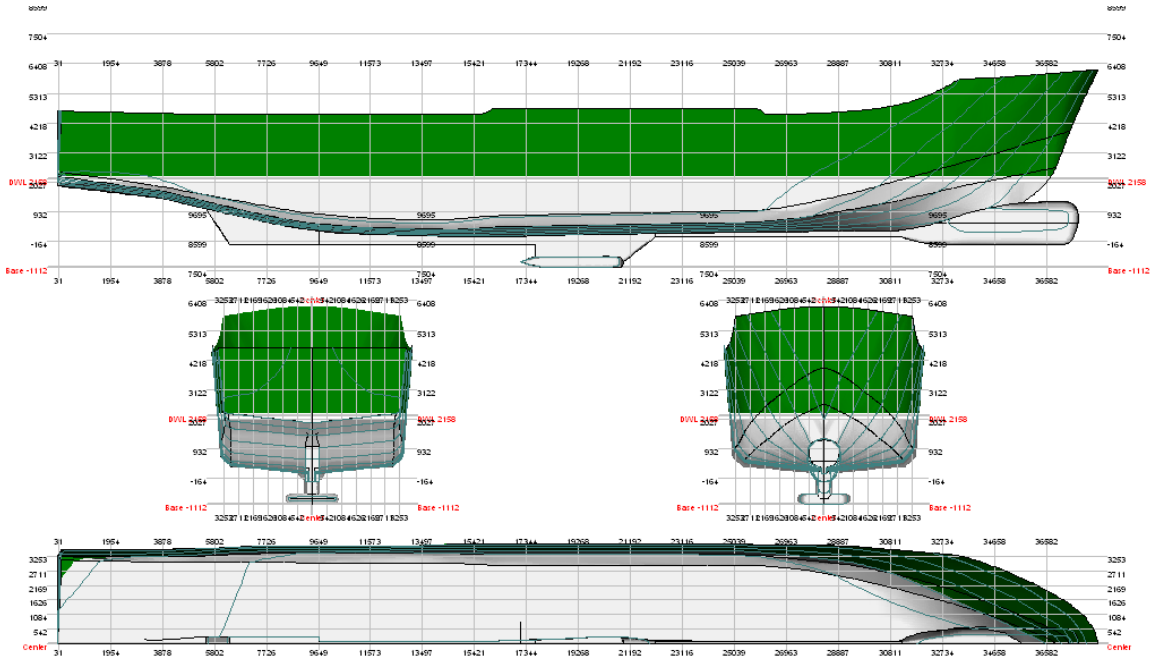

Figure 18: FS Lines Plan

The input and calculated variables extracted from the FS model are listed in Table 20. These constants are used in calculating total open water ship surge resistance in the Simulink model (Figure 19), utilizing the equations described in Section 4.1.1.

Table 20: FS Variables

General	Water density ρ_w [t/m^3]	1.025
	Water viscosity γ_w [m^2/s]	1.189e-6
Hull	Length on waterline L_{pp} [m]	36.677
	Beam on waterline B [m]	6.974
	Draught on midship T [m]	2.158
	Draught on F.P. T_F [m]	2.158
	Draught on A.P. T_A [m]	2.158
	Wetted surface area S [m^2]	351.85
	Waterplane area [m^2]	223.50
	Displacement ∇ [m^3]	338.350
	Longitudinal center of buoyancy *lcb* [%]	-0.019
Calculated Variables	Prismatic coefficient C_P	0.6580
	Block coefficient C_B	0.6130
	Midship coefficient C_M	0.9317

	Waterplane coefficient C_{WP}	0.8738
	C_{bt}	0.1086
	A_m [m^2]	14.02
	L_{pp}/B_{wl}	5.259
	B_{wl}/T	3.232
	L_{pp}/T	16.997
	Half angle of entrance i_E [˚]	27.0

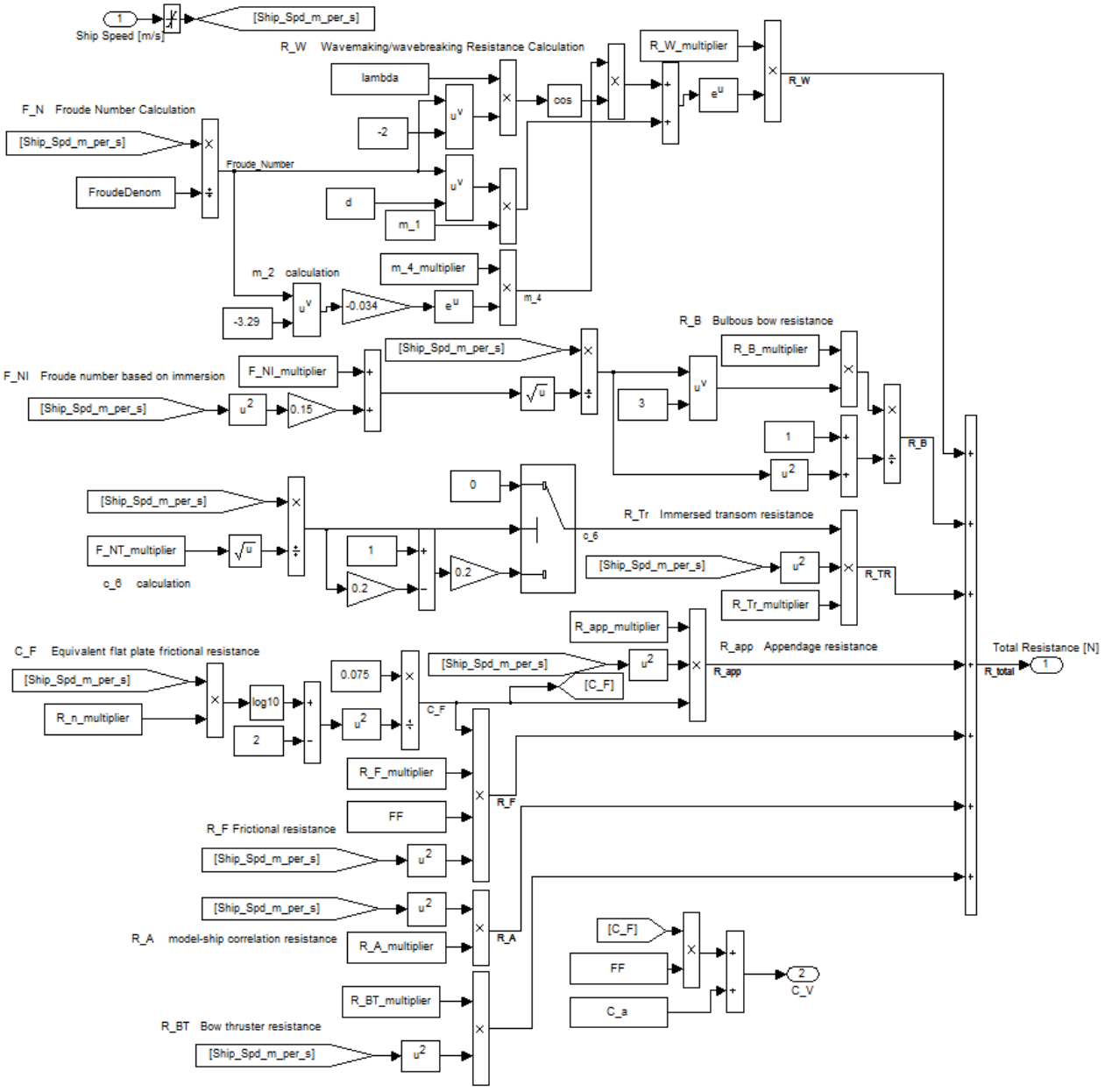

Figure 19: Vessel Open Water Drag Subsystem

The FS program is also capable of calculating ship resistance based on Holtrop 1988(84). The principal components of total ship resistance, as given in Equation 31, were calculated using the Simulink model as well as through FS in order to corroborate the Simulink model. The total open water resistance versus ship speed from industry, FS and the Simulink model is compared in Figure 20. Reports generated using FS are given in Appendix C.

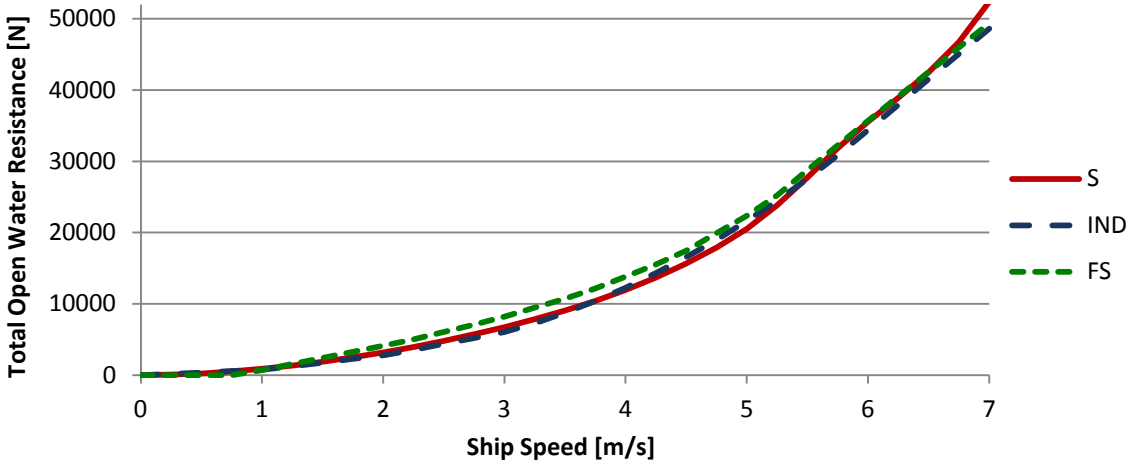

Figure 20: Total Ship Resistance

4.2.2 Wind, Waves and Current Models

The environmental disturbances subsystem is shown in Figure 21. The wind resistance model, presented in Figure 22, is based on the description given in Section 4.1.2. The model takes in the user selected Beaufort number, the user defined true wind angle, and the present speed of the ship. The true wind velocity at 10m is derived from the Beaufort number according to Equation 63. The mean wind velocity and angle of attack are fed into a MSS Wind block which outputs varying wind speed and angle within limits of the user defined sea state. The wind speed output is transformed to reflect the speed at a height of 3m above the waterline, following which the true wind values are converted to real wind speed and angle, taking into account the ship's velocity, using Equations 65 and 66. Using these values, the transverse and lateral forces experienced by the vessel due to wind are evaluated based on Equations 61 and 62, respectively. The coefficients C_{XW} and C_{YW} were calculated offline and included as lookup tables.

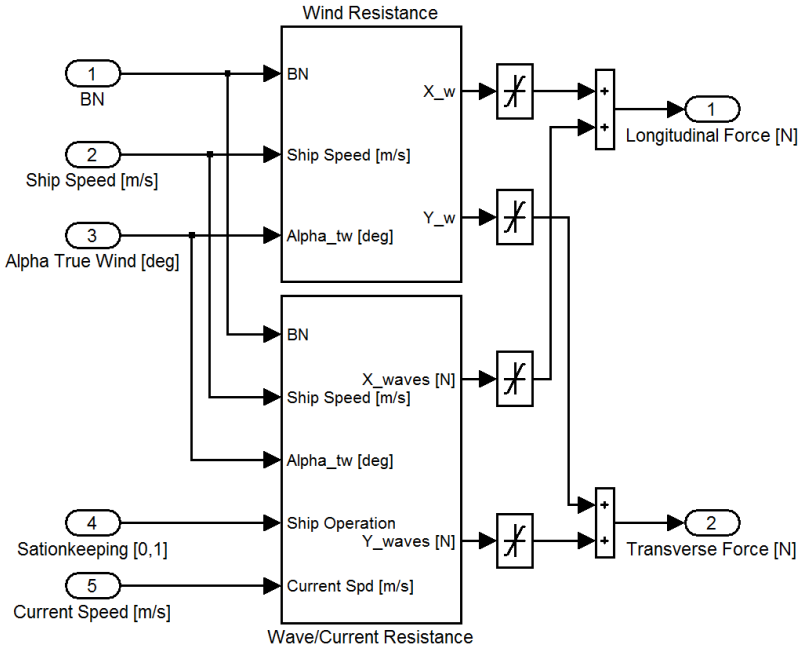

Figure 21: Environmental Disturbances Subsystem

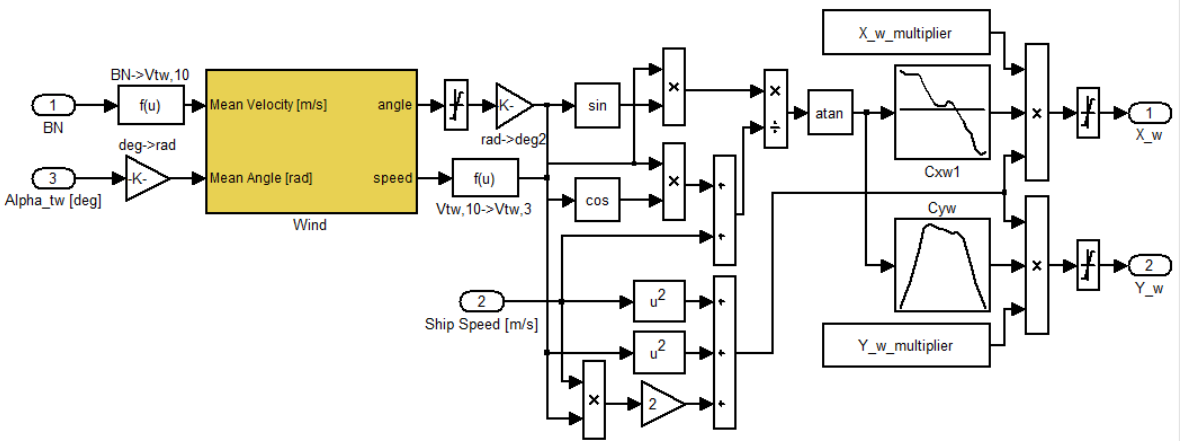

Figure 22: Wind Resistance Subsystem

The wave and current resistance subsystem is shown in Figure 23. The ship principal particulars used in selecting the seakeeping tables for determining wave and current added resistance in head seas are listed in Table 21. The Froude number ranges from 0.1 to 0.3, and the non dimensional sea state ranges from 0.015 to 0.1. The resulting added resistance based on true wind speed and ship speed is shown in Figure 24.

Table 21: Seakeeping Table Values - Ship Principal Particulars

Principal Particular	Lower Range Value	Actual Value	Upper Range Value
B/T	3	3.232	4
L_{pp}/B	5.5	5.259	7
C_B	0.6	0.613	0.65

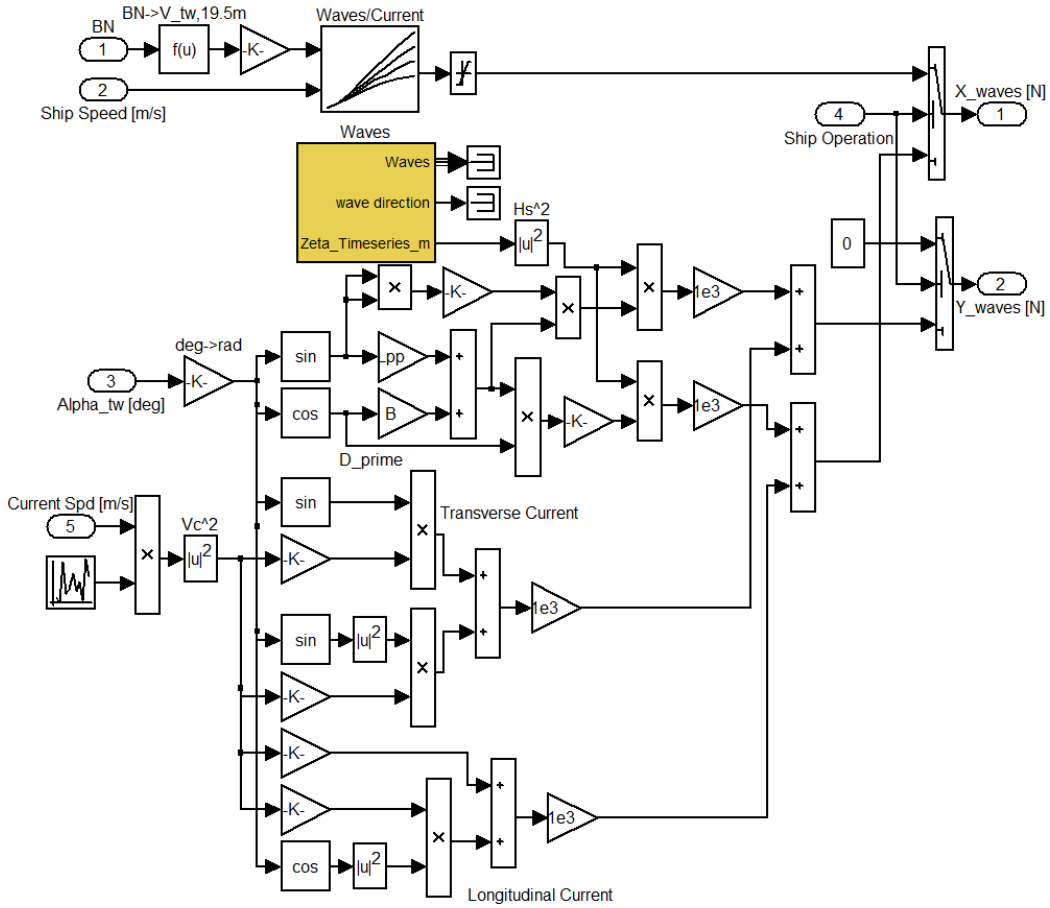

Figure 23: Wave/Current Resistance Subsystem

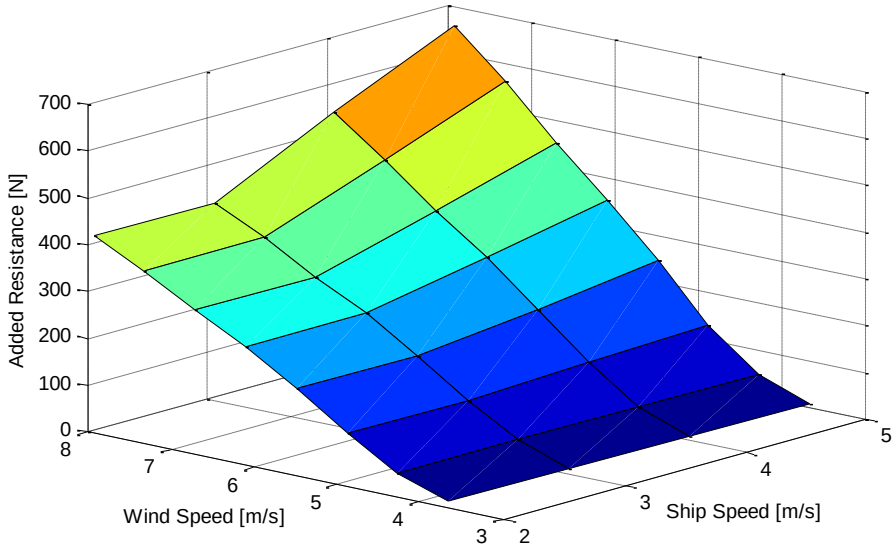

Figure 24: Wave and Current Added Resistance in Head Seas

Lastly, the wave and current resistance during station keeping operations, as described by section 4.1.3.2, was implemented with the addition of MSS environment blocks. The significant wave height is calculated using Equation 70, and the wave angle of attack is taken to be the same as the wind encounter angle. These are inputs to the MSS Waves block. The block can be parameterized to characterize long or short crested waves, various wave spectrums, etc. The MSS Wave Velocitycalc block accepts the wave spectrum and calculates the current wave height which is used to determine the transverse and longitudinal resistance according to Equations 81 and 82, respectively.

Chapter 5 Power and Energy Management System

The purpose of the power management system is to dispatch the required generation while delivering acceptable fuel economy, minimal emissions, satisfactory performance, and ensuring safety of operations. In the end, the goal of the hybrid vessel is to deliver range and performance comparable to that of a conventional vessel.

When considering power management, it is important to note that the load power demand (consumer operation) is not affected by the power generating system. Conversely, power demand impacts generation and must be managed only if it exceeds the system available power limit, creating the potential for system blackout. To prevent a blackout, load demand can be decreased by the power management system using predefined load priorities. This situation is important to ensure reliable, continuous vessel operation. However, load shedding is not addressed in this thesis. All mission simulations are created such that installed system power generation is sufficient.

For the proposed hybrid electric vessel, a rule-based supervisory control strategy was constructed. Rule based strategies are effective for real-time implementation and do not require *a priori* knowledge of a predefined driving/power demand cycle. The main vessel operational modes are conventional or high speed cruising, and low speed cruising/station keeping. During high speed cruising, the vessel will utilize the on-board generators coupled with the ESS. This is equivalent to an HEV architecture. During station keeping missions, the power will be supplied by a single source or combination of ESS, FC or generators. The possible power source combinations are equivalent to automotive vehicle types: EV, FCEV, and HEV. The supervisory power control strategy is formed from an amalgamation of the three individual vehicle type control strategies.

5.1 Operational Modes

The three operational modes include EV, FCEV and HEV. During EV mode, the load will be supplied exclusively by the ESS. While operating as a FCEV, the powertrain will be fuel cell dominant with the ESS acting as a power assist. Lastly, two HEV modes were developed. The first HEV mode is modeled after a mild hybrid in which the ESS acts as a

power assist to the engine, similar to the Honda Insight or Honda Civic. The second HEV mode developed allows for a more significant ESS power contribution.

The supervisory control strategy for the vessel is illustrated in Figure 25. At this level, mode selection is based on meeting system power demand given the mode power capability and mode fuel reserves (energy or hydrogen).

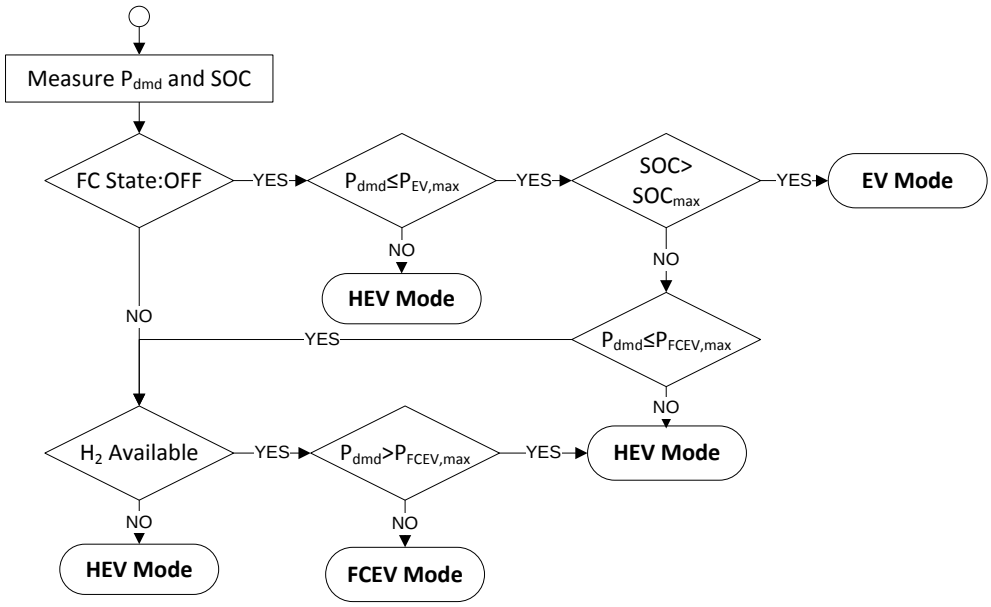

Figure 25: Supervisory Mode Control

5.2 ESS Partition

To accommodate the three operational modes in a single platform, the ESS is partitioned into operational capacity windows for each of the modes. Generally, for lithium-ion batteries, a useful SOC range to maintain reversibility is between 20% to 90% [59]. Normal SOC usage for an HEV or a PHEV is illustrated in Figure 26 [60]. For an HEV, a baseline SOC level is selected and the ESS operational range is contained within a 10% SOC window around this baseline [61]. The HEV operational range is easily translated to a PHEV - the operational SOC band is shifted to the lower spectrum of the battery capacity. With PHEVs, the installed ESS is suitable for deep discharge cycles. For this reason, the higher SOC range is reserved for EV or blended mode of operation. For the proposed vessel, the ESS partition for each of the modes is similar to the PHEV SOC utilization scheme shown in Figure 26.

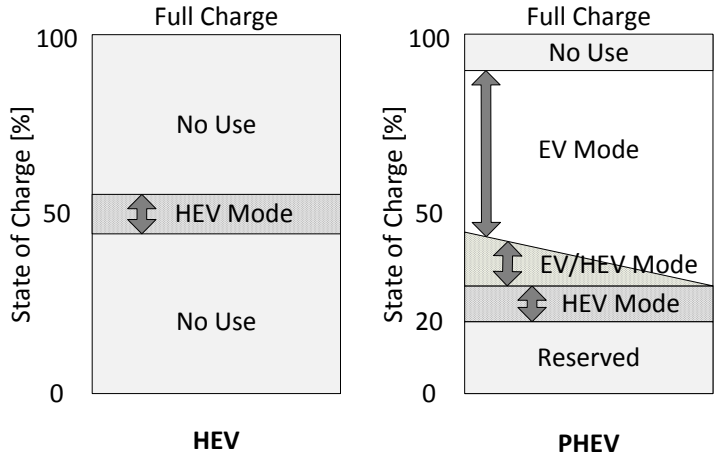

Figure 26: Schematic of SOC Utilization for HEV and PHEV

For the U24-12XP battery modules, Valance manufacturers state a drop in deep cycle life from 10000 to 4500 cycles given a 4 hour load to a depth of discharge (DOD) of 50% and 80%, respectively [62]. For a 100% DOD under the same conditions, the deep cycle life drops to 2600 cycles. Given this information, the ESS SOC useable window is defined to be between 20-95%. Of this window, the lowest 10% range will be dedicated to CS operation.

The SOC utilization scheme is shown in Figure 27. An example of a typical discharge profile, given an initial 90% SOC, is shown in Figure 28 [60]. For the given application, a CD or blended strategy is utilized when the ESS has a higher SOC. This includes ESS only or HEV modes. When the ESS SOC reaches a predefined low threshold of 30%, the supervisory controller switches to a CS strategy and utilizes FCEV or HEV modes of operation.

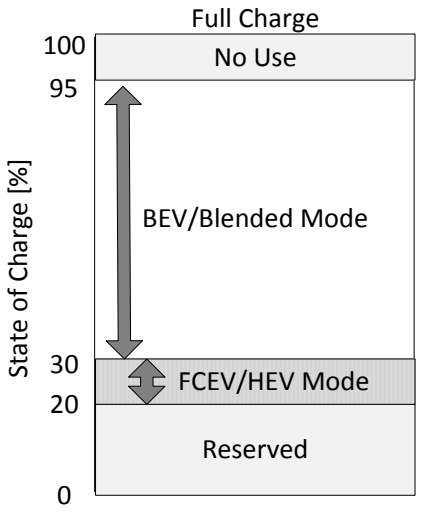

Figure 27: ESS SOC Utilization

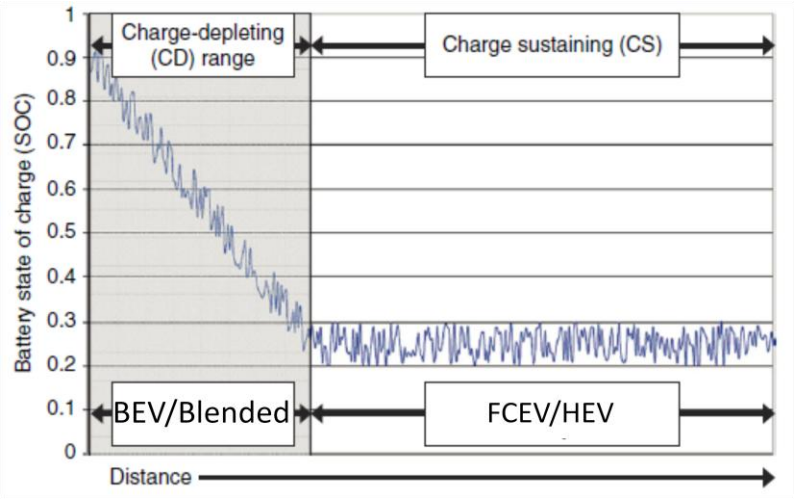

Figure 28: Typical PHEV Discharge Cycle

5.3 HEV Modes

In HEV mode, the bulk of the load is provided for by the generators with the ESS acting as a power assist. The first designed HEV mode emulates a mild HEV where the ESS assistance is minimal. This mode is referred to as conventional HEV mode and uses a CS strategy. The second HEV mode is the 30% ESS assist mode. With this strategy, the ESS provides for up to 30% of a single generator rated power or 64.5 kW. This mode utilizes a CD strategy. Generator usage for both HEV modes is governed through the use of generator start/stop tables, which is an accepted industry practice.

5.3.1 Generator Stop/Start Tables

Different generation reserves for a vessel power system are outlined in Figure 29. Spinning reserve is additional generating capacity that is available from online generators which have not reached 100% rated power output. Supplemental reserve is extra generating capacity which is not currently supplying the load, but can be brought online within a short period. This includes generators which are warmed up and/or operating under no load, but have not been connected to the system. In the case of the proposed hybrid ship, the ESS acts as a supplemental reserve. Minimum power system reserves must be maintained in order to ensure safety of operations (class rule). Power reserves can be managed though predefined generator stop/start tables.

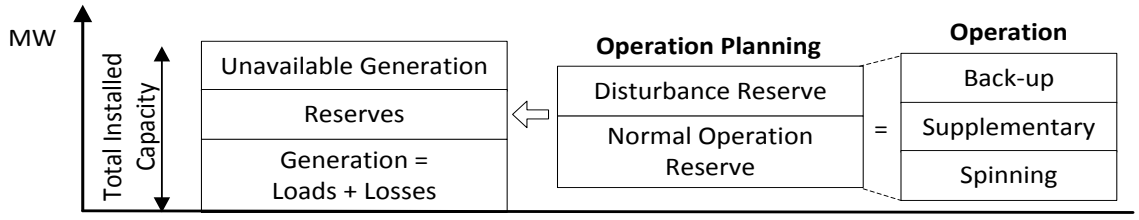

Figure 29: Different Generation Reserves in a Ship Power System

Typically, the highest operational cost for marine vessels is the fuel cost, which should always be minimized. The generator stop/start tables are created with a focus on efficient operation. Generator load $P_{gi}(k)$ for start/stop of unit i is defined by Equation 84. $P_{stop,gi}(k)$ is the power when the next unit $k\text{-}1$ stops for the situation with k units online. Likewise, $P_{start,gi}(k)$ is the power when the next unit $k+1$ starts. The generator power rating is given by $P_{r,gi}$. The minimum and maximum load on the engine, given by the constants a_{min} and a_{max}, is set to 0.3 and 1.1 respectively [36].

$$a_{min,g}P_{r,gi} \le P_{stop,gi}(k) \le P_{gi}(k) \le P_{start,gi}(k) \le min\left(P_{cont,gi}^{max}(k, N_f), P_{r,gi}\right) \quad (84)$$

The cost function $J_{FC,}$ given in Equation 85, is used to find the most advantageous load demand to bring the next generator online. Essentially, $P_{start,g}(k)=P_g(k\rightarrow k+1)$ for minimum J_{FC}. The ratio of rated power $w_{r,gi}(k)$ is equal to the generator power rating divided by the sum of all generating power capacity. As all the generating units are equally sized and rated, $w_{r,gi}(k=1)=1$ and $w_{r.gi}(k=2)=0.5$.

$$\min_{P_{start,g}(k)} J_{FC} = \min_{P_{start,g}(k)} \left(\sum_{i=1}^{k+1} FC_{gi}\left(P_{gi}(k+1)\right) w_{r,gi}(k) - \sum_{i=1}^{k} FC_{gi}\left(P_{gi}(k)\right) w_{r,gi}(k) \right) \quad (85)$$

for $k \in [1, N_g]$, $J_{FC} \geq 0$

where

$$P_{gi}(k) = \frac{P_L(k)}{k} \quad (86)$$

$$P_{gi}(k+1) = \frac{P_L(k)}{k+1} \quad (87)$$

The generator fuel consumption $FC_{gi}(P_{gi})$ and the BSFC $b_{e,gi}(P_{gi})$ is given by Equation 88 and Equation 89, respectively. The BSFC equation is derived from the generator operating data [7].

$$FC_{gi}(P_{gi}) = b_{e,gi}(P_{gi}) P_{gi} \quad (88)$$

$$b_{e,gi}(P_{gi}) = 384.28 - 459.58 \frac{P_{gi}}{P_{r,gi}} + 320.34 \left(\frac{P_{gi}}{P_{r,gi}} \right)^2 \quad (89)$$

for $i \in [1, N_g]$

The graph of J_{FC} is given in Figure 30. As the function is concave, two minima exist for each unit start commitment, $k \rightarrow k+1$. As operation at lower generator load $P_{gi}(k)$ has less efficient fuel utilization than operation in the upper engine range, $P_{start,gi}(k)$ is limited to the upper operating range: $P_{start,gi}(k) \geq 0.5 P_{r,gi}$.

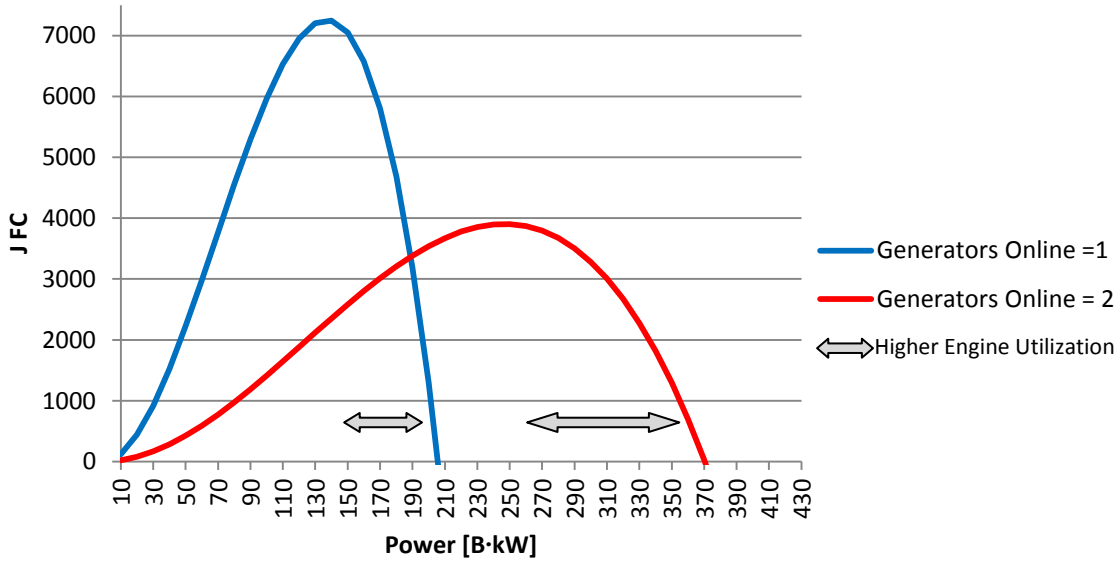

Figure 30: Instantaneous Fuel Consumption Cost Function

The fuel consumption cost function is also subject to the blackout constraint (Equation 90), which is a class requirement. The blackout constraint is based on the scenario of one or more generators failing, and the response of the fast load reduction strategy.

$$P_{gi}(k) \leq P_{start,gi}(k) \leq min\left(P_{cont,gi}^{max}(k, N_f), P_{r,gi}\right) \quad (90)$$

For equal rated units, the continuous loading limit or blackout limit of the generator is given in Equation 91. The maximum transient overload step of each of the equally rated generators is given in Equation 92, with the inertial time constant H [s] given in Equation 93. Generator continuous loading limit parameter values are listed in Table 22. The safe load time t_{SL} must be greater than or equal to the fast load reduction time t_{FLR}. The ESS is capable of providing a continuous load up to 323 kW for a period proportional to the HEV ESS window. The proposed vessel hybrid power system specifications state that the generators are can be loaded to a continuous maximum of 90% of their rated capacity [46]. Given this loading, the safe load time is calculated to be 0.125s.

$$P_{max}^{cont}(k, N_f) = P_{max}^{trans}\frac{k - N_f}{k} \quad (91)$$

$$P_{max}^{trans} = 100\% + \frac{\Delta w \cdot 2H}{t_{SL}} \quad (92)$$

$$H = 0.5\frac{J_g w_{0g}^2}{S} \quad (93)$$

Table 22: Generator Continuous Loading Limit Parameters

$w_{0g} = 2\pi f_0$	376.8
J	1.89 kg·m^2
S	269 kVA
Δw	10%
t_{SL}	0.125s

For conventional vessels, using Equations 91 through 93, the maximum continuous load for two generators online with the possibility of one unit failing is 90% each. Likewise, a third generator must be started if the load reaches 180%.

The second HEV mode, the 30% ESS assist mode, allows for the ESS to provide up to 30% of a single generator rated power. The ESS provides this power once the online generators have reached their maximum allowable contribution. In this mode, the generators are still limited to providing a maximum of 90% of their rated generator power. However, the starting of the second and subsequent generators is delayed until the

total load demand 120% and 210% of rated generator capacity, respectively [46]. This strategy takes advantage of the ESS while maintaining operational reserves. The conventional and 30% ESS assistance generator start table options are selectable for a given simulation.

The load dependent stop table, $P_{stop,gi}(k+1)$, is the same for both HEV strategies, and is set at 80% of generator rated power [46]. The BSFC hysteresis when starting/stopping a single generator and multiple generators is given in Figure 31 and Figure 32, respectively.

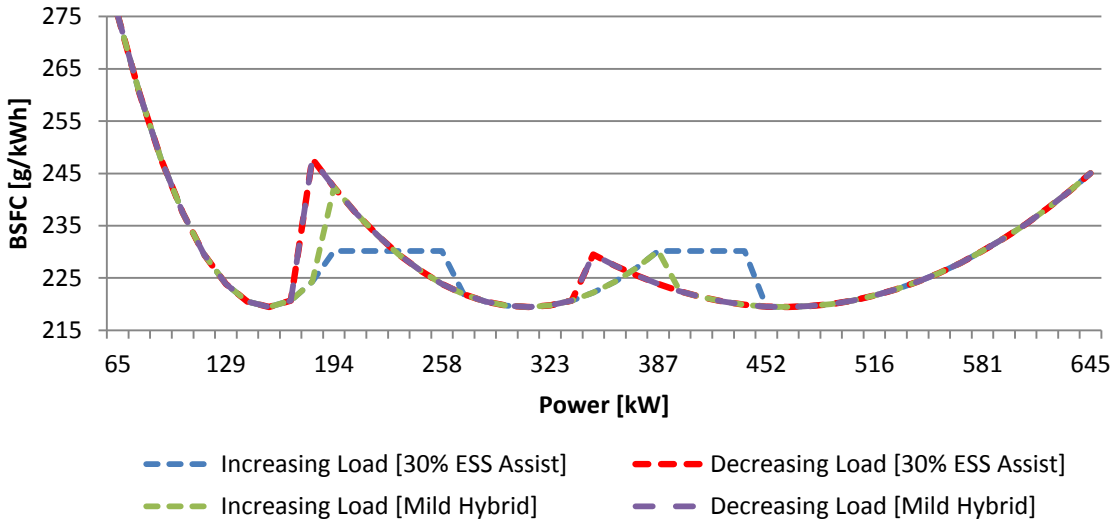

Figure 31: BSFC Hysteresis when Starting/Stopping a Single Generator

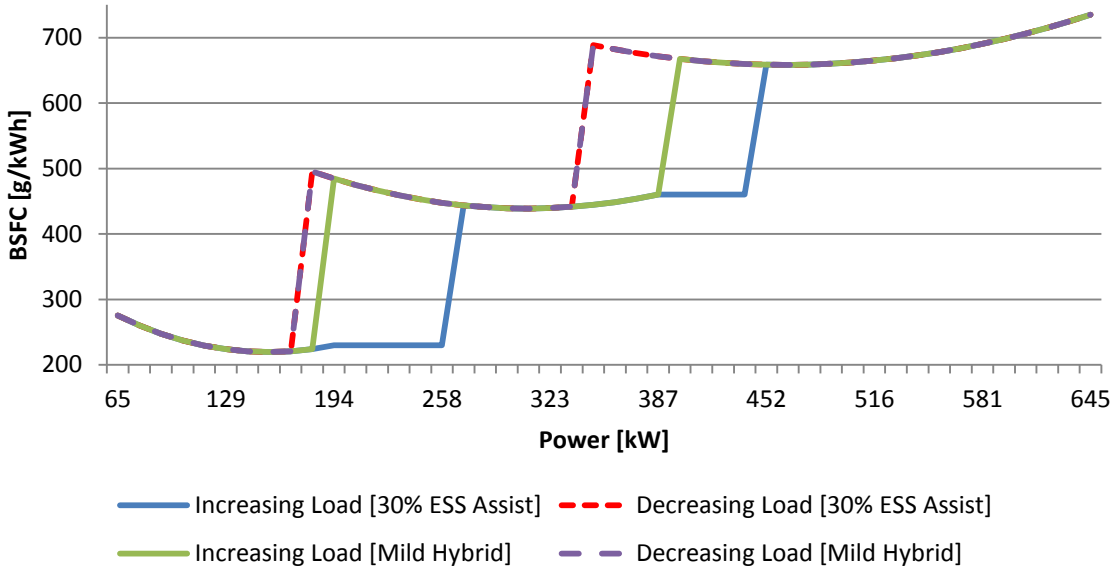

Figure 32: Total BSFC Hysteresis when Starting/Stopping Multiple Generators

In the model, the generators are assumed to be warmed up and on standby – they can be quickly brought online. A minimum generator online time of 30s was specified in the supervisory control strategy. This minimum on time is applied to HEV mode only, not to individual generators. As an example, if one generator is online, a second generator can be brought online and disconnected from the bus with no regulated minimum online time. However, the first generator must remain online for the full 30s. The starting/stopping of additional generators is regulated through use of an assertion signal which is based on power demand; a maximum/minimum power demand must be requested for a specified period before it prompts a generator start/stop. Similarly, assertion signals are used to determine when to enter HEV mode (based on current and bus voltage). This assertion period is included to prevent excessive on/off HEV mode toggles. For the 30% ESS assist HEV mode of operation, if the ESS SOC enters the CS window, the supervisory controller switches to the conventional HEV strategy.

5.4 FCEV Mode

The power balance of the system in FCEV mode can be expressed according to Equation 94. The minimum and maximum FC power is 20 kW and 150 kW, respectively. For the ESS, the minimum load is zero, and the maximum load is 177 kVA.

$$P_{FC} + P_{ESS} = P_{dmd} + P_{loss} \tag{94}$$

subject to

$$P_{FC,min} \leq P_{FC} \leq P_{FC,max} \tag{95}$$

$$P_{ESS,min} \leq P_{ESS} \leq P_{ESS,max} \tag{96}$$

A load follower scheme is used to determine the output power of the FC (Figure 33). The strategy is modified from the one given in [63]. The SOC dependent correction factor, *f(SOC)*, is given in Equation 97. A minimum 30s FC online time is included in the supervisory control strategy.

$$f(SOC) = \frac{0.5(SOC_{min} + SOC_{max}) - SOC}{0.5(SOC_{max} - SOC_{min})} \tag{97}$$

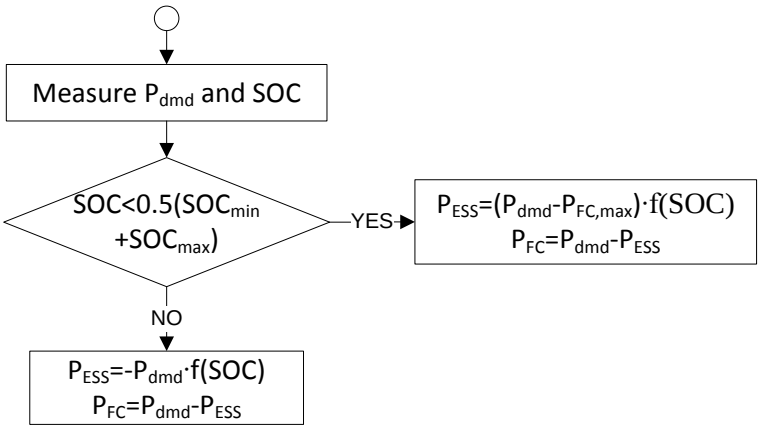

Figure 33: FCEV Load Follower Control Strategy

Chapter 6 Simulation Results and Discussion

The proposed hybrid electric ship was designed with two intended operating modes: a) generator mode or high speed cruising, and b) hybrid mode, or low speed cruising/station keeping. During high speed cruising, the generators and ESS are in operation and the surge resistance is relatively steady. During station keeping operations, the load experienced by the vessel can be more demanding on the power system as the thruster rpm is continuously adjusting to overcome the environmental resistance. Depending on the BF number, current speed and true wind angle specified, the ship may or may not be able to hold station. As well, during station keeping, ROPOS is assumed to be in operation. Vessel and power system response to various mission cycles are presented in this section.

6.1 Vessel Surge Performance

The resultant vessel surge speed versus rpm input for open water BF1 is shown in Figure 34. The surge speed is attained with both azimuthing thrusters in use (same rpm input to both thrusters).

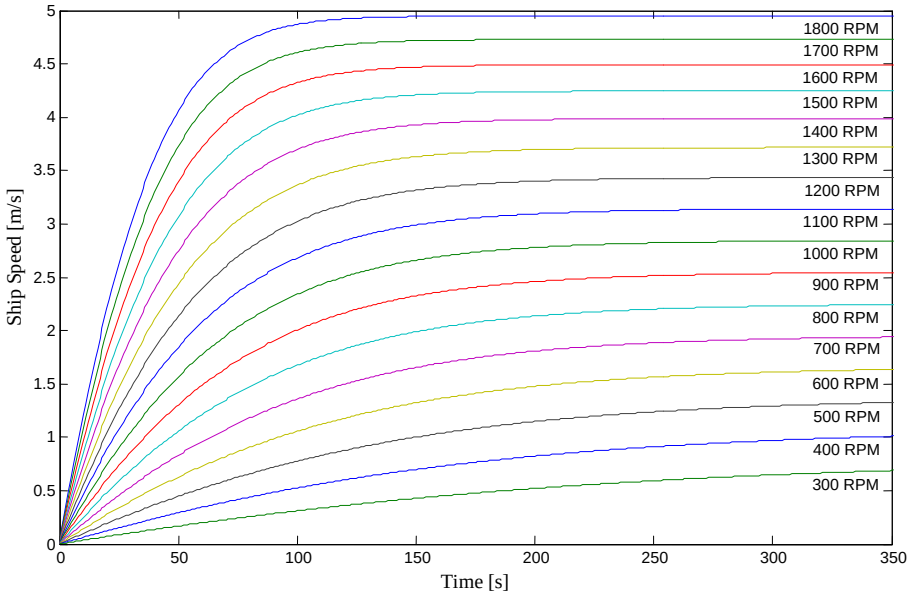

Figure 34: Ship Speed based on rpm Setpoint

6.2 Model Issues & Modifications

6.2.1 Generator Synchronization

During initial simulations, the main AC bus voltage failed at arbitrary times during the simulation, as shown in Figure 35. In the figure, high mode level is equivalent to HEV mode, and zero is ESS only mode. The failure occurs during the transition from ESS only mode to HEV mode. Once the breakdown in bus voltage occurred, it continued to reoccur during each HEV mode entry. The cause of the bus failure was traced back to the generator subsystems. When a generator is not in use, a three phase voltage source is connected at the generator output terminals. Two sets of contactors are used to toggle between a three phase voltage source and the main AC bus. As shown in Figure 35, connecting the generator to the bus the first three times resulted in no bus disturbance. On the fourth connection, the bus voltage fails. At the start of the simulation, the three phase voltage source is in phase with the bus voltage. During simulation runtime, the bus voltage phase starts to drift from the fixed voltage source phase. When the difference in phase becomes overly large, the generators do not correctly synchronize when connecting to the bus; there is frequency synchronization but no phase synchronization. This situation was corrected by replacing the fixed voltage source with a controlled voltage source which is in phase with the bus.

Other methods of ensuring synchronization when connecting the generators to the bus were explored, including a straight connection with the bus (no contactors) with a zero power demand to the generators. However, due to the automatic voltage regulator (AVR), a zero power demand does not ensure the generators do not provide power to the bus. This behavior was not desired; in ESS or FCEV mode, voltage regulation is to be maintained by the ESS converter. The AVR does not include any phase synchronization control. The AVR could be modified to include this control in future model iterations. For the current model, a phase controlled voltage source is employed as a simple fix.

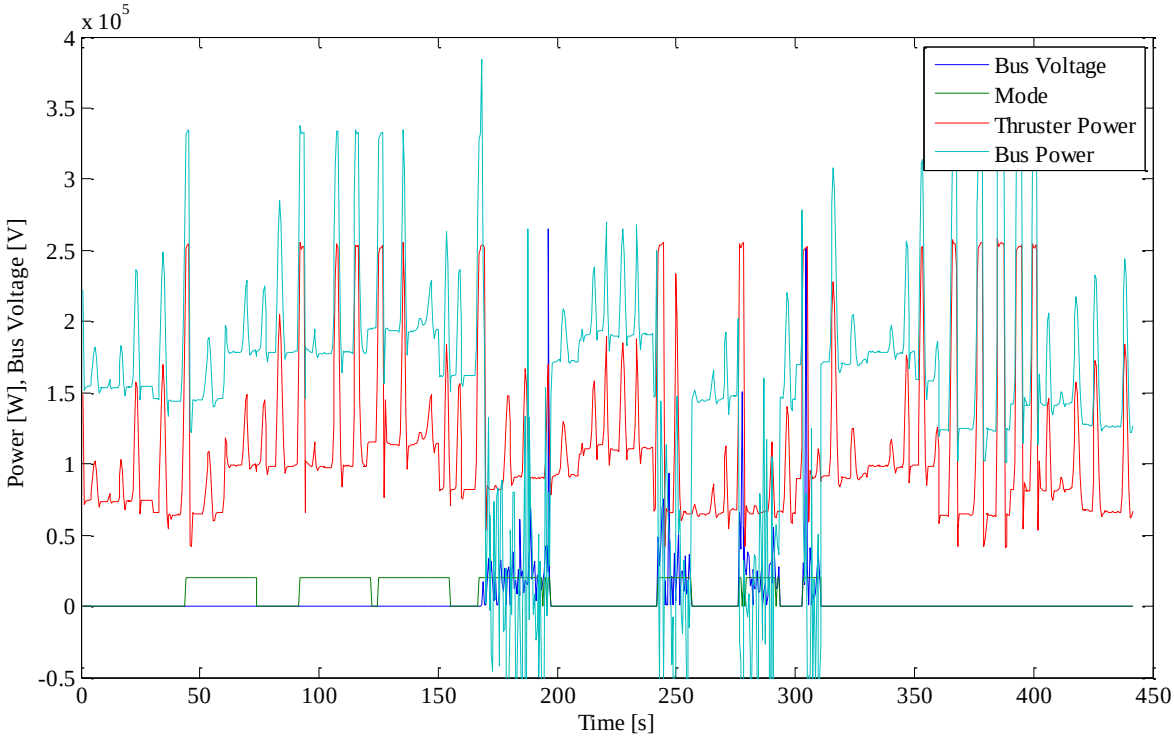

Figure 35: Bus Failure during HEV Mode Entry

6.2.2 Bus Voltage Fluctuation

With the previously mentioned model modification implemented, re-running the simulation produced results as shown in Figure 36. A high value of mode equates to HEV mode, while zero represents ESS only mode. It can be seen that in HEV mode, the bus voltage dips from 460 VAC. However, in ESS only mode, this behavior does not occur. These voltage dips are believed to be triggered by inadequate reactive power compensation and/or harmonics generated by the VFDs. A potential solution could be the inclusion of a FACTS device at the main bus, either a Static Var Compensator or a more complex derivative. However, exploring the design of a FACTS device would not contribute to the scope of the thesis aside from ensuring normal system operation. As only power consumption at the thrusters is of interest, the model was modified so as to neglect the effect of reactive power and the possible presence of harmonics. This was done by splitting the thruster subsystem off from the main model. A three phase voltage source was connected to the input of the VFDs, and power consumed by the thruster subsystem is measured. This power value serves as the demand input to a controlled three

phase dynamic load attached to the main AC bus (with reactive power demand set to zero).

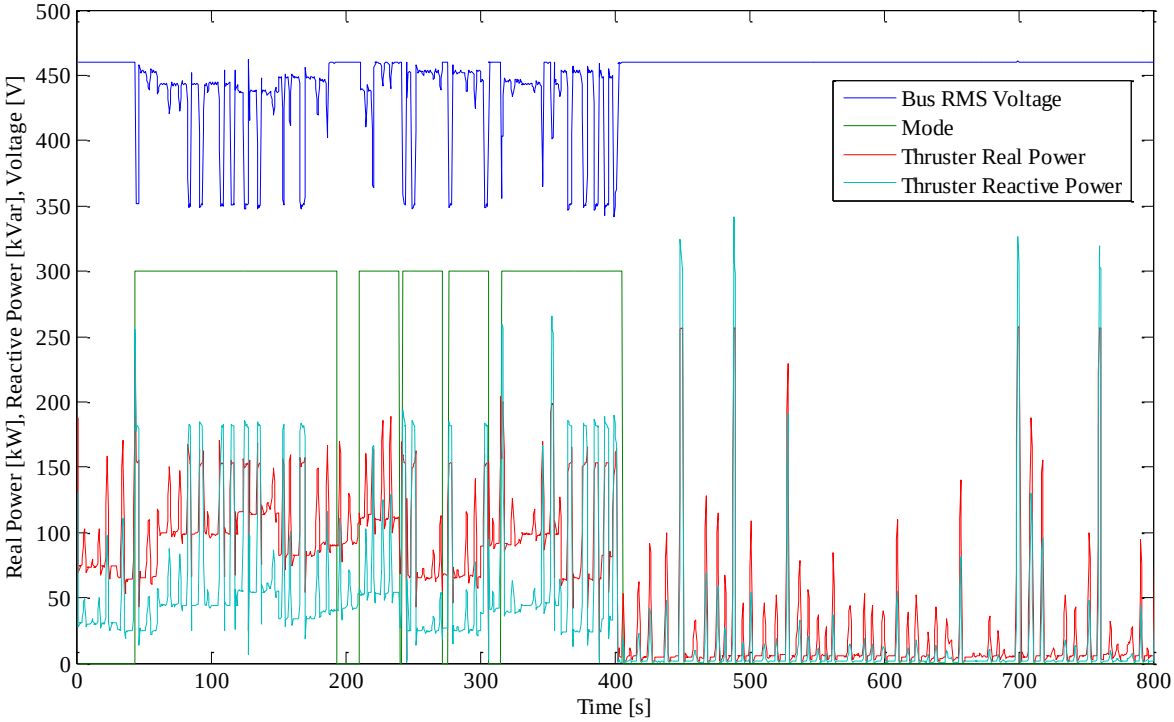

Figure 36: Bus Voltage Fluctuation with Direct Connection to Thrusters

6.3 Mission Cycle Simulation Results

Simulations are presented which provide an operational comparison between the two HEV modes. As well, ship station keeping mission cycles were completed for various combinations of BF number, current speed, true wind angle, and initial ESS SOC.

6.3.1 HEV Modes: Load Power Specified

In order to evaluate and compare fuel consumption and emissions of the conventional and 30% ESS assist HEV modes, each mode was subject to the same load profile (Figure 37). This load profile is designed to operate within the two windows where the ESS assist would be utilized: approximately 195 to 250 kW, and 390 to 450 kW. The rpm input signal to the azimuthing thrusters (cruising mode) is given in Figure 38. During the lower rpm input, a static load of 40 kW is connected to the bus, and after 450s, the static load is increased to 80 kW. The initial SOC for the cycle is 50%. As well, the supervisory mode controller is disabled during the simulation; the ship cannot shift out of HEV mode. The

simulation results for each of the HEV modes are compared in Figure 39 through Figure 43.

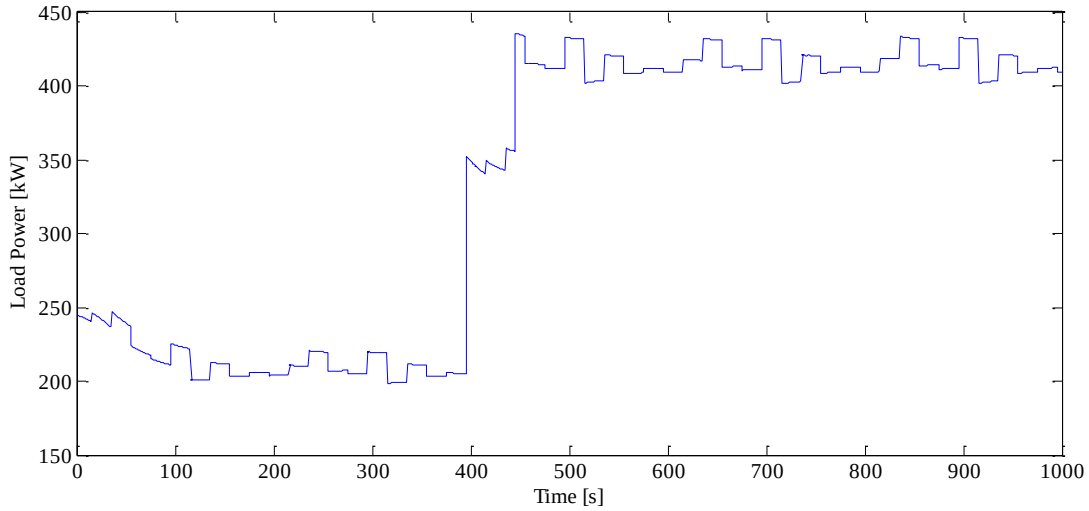

Figure 37: HEV Load Power Profile

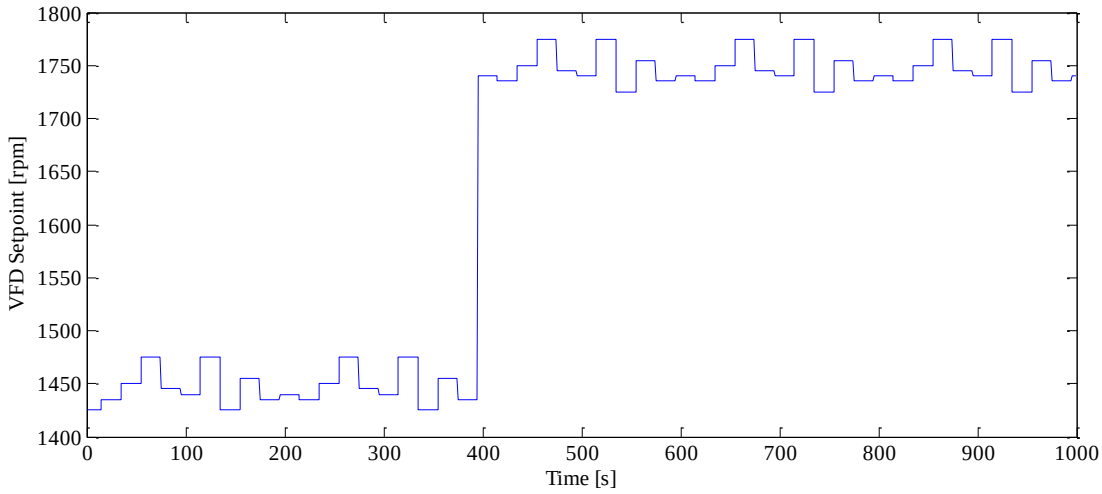

Figure 38: VFD RPM Input

Figure 39 shows the power contribution from the generators throughout the mission cycle. The blue and green lines represent generator one and generator two power contribution during 30% ESS assist mode, respectively. At the start of the cycle, the load is just above the 90% single generator maximum allowable contribution, so the generator output is capped at 193.5 kW. At approximately 400s, the load is increased beyond the 30% ESS assist lower window. At this step, the second generator is brought online, and shares the load equally with the first generator. The load is increased further at approximately 450s. At this point, the load exceeds the maximum power contribution

allowed from both generators, but not beyond the 30% ESS assist range. Thus, the two online generators are operated at their maximum allowed power output for the remainder of the cycle.

The conventional HEV mode is represented by the red, light blue, and magenta lines, which correspond to generators one, two and three, respectively. During the first part of the mission cycle, generators one and two are in operation. When the load is increased at 400s, the third generator is brought online. This generator only remains in operation for the 30s minimum time before turning off. At 450s, it is brought online again, with each generator sharing a third of the load.

The temporary start/stop of generator three at 400s is due to a sudden spike in power demand at that time - over the 90% generator maximum. It is not shown in the load power profile in Figure 37 due to the sampling time of 0.5s. Looking at the load profile, between 400s and 450s, the power demand is just short of 90% maximum for two generators. This is why the third generator shuts down until the load step changes at 450s.

A breakdown of the generator and ESS power contributions for the 30% ESS assist and conventional HEV modes for the load power profile is shown in Figure 40 and Figure 41, respectively.

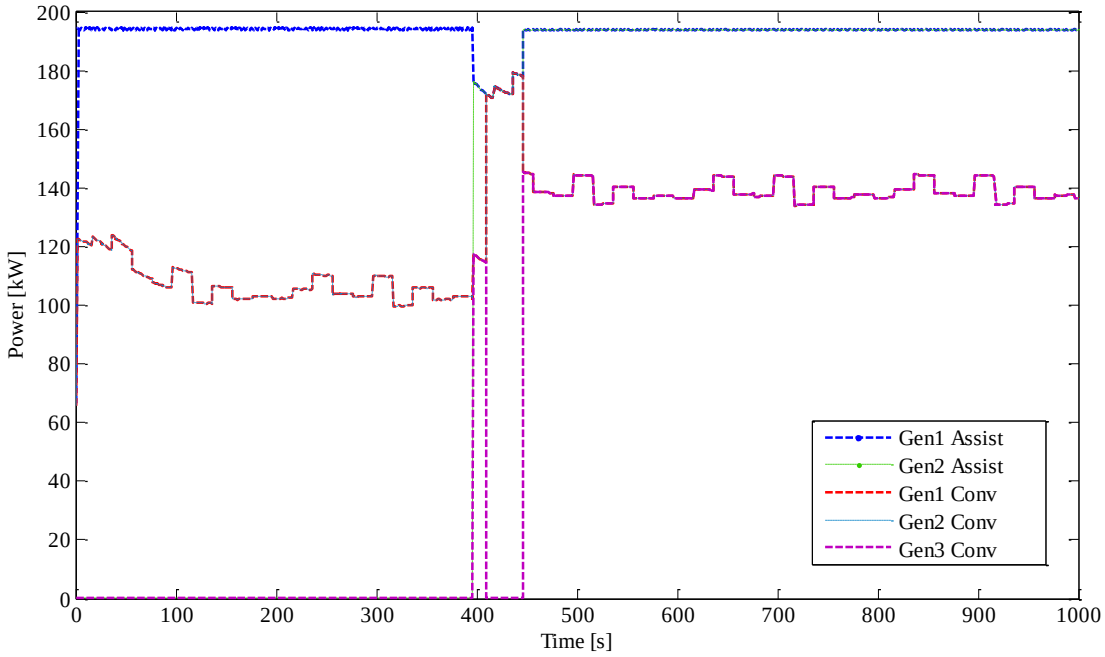

Figure 39: Generator Power Contributions

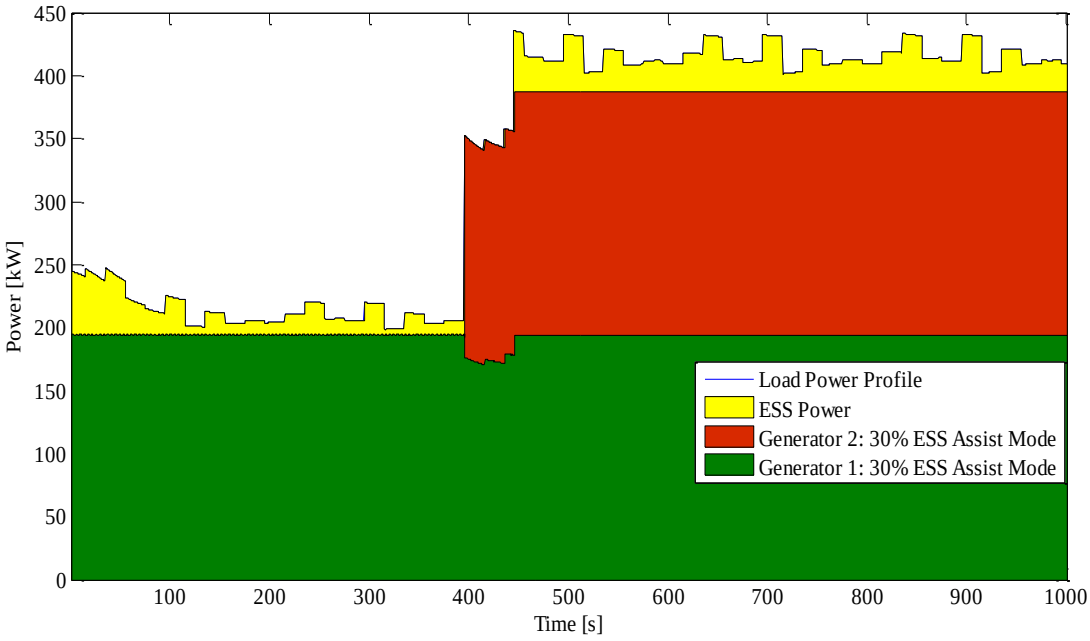

Figure 40: 30% ESS Assist HEV Mode: Generator & ESS Power Contributions

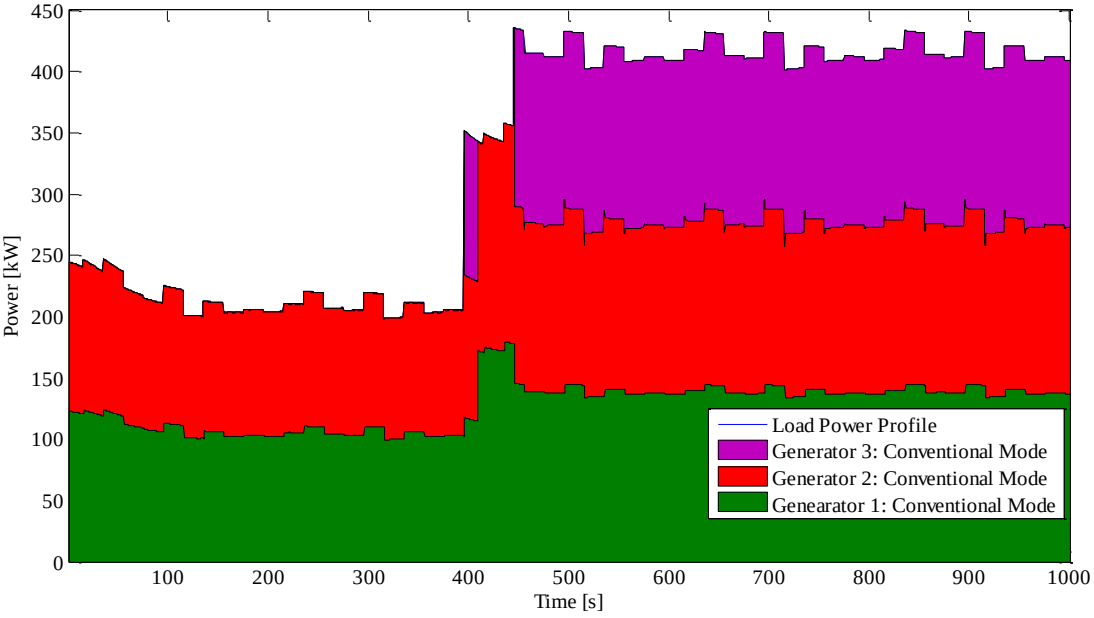

Figure 41: Conventional HEV Mode: Generator Power Contributions

Figure 42 shows the ESS power contribution for each HEV mode. The blue line represents the ESS power during the 30% ESS assist mode, while the green line shows the power assist during the conventional HEV mode. For both cases, the ESS initial SOC is 50%. The red and cyan lines show the SOC for the 30% ESS assist and conventional HEV modes, respectively. The 30% ESS assist mode depleted the ESS SOC to 46.91%

over the mission cycle. During the 30% ESS assist mode, when the demand load is within the assist window ranges, the ESS will be charge depleting as shown. However, if the load demand is not within those windows, the ESS usage will act similar to the conventional HEV mode. The ESS will deplete minimally and maintain an SOC near the level at which it entered into HEV mode; significant ESS assistance is provided once the generator power contribution has reached its maximum.

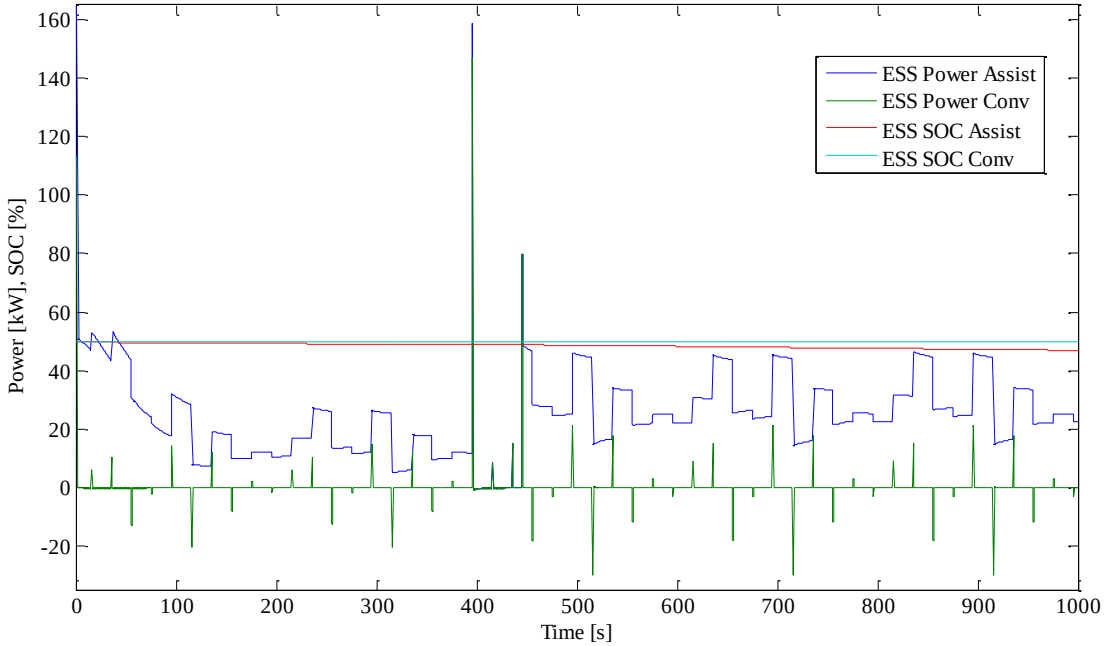

Figure 42: ESS Power and SOC

The total emissions and fuel consumption over the mission cycle are given in Figure 43. (These values include the ESS charging contribution up to the initial SOC for the cycle.) The final emissions value for the conventional HEV mode is 125.2 kg $C0_2e$ and for the 30% ESS assist mode is 116.5 kg $C0_2e$. Similarly, the total fuel consumption is 38.2 kg and 35.5 kg for conventional HEV and 30% ESS assist modes, respectively. Using a the same cycle repeated over a 5 hour period, the emissions savings using the 30% ESS assist mode compared to the conventional HEV mode would be approximately 156.6 kg $C0_2e$, and the fuel savings would amount to 48.6 kg. Given these results, it is clear that a delayed start time for a subsequent generator while incorporating a significant ESS contribution (SOC allowing), amounts to considerable reduced emissions and fuel consumption.

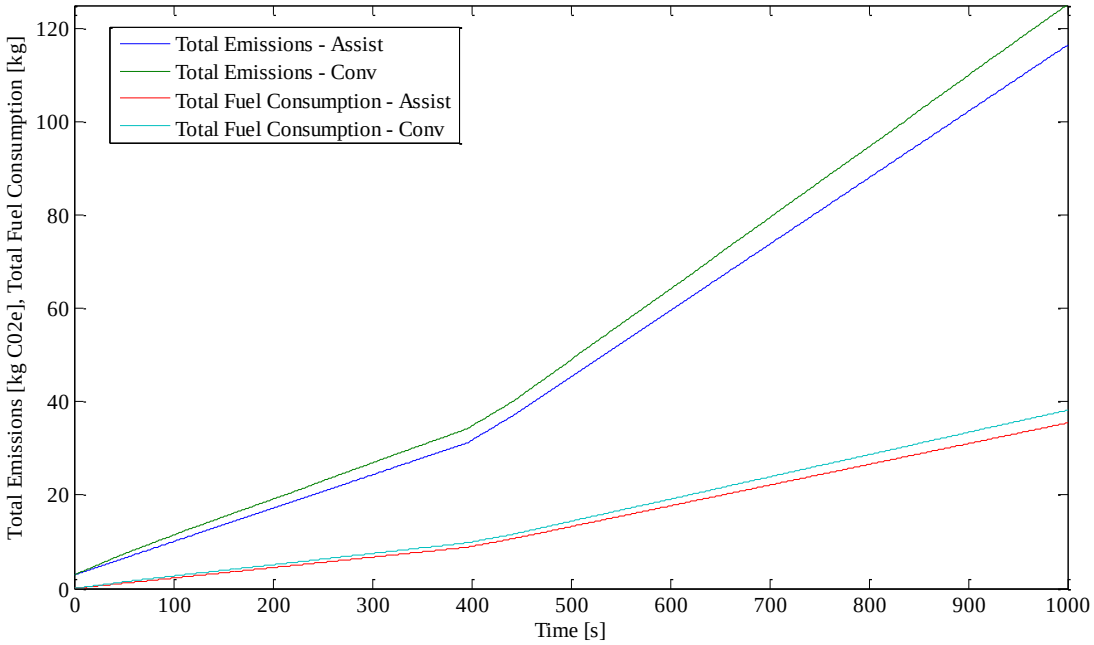

Figure 43: Total Emissions and Total Fuel Consumption

6.3.2 Full Hybrid Functionality: Environment Specified

The load profile to evaluate full hybrid functionality is derived from a station keeping mission cycle with BF5 condition and a wave height of 1.83m. The current is 1 m/s and static load is 100 kW up to 500s. After 500s, the current is decreased to 0.3 m/s and the static load reduced to 40 kW. The load power profile is shown in Figure 44. The decrease in load at 500s is to allow for a load profile within the FCEV operation range. At the start of the simulation, the ESS SOC is 35% and 86.4 kg of hydrogen is available. As well, the 30% ESS assist mode is selected.

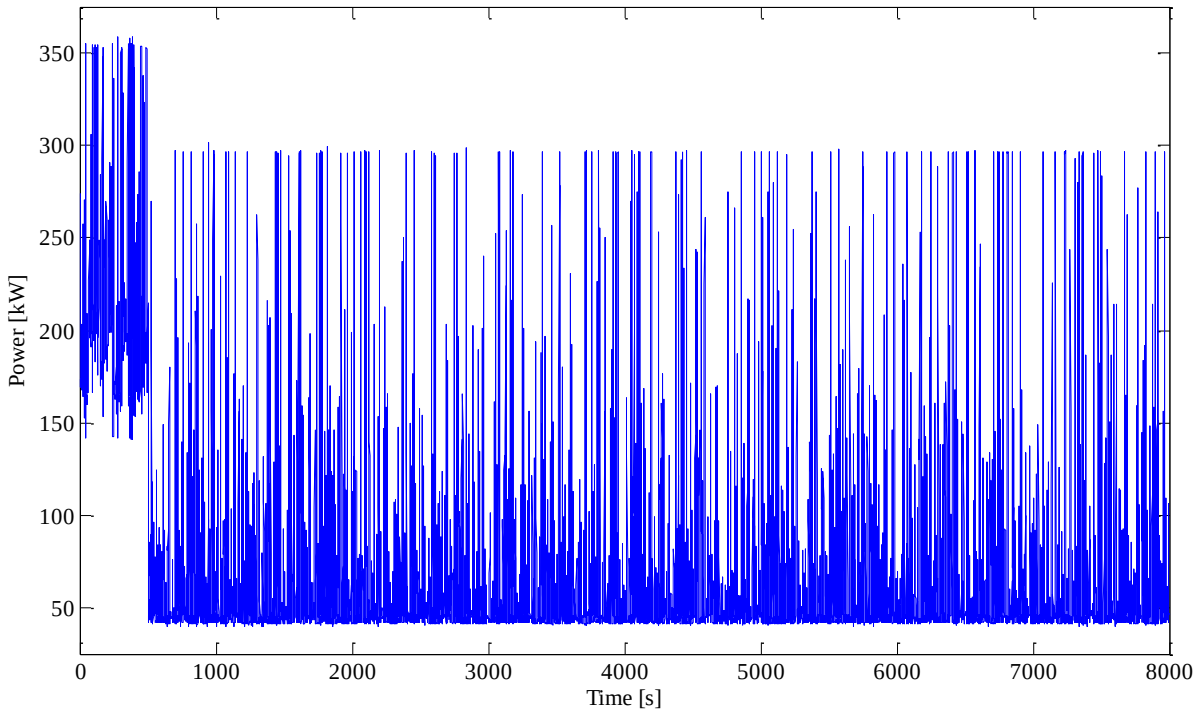

Figure 44: Load Power Profile

The ESS SOC profile is shown in Figure 45. The dashed line represents the CS window mid-range SOC – 25%. At approximately 640s, the ESS SOC has depleted to 30% and the system now operates in CS mode (conventional HEV mode). The load at this point is low enough for FC operation to be employed. However, due to load fluctuations beyond the power capability of the FC, the mode continuously toggles between FCEV and HEV. Both modes must be maintained for a minimum of 30s. The mode throughout the mission cycle is shown in Figure 46. Looking at the load power profile, it can be seen that the high power fluctuations are short lived. The high number of mode changes is not desirable; further development of the supervisory control strategy is needed to reduce the number of mode toggles.

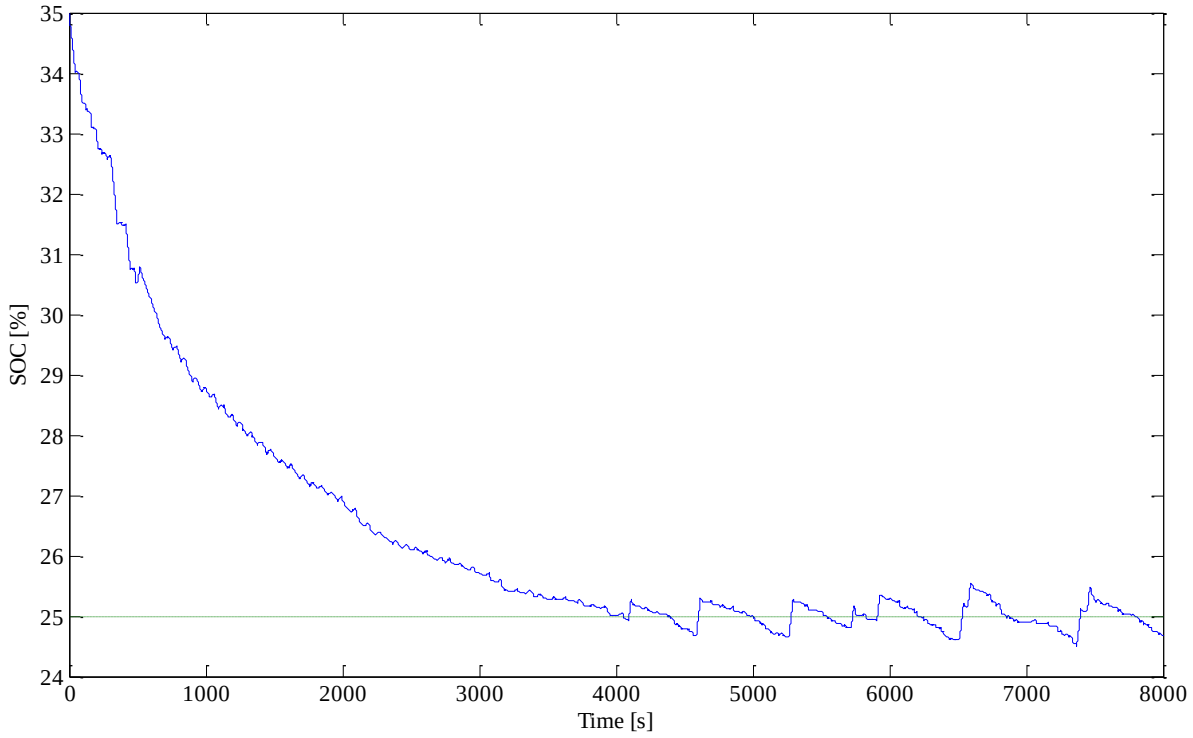

Figure 45: ESS SOC Profile

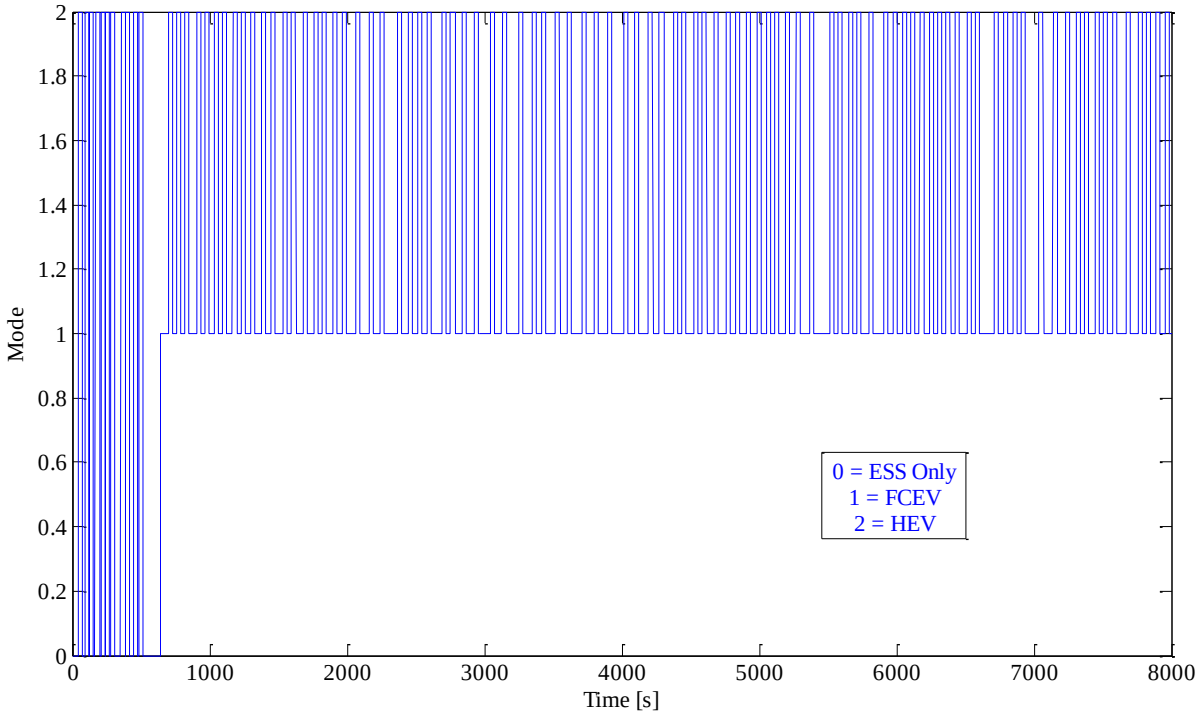

Figure 46: Supervisory Control Mode

The power contribution from each of the generators, along with the FC and the ESS are shown in Figure 47 and Figure 48, respectively. The total generator fuel consumption and resultant GHG emissions are given in Figure 49. Over the cycle, 3.74 kg of hydrogen is consumed. The GHG emissions resulting from the production of this amount of hydrogen is 7.98 kg $C0_2e$. Likewise, the GHG emissions produced to charge the ESS to its initial SOC of 35% is 2.03 kg $C0_2e$.

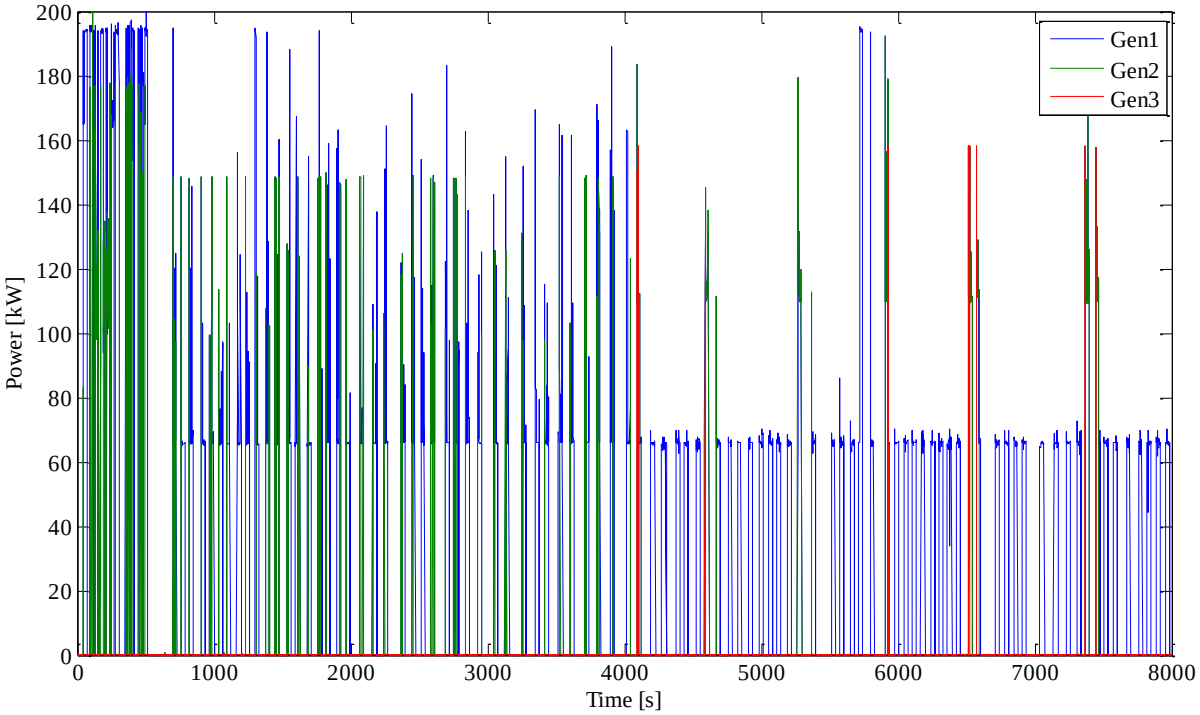

Figure 47: Generator Power Contributions

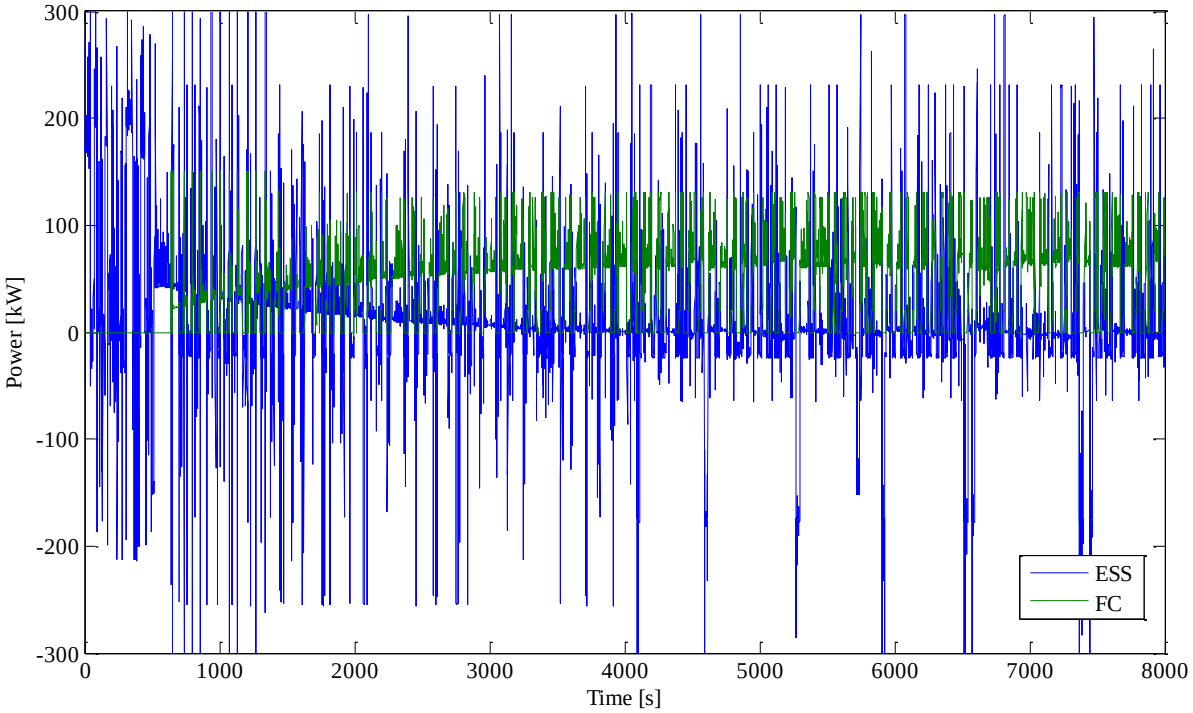

Figure 48: ESS and FC Power Contributions

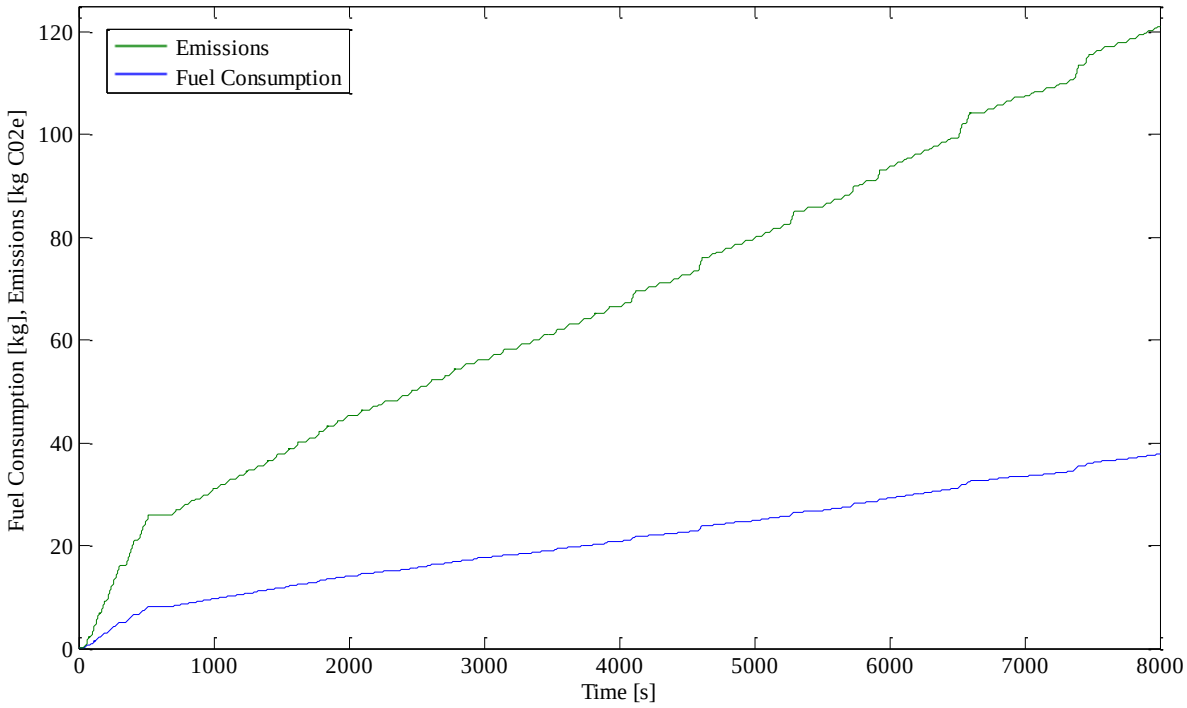

Figure 49: Generator Fuel Consumption and GHG Emissions

6.3.3 EV and HEV Modes: Environment Specified

An eight hour station keeping mission cycle was developed. During the first and last half hour of the cycle, the ROV is deployed/recovered. During these periods, a 30 kW power pack is in use; during the middle 7 hours of the cycle, the 46 kW ROV is in operation. Both the ROV and power pack loads are created by multiplying a random number generator between zero and one with the component power rating (sample time of 30s). The environment specified for this mission is as follows: BF5, wave height of 1.83m, current speed of 0.8 m/s, and true wind angle of 10°. A static load of 60 kW was applied throughout the mission and the initial SOC was set to 95%. The 30% assist HEV mode was selected, and no hydrogen was available for this cycle.

The total load profile over the eight hour period is shown in Figure 50. For the first 2 hours, the mode switches between ESS only mode (0) and HEV mode (2), depending on the magnitude of the load applied to the bus, as shown in Figure 51. At the 2 hour mark, the ESS has depleted to the HEV CS range and the supervisory control strategy switches to HEV conventional mode for the remainder of the simulation. The ESS SOC profile is given in Figure 52. The power contribution from a combination of the generators and the ESS is shown in Figure 53, with their associated GHG emissions and fuel consumption given in Figure 54.

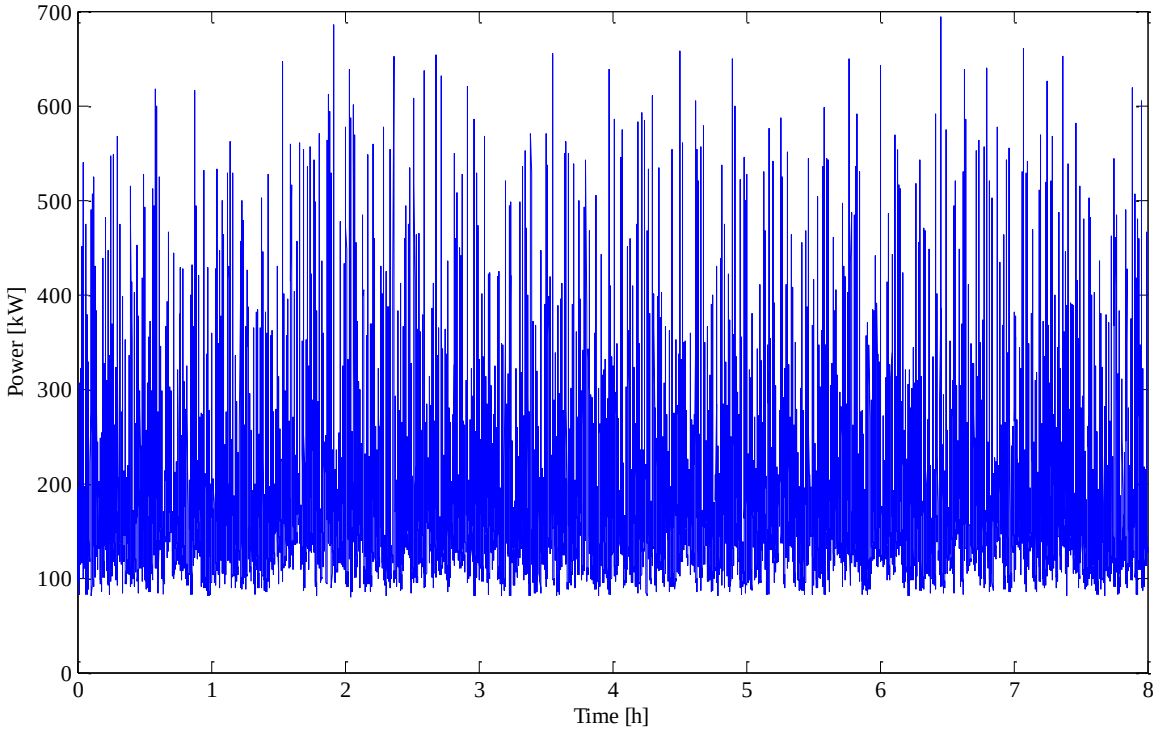

Figure 50: Load Power Profile

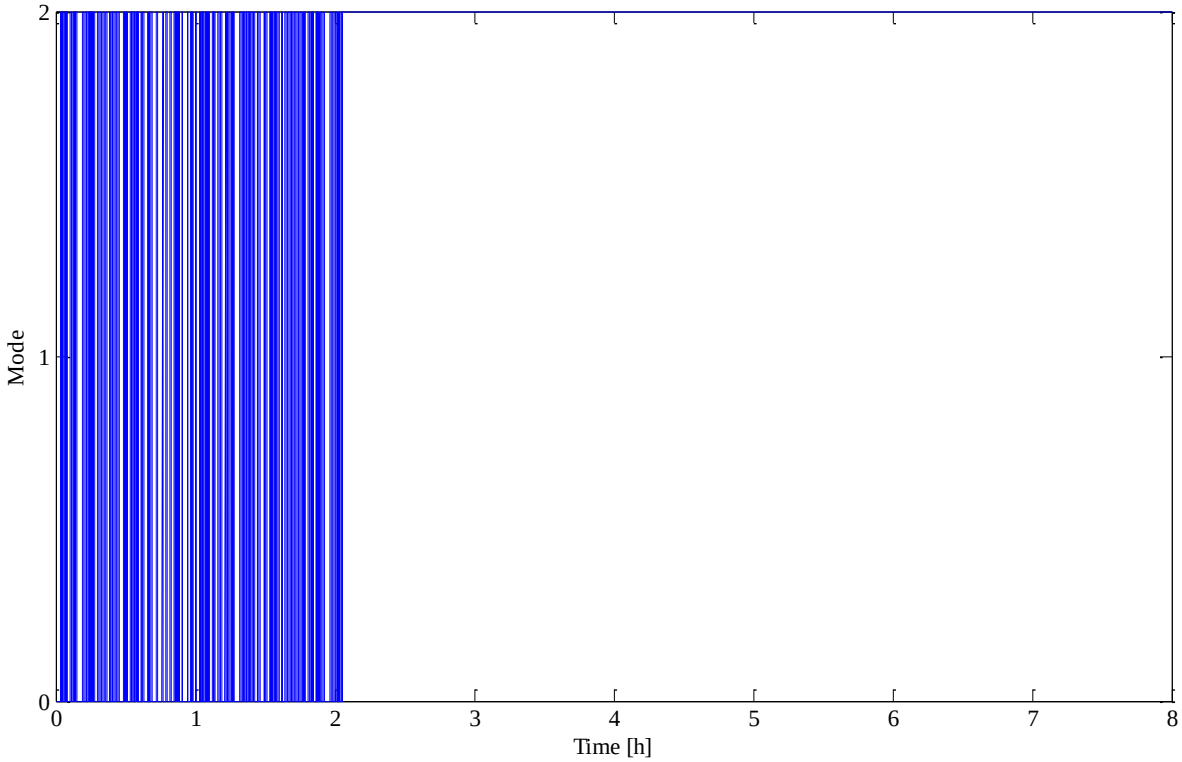

Figure 51: Supervisory Control Mode

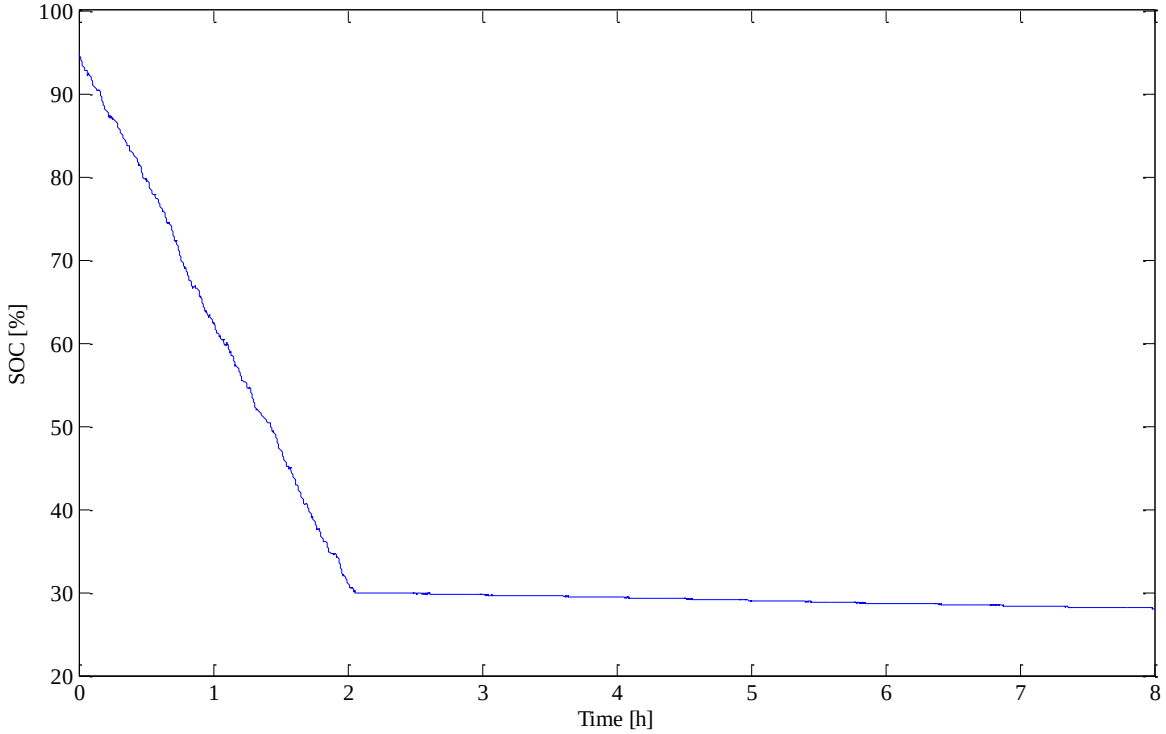

Figure 52: ESS SOC Profile

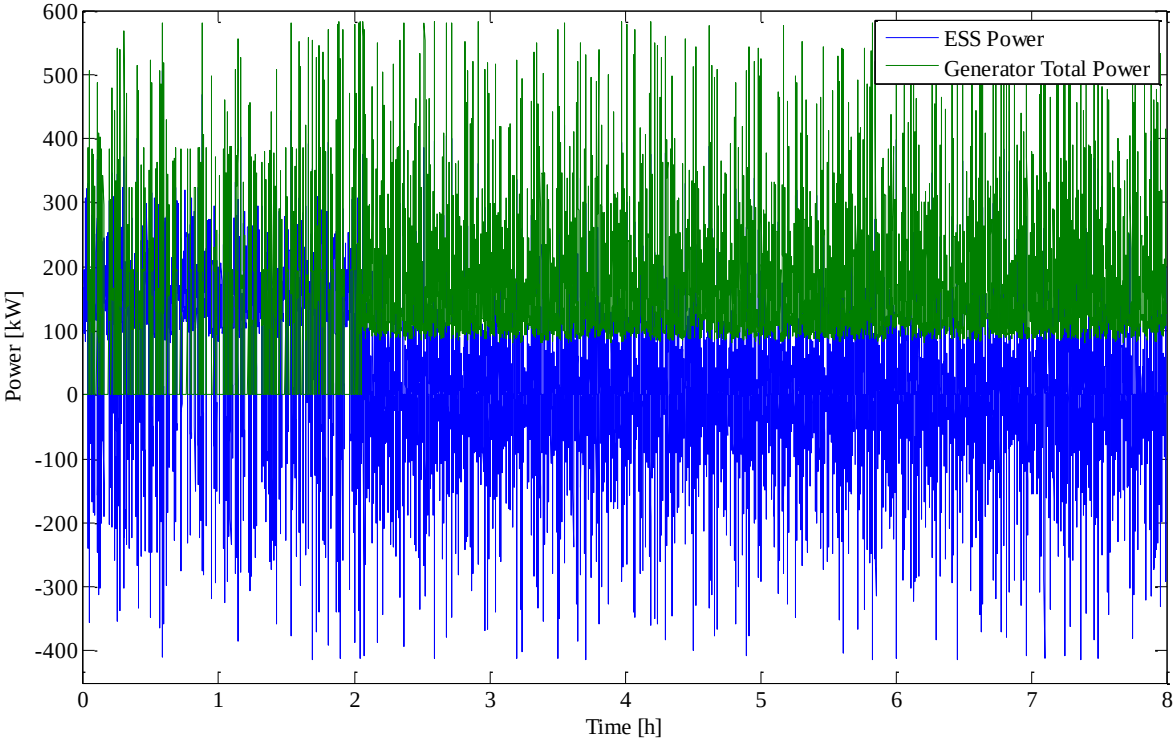

Figure 53: ESS and Generator Total Power Contributions

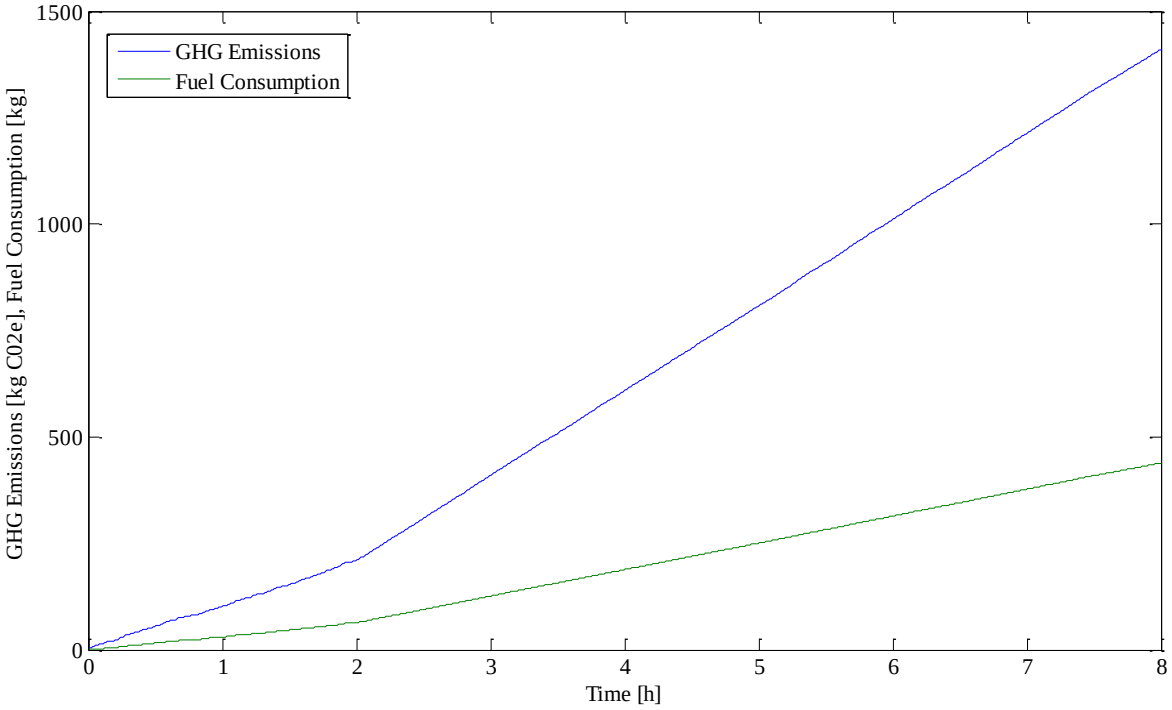

Figure 54: Generator Fuel Consumption and GHG Emissions

6.3.4 Station Keeping Capability

The mission cycles presented previously were all designed so as to ensure the vessel would be capable of holding station. A snapshot of the azimuthing propeller thrust and associated surge resistance for the 8 hour mission cycle is presented in Figure 55. Similarly, the bow thruster force and coupled lateral resistance is given in Figure 56. From the figures, it can be noted that the ship does not lose station in the specified environment. Given the same environment scenario with the current speed increased to 2 m/s, the vessel is no longer capable of holding station and will drift laterally. The resulting lateral resistance and bow thruster force is given in Figure 57. It can be seen that the bow thruster maximum output thrust does not come close to overcoming the lateral resistance.

It should be noted that the propeller thrust generated closely follows the resistance load during station keeping scenarios. The input rpm to the thruster VFDs is generated through use of simple PI controllers which use the error signal of resistance minus thrust. This does not accurately reflect ship propeller control. As stated in the ship requirements, station keeping should be accurate to ±5 m. This allowance for drift was not taken into

account when designing the PI controllers for thruster rpm setpoint. With improvement in the PI controllers to allow for a slower response rpm setpoint transition, keeping within the drift limitations, this may allow for a smoother load power demand. Possibly, this may reduce the power spikes seen by the system, in turn reducing mode toggling.

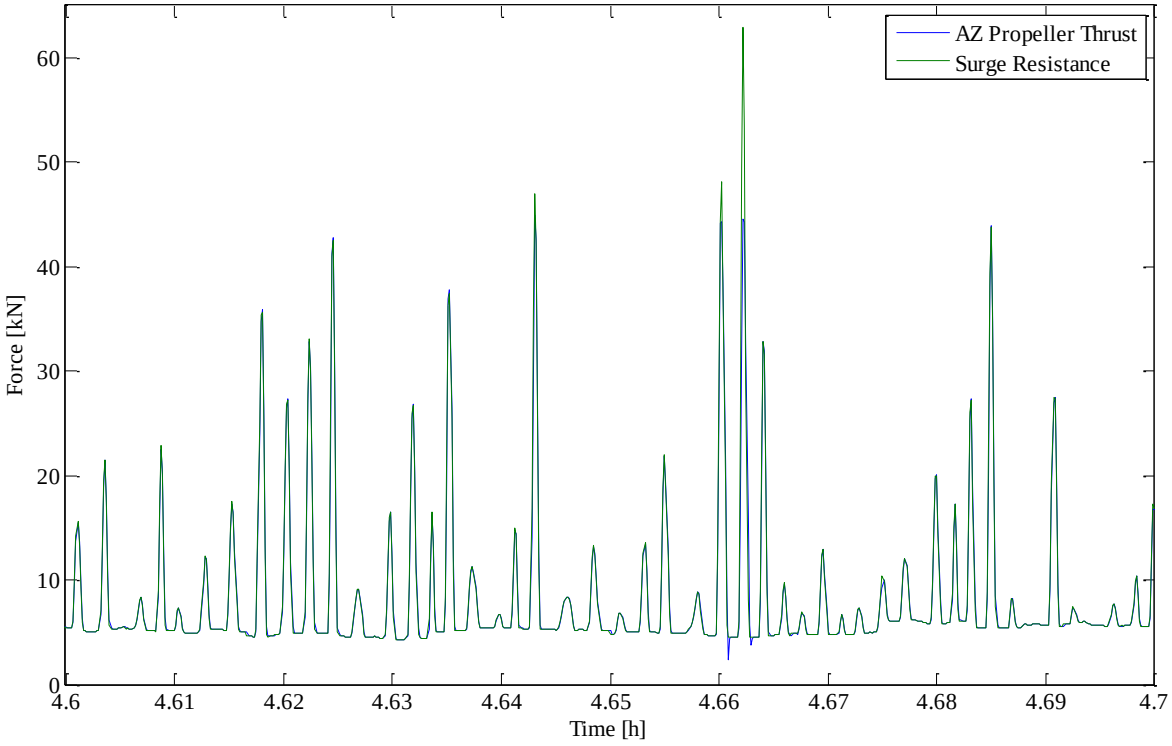

Figure 55: Station Keeping – Surge Resistance & Azimuthing Propeller Thrust

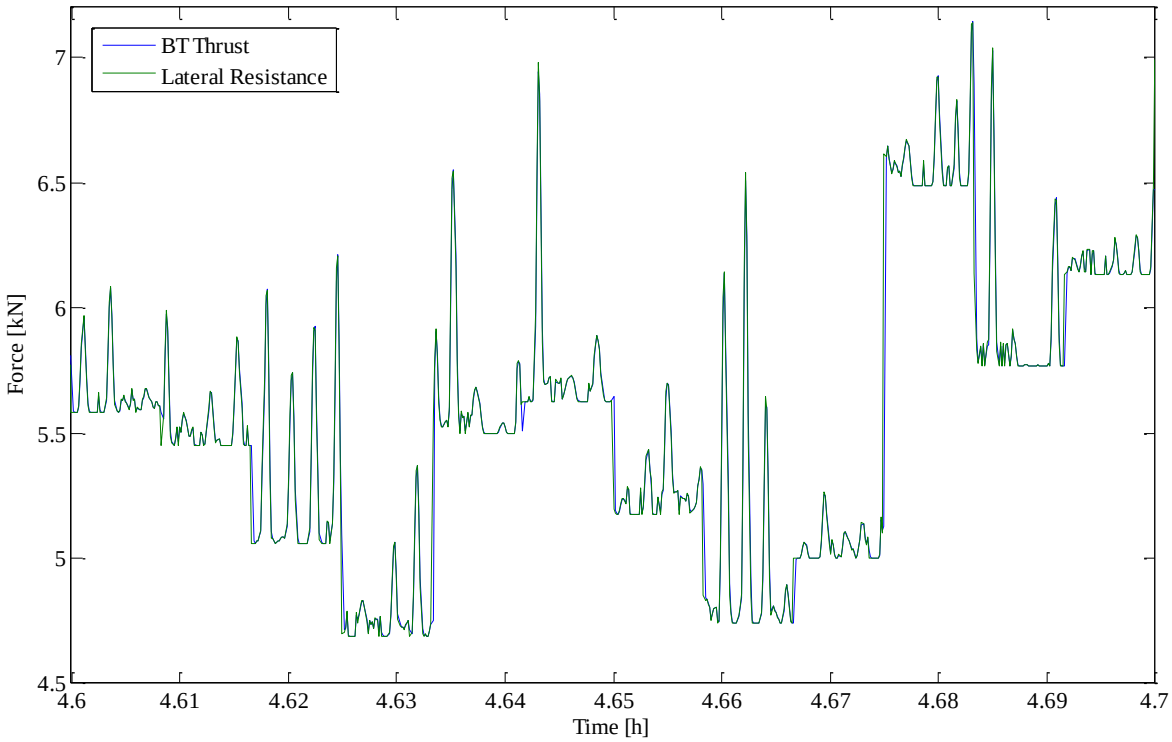

Figure 56: Station Keeping – Lateral Resistance & Bow Thruster Force

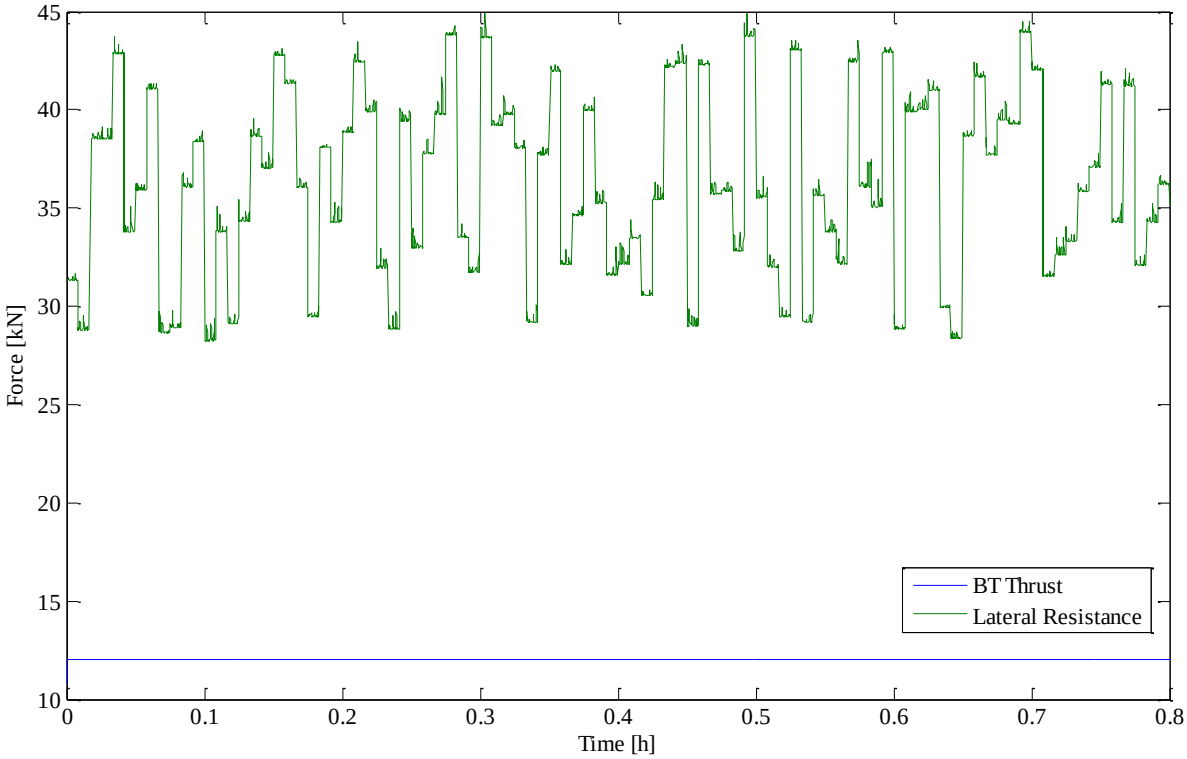

Figure 57: Lateral Drift during Station Keeping Mission

6.4 Conclusions

The hybrid electric propulsion model functions as intended. Power can be drawn from one or a combination of the three onboard sources, the ESS, the fuel cell and the generators, as specified by the supervisory controller. System operation was observed though the use of three predefined load cycles – one with VFD rpm input given, and two with the environment specified. The environment specified missions were designed as aggressive cycles. This approach was chosen in order to test the threshold of the power system.

The ESS operates in CD mode during high SOC, and switches to CS mode when the SOC enters the 20-30% window, irrespective of the power sources in operation. For the eight hour mission cycle with a continually high load demand, the ESS operates in CD mode for approximately 2 hours (given an initial 95% SOC). During this period, the mode toggled between EV and 30% ESS assist HEV mode. This ensured a continual SOC depletion. To increase the length of the ESS contribution period, a larger capacity ESS can be used. As well, this period will be extended given a less aggressive load demand cycle.

The fuel consumption and emissions generation improvement of the 30% ESS assist HEV mode as compared to a conventional HEV mode was demonstrated in the simulations. This performance, which was expected, supports the case for plug-in hybrid electric vessels with a large capacity ESS. The capacity of the ESS and the percentage power contribution during HEV mode can be adjusted to provide further improvements.

A high number of mode toggles occur during the simulations (when another mode is available). This behavior is present in part due to the challenging mission cycles. If the load demand was more stable, with reduced fluctuations, fewer mode changes would occur. Another means to reduce the mode switching is through modification of the supervisory controller. Reducing the number of mode changes is significant as it affects component operation/life. Presently, when the FC is in use during an aggressive load cycle, it is not on for more than a couple minutes at most. In reality, the fuel cell would be operated with a steady, stable load demand as this will assist in prolonging the life of the fuel cell. This issue can be addressed by ensuring the FC remains in operation for a

longer period. This may be unreasonable with a high load peaking cycle without additional assistance from the ESS or generators. As the ESS is operated as CS during FC mode, the combination of the two may be incapable of providing enough power to the bus. A more reasonable approach may be to use a combination of ESS, FC and generators once the FC has been brought online. With this method, the supervisory controller can specify a stable power demand for the FC, with the ESS and generators providing for the remainder of the load. Yet again, this may cause issues with the generators being brought on and offline excessively. The generators may have to remain in a warmed up, idle state to enable quick connection to the bus. In this model, the generators are operated in this manner. Mode control by the supervisory controller requires further investigation.

The simulations provide insight into ESS energy usage – charging and discharging. Given the aggressive load cycles, the ESS charge and discharge profiles fluctuate greatly. These power spikes may need further examination to ensure they are within the physical limits of the actual component.

The vessel resistance subsystem serves the purpose of providing a method of designing a meaningful mission cycle to evaluate a given propulsion system. The approach utilizes industry accepted empirical equations. It is not intended to assist with a sensitivity study of the ship hull form. However, coupled with the industry accepted, empirically based thruster model, the model provides an estimation of the thruster capabilities. This includes the maximum speed capability of the vessel as well as the environmental conditions in which the ship will lose station. This may not affect the power system; it is an inherent limitation of the components. However, knowing these constraints, different propellers options can be explored which may require size adjustments of the VFD drives, in turn affecting system power demand.

Chapter 7 Summary and Recommendations

7.1 Summary

The objective of this thesis was to model, simulate and evaluate a proposed marine vessel hybrid electric propulsion system, utilizing MATLAB Simulink and the SPS toolbox.

Models for each of the individual powertrain components were developed and incorporated into a complete hybrid propulsion model. A vessel resistance model was created to support vessel performance and energy requirement evaluation. The model incorporates data based on the ship principal parameters and hull form. Ship open water resistance simulations were compared with industry provided data (industry data is predicted via commercial calculation programs). The simulation results and industry predicted results are in good agreement.

A rule-based supervisory controller for the proposed vessel was constructed. It is an amalgamation of control strategies for three vehicle architectures: EV, FCEV, and HEV. Additional logic was included in the controller so as to adjust the occurrence of a mode toggle and generator turn on/off. The ESS was partitioned so as to assign SOC windows for each of the modes. It takes into account typical SOC operational ranges for each vehicle type and as well as the ESS characteristics.

The complete model of the hybrid electric propulsion, control, and resistance subsystems was simulated on a dSPACE HIL platform. For each run, the ESS SOC, station keeping/cruising mode, HEV assist, BF number, current speed, true wind angle, and hotel load were specified. From the simulations, it was demonstrated that using an ESS assisted HEV mode results in reduced emissions and fuel consumption as compared to the conventional HEV mode. A larger capacity ESS has the potential to reduce emissions and fuel consumption further, depending on ship usage. The rule-based supervisory controller proved inadequate in situations with frequent large load changes. In these cases, often the controller would not change mode in a timely manner to prevent bus failure.

7.2 Research Contributions

This research presents a first pass at blending an industry standard automotive modeling approach with marine engineering/naval architecture principles. The generated modeling tool introduces established empirical naval architecture equations, which describe ship resistance estimation along with effects of environment applied to a vessel form, into a time domain simulation. Coupled with the established automotive tools, the modeling platform allows for simulation, component size sensitivity analysis, and ship performance analysis of a vessel power system and associated ship architecture. This tool was modified as necessary to enable model simulation on a dSPACE HIL platform.

7.3 Recommendations

There is potential for improvement in any of the subsystem models, depending on the fidelity required. Modifications to the thruster subsystem are necessary to allow for direct connection to the AC bus. The thruster drives are modeled using SPS AC3 blocks. These blocks do not use the average-model type of voltage source converter to represent the power electronics used to convert AC/DC or DC/AC. As a result, this system includes the effect of harmonics. As well, reactive power consumption at the thrusters can become unmanageable given the current power system and control strategy. To reduce the harmonic generation of this system, the SPS block can be modified to use the average-value type voltage source converter with no harmonics generated. This may require a somewhat substantial modification in the drive control strategy. Furthermore, possible reactive power mitigation measures may include a FACTS device sized for the system, which can be included at the AC bus, or an LCL filter included at the input to the drive block. With these improvements, direct connection of the thruster subsystem to the bus without experiencing bus voltage fluctuations may be possible.

Another modification which can be explored to further improve the HEV ESS assist mode could be to allow the ESS contribution before the maximum generator power is reached, at a point when the fuel consumption and emissions produced by the generator is within an efficient operation region. Power output by the generator could be held at a

lower value, with the ESS contributing a larger portion but not beyond its specified maximum.

Assert signals were used to serve as mode switch de-bouncing, however, these proved not to be adequate in all situations. With fast load changes, resulting in load beyond the capability of the ESS, the time delay until the supervisory controller switches to HEV mode can result in system instability. In these cases, the bus voltage and system frequency becomes unstable and the system cannot recover. Replacing the assert signals with fuzzy logic controllers may allow for more effective mode changes – before the bus voltage/frequency becomes unstable, but not when it is unnecessary to change mode (short load peaks).

The size and complexity of the model proved to be overly extensive for real-time HIL simulation; the model could only run in ‘as fast as possible’ mode. For future research, given a large scale powertrain simulation where the focus is on power/energy usage, restricting the model to using Simulink/SimDriveLine blocksets which can run with a higher simulation step size may be beneficial to achieving real-time simulation. Ability to run in real-time is favorable for addition of an external controller with CAN communication.

Simulation of the Simulink/SPS model has been shown to provide insight into performance of the proposed hybrid power system under various operating conditions. This information can further be used to re-examine the sizes/types of the initial specified powertrain components and/or improve the rule-based supervisory control strategy or replace it altogether with a more advanced strategy; the information promotes potential improvement and/or optimization in powertrain design, control development, and system modelling.

References

[1] The Organization for Economic Co-operation and Development/International Transport Forum. Greenhouse Gas Reduction Strategies in the Transport Sector: Preliminary Report 2008.

[2] The Organization for Economic Co-operation and Development/International Transport Forum. Canada 1990-2007 CO_2 Emissions by Transportation Sector, 2010.

[3] UniCredit, Corporate Banking, Study: Green Shipping, January 2009.

[4] International Maritime Organization. IMO at COP17, 2010. Available: http://www.imo.org/ourwork/environment/pollutionprevention/airpollution/pages/imo-at-cop-17.aspx

[5] European Maritime Safety Agency. Final Report: Study on Ships producing reduced quantities of ships generated - present situation and future opportunities to encourage the development of cleaner ships. EMSA/OP/05/05. January 2007.

[6] INTERTANKO. Poseidon Challenge Award, June 2007. Available: http://www.intertanko.com/News-Desk/Home-Page-Article/Poseidon-Challenge-Award/

[7] Caterpillar, Marine C9 Generator Set Performance Data: PRIME-DM7758-01.

[8] The Center for Energy Analysis and Policy, The Total Energy and Emissions Analysis for Marine Systems Model, Rochester Institute of Technology, 2005.

[9] British Columbia: Ministry of Environment. Methodology for Reporting B.C. Public Sector Greenhouse Gas Emissions, Version 1.0. Victoria, BC. February 2011.

[10] S.G. Wirasingha and A.Emadi, "Classification and review of control strategies for plug-in hybrid electric vehicles," *Vehicular Technology, IEEE Transactions on*, Vol. 60, pp. 111-122, 2011.

[11] K. Bragadottir. Iceland's hydrogen ship heralds fossil-free future. Environmental News Network, 2008. Available: http://www.enn.com/energy/article/29805

[12] Alcatraz Cruises. Hornblower Hybrid. Available: http://www.alcatrazcruises.com/website/hybrid.aspx

[13] D. Biello. World's First Fuel Cell Ship Docks in Copenhagen. Scientific American Magazine, 2009. Available: http://www.scientificamerican.com/article.cfm?id=worlds-first-fuel-cell-ship

[14] The World's First Hydrogen Boat on the Alster. Available: http://www.zemships.eu/das-erste-wasserstoffschiff-der-welt-in-hamburg/

[15] J. Steele, "Navy's First Hybrid-Drive Warship Goes To Sea," San Diego Union-Tribune, 2011.

[16] KOTUG. Europe's first Hybrid Rotortug E-KOTUG Operating in Port of Rotterdam. 2012. Available: http://www.kotug.nl/en-GB/news-events/33_europe-s-first-hybrid-rotor-r-tug-e-kotug-operating-in-port-of-rotterdam.html

[17] Wärtsilä installs fuel cell unit on vessel – unique SOFC technology provides power to Wallenius' car-carrier 'Undine', FuelCellsWorks. Available: http://fuelcellsworks.com/news/2010/06/11/wartsila-installs-fuel-cell-unit-on-vessel-unique-sofc-technology-provides-power-to-wallenius-car-carrier-undine/

[18] T. Markel, A. Brooker, T. Hendricks, V. Johnson, K. Kelly, B. Kramer, M. O'Keefe, S. Sprik, and K. Wipke, "ADVISOR: a systems analysis tool for advanced vehicle modeling," *Journal of Power Sources*, vol. 110, pp. 255-266, 2002.

[19] Argonne National Laboratory. Transportation Technology R&D Center. PSAT. Available: http://www.transportation.anl.gov/modeling_simulation/PSAT/psat.html

[20] Autonomie, Argonne National Laboratory. Available: http://www.autonomie.net

[21] R.D. Moody, "Preliminary power prediction during early design stages of a ship," Cape Town, South Africa, November 1996.

[22] Performance Prediction Software, Hydrocomp Inc. Available: http://www.hydrocompinc.com

[23] Maritime Research Institue Netherlands. Available: http://www.marin.nl

[24] Theoretical Manual of SEAWAY (Release 4.19, 12-02-2001), J.M.J. Journée, Report 1216a, February 2001, The Netherlands, Delft University of Technology, Shiphydromechanics Laboratory

[25] Mathematical Model for MANSIM Version 2: A Surface Ship Manoevring, Stationkeeping, and Seakeeping Simulator Computer Program, P.J. Kopp, October 1996, CRDKNSWC/HD-1427-02

[26] Marine Systems Simulator, 2013. Available: www.marinecontrol.org

[27] H. Zhang, K.L. Butler, N.D.R. Sarma, H. DoCarmo, S. Gopalakrishnan, A. Adediran, "Analysis of Tools for Simulation of Shipboard Electric Power Systems," in *Electric Power Systems Research*, vol. 58, 2001, pp. 111-122.

[28] K. Schmitt, "Modeling and Simulation of an All Electric Ship in Random Seas," 2010.

[29] T. Nord, "Voltage Stability in an Electric Propulsion System for Ships," 2006.

[30] J. M. Apsley, A. G. Villasenor, M. Barnes, A. C. Smith, S. Williamson, J. D. Schuddebeurs, P. J. Norman, C. D. Booth, G. M. Burt and J. R. McDonald, "Propulsion drive models for full electric marine propulsion systems," in *Electric Machines & Drives Conference, 2007. IEMDC '07. IEEE International*, 2007, pp. 118-123.

[31] R. Arendt, "Simulation investigations of ship power systems," in *Environment and Electrical Engineering (EEEIC), 2011 10th International Conference on*, 2011, pp. 1-4.

[32] L. Luckose, H. L. Hess and B. K. Johnson, "Fuel cell propulsion system for marine applications," in *Electric Ship Technologies Symposium, 2009. ESTS 2009. IEEE*, 2009, pp. 574-580.

[33] W. Jiang, R. Fang, J. Khan and R. Dougal, "Performance prediction and dynamic simulation of electric ship hybrid power system," in *Electric Ship Technologies Symposium, 2007. ESTS '07. IEEE*, 2007, pp. 490-497.

[34] S. S. Kalsi and O. Nayak, "Ship electrical system simulation," in *Electric Ship Technologies Symposium, 2005 IEEE*, 2005, pp. 63-69.

[35] G. Seenumani, "Real-time Power Management of Hybrid Power Systems in All Electric Ship Applications," 2010.

[36] D. Radan, “Integrated Control of Marine Electrical Power Systems,” 2008.

[37] C. Mulder, M. Mulligan, “Project to Build a Prototype Hydrogen-Powered Hybrid Electric Tug,” ITS 2010, Capilano Maritime Design Ltd., Paper No. G4.

[38] Weifeng Shi, Tianhao Tang and Jianmin Yang, "Simulation of a large marine container ship power system," in *SICE 2004 Annual Conference*, 2004, pp. 39-44 vol. 1.

[39] C. Xie, C. Zhang, J-Y.J. Chang, "Research on Simulation of Ship Electric Propulsion System with Flywheel Energy Storage System," Microsystem Technologies, pp. 1161-1167, Vol. 17, Issue 5, June 2011.

[40] EPA, United States Environmental Protection Agency, Air and Radiation, EPA420-R-99-027, “In-Use Marine Diesel Fuel,” August 1999.

[41] The Greenhouse Gasses, Regulated Emissions, and Energy Use in Transportation Model, Argonne National Laboratory. Available: http://greet.es.anl.gov/

[42] David, C, "Representative emissions factors for use in quantification of emissions from ships associated with ship movements between port in the European Community," IVL Swedish Environmental Research Institute Ltd, ENV.C.1/ETU/2001/0090, 2002, pp. 13-15.

[43] Kirk-Othmer, "Encyclopedia of Chemical Technology," John-Wiley & Sons, 2001. Vol. 9, pp.646, Vol. 6, pp. 108-109.

[44] Ballard FCvelocity™-HD6 Specification Sheet, 04/2010

[45] Sacré-Davey, Hydrogen Energy Group Report, "Engineering Innovation for the Emerging Hydrogen Age," Issued: March 2009.

[46] Techsol Marine Electrotechnology, P11-7001-SP, Hybrid Power System Specifications, University of Victoria, Science Vessel. 2011, R.0A.

[47] M.N. Souleman, "A generic fuel cell model and experimental validation," 2008.

[48] I. Zamora, J.I. San Martín, J. García, F.J. Asensio, O. Oñederra, J.J. San Martín, V. Aperribay, "PEM fuel cells in applications of urban public transport," in Renewable Energies and Power Quality (ICREPQ), 2011, International Conference on, 2011.

[49] Valence U-Charge XP Battery Modules Datasheet, 2011.

[50] M. W. C Oosterveld, "Wake Adapted Ducted Propellers," NSMB Wageningen Publication No. 345, June 1970, pp. 30-35.

[51] J.M.J Journée and W.W. Massie, *Offshore Hydromechanics*. Delft University of Technology, 2001.

[52] J. Holtrop and G.G. J. Mennen, "An Approximate Power Prediction Method, " *in International Shipbuilding Progress*, 1982, Vol. 29, No. 335.

[53] J. Holtrop, “A statistical re-analysis of resistance and propulsion data,” *in International Shipbuilding Progress*, 1984, No. 31, pp. 272-276.

[54] K.J. Rawson and E.C. Tupper, *Basic Ship Theory, 5E V2*. Oxford: Butterworth-Heinemann, 2001.

[55] R.M. Isherwood, Wind resistance of merchant ships, *in Transactions of Royal Institution of Naval Architects*, Vol. 115, 1973, pp. 327-338.

[56] T.A. Loukakis, C. Chryssostomidis, "Seakeeping standard series for cruiser-stern ships," *in Transactions SNAME,* vol. 83, 1975, pp. 67-127.

[57] G.J. Grigoropoulos, T.A. Loukakis, A.N. Perakis, "Seakeeping standard series for oblique seas." Rept. NAL 114-F-1994, Department of NA and ME, National Technical University of Athens.

[58] C.A. Thoresen, *Port Designer's Handbook: Recommendations and Guidelines*, London: Thomas Telford Publishing, 2003.

[59] P. T. Krein, "Battery management for maximum performance in plug-in electric and hybrid vehicles," in *Vehicle Power and Propulsion Conference, 2007. VPPC 2007. IEEE*, 2007, pp. 2-5.

[60] G. Pistoia, *Electric and Hybrid Vehicles : Power Sources, Models, Sustainability, Infrastructure and the Market*. Amsterdam: Elsevier, 2010.

[61] R.F. Nelson, “Power requirements for batteries in hybrid electric vehicles,” *Journal of Power Sources*, vol. 91, pp. 2-26, 2000.

[62] Valance Energy Storage Solutions, "Application: U24-12XP Rev 2, 55s3p, Diesel Electric Propulsion Ship Vessel Conversion," May 31, 2011.

[63] D. Wu, S.S Williamson, Status review of power control strategies for fuel cell Based hybrid electric vehicles, in *Proc. IEEE Electrical Power Conf.*, Montreal, QC, Canada, Oct. 2007. 2007

.Appendix A: Tsekoa II General Information

CCGS TSEKOA II

Official Number: 804446

Call Sign: CY 5282

Details

Vessel Type:	Specialty Vessel
Port of Registry:	Ottawa
Region:	Pacific
Home Port:	Victoria, BC, Canada
Year Built:	1984
Material:	Steel
Builder:	Allied Shipbuilders Ltd, North Vancouver, BC, BC, Canada
Modernized:	
Complement:	Officers: 3 Crew: 4
Total:	7
Crewing Regime:	Lay Day
Available Berths:	1

Certificates

Class of Voyage:	Home Trade II
Ice Class:	N/A
MARPOL:	0
IMO:	8320418

Scientific Equipment

Laboratory Types:

LAN:	No
Winches:	
Sounders:	No
Power on Deck:	Hydraulic: No Electrical: No
Container Capacity:	No

Engineering

Propulsion:	Geared Diesel
Description:	(2x) Caterpillar 8 cyl
Power:	537
Propellers:	2 - fixed pitch
Generators:	
Emergency Gen.:	
Thrusters:	Bow: No Stern: No
UPS:	

Holds and Decks

Hold 1:	33 m3 Hatch Size:2.5 m X 1.3 m
Hold 2:	0 m3 Hatch Size: X
Main Deck Area:	71 m2
Boat Deck Area:	
Forcastle:	
After Deck Area:	

Navigation Equipment

Auto Pilot:	(1x) Comnav 2001
Depth Sounder:	(1x) Furuno FCV-1000
Elec. Charts:	
GPS:	(1x) Furuno GA70 Mk2
Gyro:	(1x) Sperry Rascar SR 120
LORAN:	
MF DF:	
Radar:	(1x) Raytheon R80XX (1x) Raytheon R81 - X Band
Speed Log:	
VHF DF:	(1x) OAR 320 E
Other Equipment:	

Deck Equipment

Main Hoist:	(1x) Crane
Cranes:	(1x) Boat crane
Towing Equipment:	(1x) Nylon rope
Workboats:	1 - RHI Mark V Zodiac (Crane)

Communications Equipment

VHF FM:	
VHF AM:	
HF:	
SatComm:	
Weather Fax:	

Helicopter Accomodations

Flight Deck Area:	
Hangar Area:	
Hangar Gear:	No
Fuel Capacity:	No

CCGS TSEKOA II

Official Number: 804446 **Call Sign: CY 5282**

Dimensions

Length:	26.7 m	**Gross Tonnage:**	160.75 grt	**Cruising Range:**	500 nm	**Fresh Water:**	3.6 m3
Breadth:	7.25 m	**Net Tonnage:**	53.68 nrt	**Endurance:**	7 days	**Fuel Capacity:**	13 m3
Draft:	2 m	**Freeboard:**		**Cruising Speed:**	11 kts	**Fuel Consumption:**	

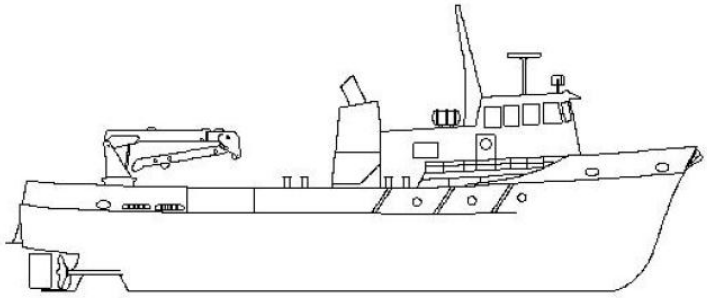

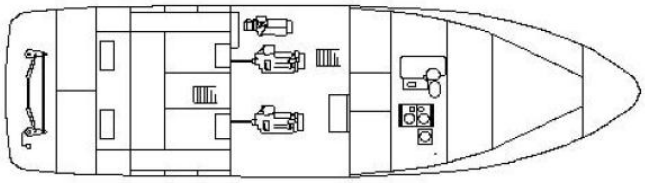

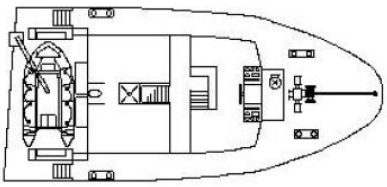

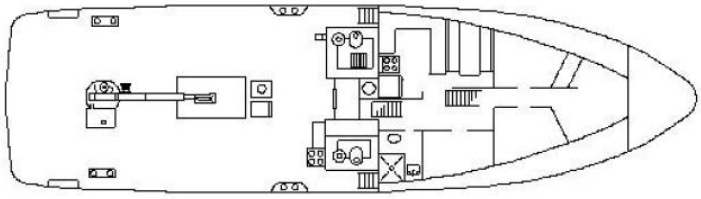

Appendix B: Isherwood Wind Coefficients

Table 23: C_{XW} Wind Coefficients

α_{rw} [°]	A_0	A_1	A_2	A_3	A_4	A_5	A_6
0	2.152	-5.000	0.243	-0.164	0.000	0.000	0.000
10	1.714	-3.330	0.145	-0.121	0.000	0.000	0.000
20	1.818	-3.970	0.211	-0.143	0.000	0.000	0.033
30	1.965	-4.810	0.243	-0.154	0.000	0.000	0.041
40	2.333	-5.990	0.247	-0.190	0.000	0.000	0.042
50	1.726	-6.540	0.189	-0.173	0.348	0.000	0.048
60	0.913	-4.680	0.000	-0.104	0.482	0.000	0.052
70	0.457	-2.880	0.000	-0.068	0.346	0.000	0.043
80	0.341	-0.910	0.000	-0.031	0.000	0.000	0.052
90	0.355	0.000	0.000	0.000	-0.247	0.000	0.018
100	0.601	0.000	0.000	0.000	-0.347	0.000	-0.020
110	0.651	1.290	0.000	0.000	-0.582	0.000	-0.031
120	0.564	2.540	0.000	0.000	-0.748	0.000	-0.024
130	-0.142	3.580	0.000	0.047	-0.700	0.000	-0.028
140	-0.677	3.640	0.000	0.069	-0.529	0.000	-0.032
150	-0.723	3.140	0.000	0.064	-0.475	0.000	-0.032
160	-2.148	2.560	0.000	0.081	0.000	1.270	-0.027
170	-2.707	3.970	-0.175	0.126	0.000	1.810	0.000
180	-2.529	3.760	-0.174	0.128	0.000	1.550	0.000

Table 24: C_{YW} Wind Coefficients

α_{rw} [°]	B_0	B_1	B_2	B_3	B_4	B_5	B_6
10	0.096	0.220	0.000	0.000	0.000	0.000	0.000
20	0.176	0.710	0.000	0.000	0.000	0.000	0.000
30	0.225	1.380	0.000	0.023	0.000	-0.290	0.000
40	0.329	1.820	0.000	0.043	0.000	-0.590	0.000
50	1.164	1.260	0.121	0.000	-0.242	-0.950	0.000
60	1.163	0.950	0.101	0.000	-0.177	-0.880	0.000
70	0.916	0.530	0.069	0.000	0.000	-0.650	0.000
80	0.844	0.550	0.082	0.000	0.000	-0.540	0.000
90	0.889	0.000	0.138	0.000	0.000	-0.660	0.000
100	0.799	0.000	0.155	0.000	0.000	-0.550	0.000
110	0.797	0.000	0.151	0.000	0.000	-0.550	0.000
120	0.996	0.000	0.184	0.000	-0.212	-0.660	0.340
130	1.014	0.000	0.191	0.000	-0.280	-0.690	0.440
140	0.784	0.000	0.166	0.000	-0.209	-0.530	0.380
150	0.536	0.000	0.176	-0.029	-0.163	0.000	0.270
160	0.251	0.000	0.106	-0.022	0.000	0.000	0.000
170	0.125	0.000	0.046	-0.012	0.000	0.000	0.000

Appendix C: FreeShip Reports

```
Design length         :     38.475 m
Design beam           :      7.400 m
Design draft          :      3.270 m
Midship location      :     19.237 m
Water density         :      1.025 t/m^3
Appendage coefficient :     1.0000

--------------------------------------------------------------------------------


Input variables
--------------------------------------------------------------------------------


General
      Start speed                              : 0.00 kn
      End speed                                : 5.71 kn
      Water density                            : 1.025 t/m^3
      Water viscosity                          : 1.1890*10^(-6) m^2/s

Hull
      Length on waterline                      : 36.677 m
      Beam on waterline                        : 6.974 m
      Draught on midship                       : 2.158 m
      Draught on F.P.                          : 2.158 m
      Draught on F.A.                          : 2.158 m
      Wetted surface area                      : 351.85 m^2
      Waterplane area                          : 223.50 m^2
      Displacement                             : 338.350 m^3
      Longitudinal center of buoyancy          : -0.019 %
      Prismatic coefficient                    : 0.6580



Appendages areas:
      Shaft brackets area                      : 0.000 m^2
      Strut bossing area                       : 0.000 m^2
      Hull bossing area                        : 0.000 m^2
      Stabiliser fins area                     : 0.000 m^2
      Dome area                                : 13.326 m^2
Exposed shafts area:
      Angle vs buttoks about 10 °              : 0.000 m^2
      Angle vs buttoks about 20 °              : 0.000 m^2

Areas of keels
      Skeg                                     : 0.000 m^2
      Bilge keels                              : 0.000 m^2

Areas of rudders
      Rudder behind skeg/stern                 : 0.000 m^2
      2-screw rudder slender/thick             : 0.000 m^2
```

Data for Sea margin coefficient:

Time of ship hull is in water, month	: 6.0
Height of 3% wave, m	: 0.000
Course angle of moving wave, degree	: 0.00
Wind speed, m/s	: 0.00
Course wind angle, degree	: 0.00
Height of a board above DWL, m	: 0.500
Air density, kg/m^3	: 1.226
Middle height of superstructure above DWL, m	: 2.500
Depth of water, m	: 100.00
Wetted area of midsection, m^2	: 14.02
The Ship types (1-11):	: 10
Absolute roughness, mkm	: 150

Calculated variables

Cp	= 0.6580
Cb	= 0.6130
Cwp	= 0.8738
Cm	= 0.9317
Cbt	= 0.1086
Am	= 14.02 m^2
Lwl/Bwl	= 5.259
Tc	= 2.158 m
Bwl/T	= 3.232
Lwl/T	= 16.997
Cstrn	= 0
Np	= 2
ie	= 27.000 degr

Final calculations of resistance by a method Holtrop-1988

Speed [kn]	Speed [m/s]	Fr [-]	R_f [kN]	R_r [kN]	R_T [kN]	Power [kW]	R_T_e [kN]	Power_e [kW]
Fr is outside valid domain 0,05 ... 1,0								
Fr is outside valid domain 0,05 ... 1,0								
Fr is outside valid domain 0,05 ... 1,0								
0.00	0.00	0.000	0.0					
1.43	0.73	0.039	0.3					
2.86	1.47	0.077	1.1	1.2	2.3	3.4	2.3	3.4
4.29	2.20	0.116	2.4	2.4	4.8	10.6	4.8	10.6
5.71	2.94	0.155	4.1	3.8	7.9	23.1	7.9	23.1

7.14	3.67	0.194	6.1	5.5	11.6	42.7	11.6	42.7
8.57	4.41	0.232	8.6	8.0	16.6	73.2	16.6	73.2
10.00	5.14	0.271	11.5	12.2	23.7	121.8	23.7	121.8
11.00	5.66	0.298	13.7	17.4	31.0	175.6	31.0	175.6
12.00	6.17	0.325	16.1	21.9	38.0	234.4	38.0	234.4

```
Tb        =  14.135 kN
Kdt       =  1.042
Dp        =  0.750 m
Z         =  4
Ae/Ao     =  0.786 - calculated
Ae/Ao     =  0.786 - for selection of propeller diagram
P/Dp      =  0.900 - by curve of propeller optimal frequency
Ke        =  1.000
Wt        =  0.1643
t         =  0.1628
EtaR      =  0.9899
EtaH      =  1.0018
EtaH*EtaR=  0.9917

NOTE: Coefficients Wt, t and ETAr are calcs by formulaes of method Holtrop-1988
```

Appendix D: Industry Powering Check with 9.9M Plug

Prediction results							
Vel [kts]	PEtotal [kW]	WakeFr	ThrDed	RelRot	EngRPM	PB/prop [kW]	
0.1	**0**	**0**	**0**	**1**	**21.8**	**0**	
2	**1**	**0**	**0**	**1**	**392.7**	**1**	
4	**11**	**0**	**0**	**1**	**766.6**	**10**	
6	**35**	**0**	**0**	**1**	**1136.6**	**31**	
7	**60**	**0**	**0**	**1**	**1362.9**	**55**	
8	**98**	**0**	**0**	**1**	**1602.1**	**90**	
9	**150**	**0**	**0**	**1**	**1849**	**141**	
10	**221**	**0**	**0**	**1**	**2103.4**	**209**	
11	**313**	**0**	**0**	**1**	**2364.8**	**299**	
12	**431**	**0**	**0**	**1**	**2633.1**	**416**	
Vel [kts]	PropRPM	J	Kt	Kq	PropEff	HullEff	OPC
0.1	**9**	**0.4578**	**0.3258**	**0.0448**	**0.5302**	**1**	**0.5196**
2	**162.1**	**0.5078**	**0.2952**	**0.0429**	**0.5565**	**1**	**0.5454**
4	**316.4**	**0.5203**	**0.2874**	**0.0424**	**0.5617**	**1**	**0.5505**
6	**469.1**	**0.5264**	**0.2835**	**0.0421**	**0.564**	**1**	**0.5528**
7	**562.5**	**0.5122**	**0.2925**	**0.0427**	**0.5584**	**1**	**0.5472**
8	**661.2**	**0.498**	**0.3013**	**0.0433**	**0.552**	**1**	**0.5409**
9	**763.1**	**0.4854**	**0.3091**	**0.0438**	**0.5457**	**1**	**0.5348**
10	**868.1**	**0.4741**	**0.316**	**0.0442**	**0.5396**	**1**	**0.5288**
11	**976**	**0.4639**	**0.3221**	**0.0446**	**0.5338**	**1**	**0.5231**
12	**1086.7**	**0.4545**	**0.3278**	**0.0449**	**0.5281**	**1**	**0.5175**
Vel [kts]	Thrust [N]	Thr/prop [N]	DelThr [N]	PropTorq [Nm]	PD/prop [kW]	PS/prop [kW]	PBtotal [kW]
0.1	**5**	**2**	**5**	**0**	**0**	**0**	**0**
2	**1398**	**699**	**1398**	**76**	**1**	**1**	**3**
4	**5187**	**2594**	**5187**	**287**	**10**	**10**	**19**
6	**11248**	**5624**	**11248**	**627**	**31**	**31**	**63**
7	**16686**	**8343**	**16686**	**913**	**54**	**55**	**110**
8	**23756**	**11878**	**23756**	**1279**	**89**	**90**	**181**
9	**32457**	**16228**	**32457**	**1723**	**138**	**141**	**281**
10	**42937**	**21469**	**42937**	**2251**	**205**	**209**	**418**
11	**55333**	**27667**	**55333**	**2870**	**293**	**299**	**599**
12	**69798**	**34899**	**69798**	**3585**	**408**	**416**	**833**
Vel [kts]	Sigma	MinP/D	TipSpd [mps]	Press [kPa]	MinBAR	%CavAvg	%CavPeak
0.1	**80803.44**	**0.739**	**0.4**	**0**	**0.0696**	**2**	**2**
2	**202.01**	**0.756**	**6.4**	**1.6**	**0.0979**	**2**	**2**
4	**50.5**	**0.761**	**12.4**	**6.1**	**0.183**	**2**	**2**
6	**22.45**	**0.763**	**18.4**	**13.3**	**0.3201**	**2**	**2**
7	**16.49**	**0.758**	**22.1**	**19.5**	**0.4445**	**3.5**	**3.5**
8	**12.63**	**0.753**	**26**	**27.4**	**0.6058**	**6.3**	**6.3**
9	**9.98**	**0.748**	**30**	**37**	**0.8041** **	**11.1**	**11.1**
10	**8.08**	**0.744**	**34.1** **	**48.4**	**1.0427** **	**18.5**	**18.5**
11	**6.68**	**0.741**	**38.3** **	**61.9** **	**1.3246** **	**30.0** **	**30**
12	**5.61**	**0.737**	**42.7** **	**77.4** **	**1.6534** **	**48.2** **	**48.2**

Vel [kts]	PropRn	Kt/J2	Kq/J3	Cth	Cp	Fuel/eng [lph]	
0.1	**5.29E+04**	**1.554**	**0.4665**	**3.957**	**0.01357**	**0**	
2	**9.58E+05**	**1.145**	**0.3274**	**2.915**	**0.00952**	**0**	
4	**1.87E+06**	**1.061**	**0.3007**	**2.703**	**0.00875**	**0**	
6	**2.78E+06**	**1.023**	**0.2887**	**2.605**	**0.0084**	**0**	
7	**3.33E+06**	**1.115**	**0.3178**	**2.839**	**0.00924**	**0**	
8	**3.91E+06**	**1.215**	**0.3504**	**3.095**	**0.01019**	**0**	
9	**4.50E+06**	**1.312**	**0.3826**	**3.341**	**0.01113**	**0**	
10	**5.12E+06**	**1.406**	**0.4146**	**3.58**	**0.01206**	**0**	
11	**5.75E+06**	**1.497**	**0.4464**	**3.813**	**0.01299**	**0**	
12	**6.40E+06**	**1.587**	**0.4783**	**4.041**	**0.01391**	**0**	

Monohull/Propulsion					Project: 6692 - Powering Check with 9.9M Plug.no				
Powering Check with 9.9M Plug									
Propulsive coefficients									
Wake fraction	**[Off]**		Wake fract scale correctio	**[Off]**					
Thrust deduction	**[Off]**		Rudder loc		**Free stream**				
Relative rotative efficienc	**[Off]**		Wake fract duct correction	**[Off]**					
Friction line		**ITTC-57**	Tunnel stern correction	**[Off]**					
Correlation allowance		**0.00104**	Effective tunnel diam		**0.000 m**				
3D form factor		**1.2715**	Tunnel depth		**0.000 m**				
Hull data									
[General]					**[Ct-based]**				
Length between PP			**35.100 m**		Max section area		[0.904 Cx]	**13.580 m2**	
WL bow pt aft FP			**0.000 m**		Waterplane area		[0.864 Cw]	**224.800 m2**	
Length on WL			**36.900 m**		Trim by stern			**0.400 m**	
Max beam on WL			**7.049 m**		LCB aft of FP		[0.534 Lpp]	**18.750 m**	
Max molded draft			**2.130 m**		Bulb ext fwd FP			**0.000 m**	
Displacement bare			**339.40 t**		Bulb area at FP			**0.000 m2**	
Wetted surface			**325.200 m2**		Bulb ctr above BL			**0.000 m**	
Chine type			**Hard chine**		Transom area		[0.123 of Ax]	**1.670 m2**	
[Principal parameters]					Transom beam		[0.851 of B]	**6.000 m**	
Lwl/B			**5.2348**		Transom draft		[0.127 of T]	**0.270 m**	
B/T			**3.3094**		Half ent angle			**25.00 deg**	
Cb			**0.5972**		Bow shape		[V-shape]	**Buttock flow**	
Cws			**2.9432**		Stern shape		[U-shape]	**WL flow**	
Prediction method check									

Monohull/Propulsion			Project: 6692 - Powering Check with 9.9M Plug.no		
Powering Check with 9.9M Plug					
System analysis					
Analysis type		**Free run**	Water type		**Standard Salt**
Cav criteria		**Keller eqn**	Mass density		**1025.8600 kg/m3**
CPP analysis method	**[Off]**		Mass density		**1.1883e-06 m2/s**
Propulsor data					
Description		**9.9 M PLug**	Blades		**5**
Propulsors		**2**	Exp area ratio		**0.750**
Propulsor type		**Series**	Diameter		**0.750 m**
Propeller series		**Kaplan Ka 19A**	Pitch		**0.800 m**
			Immersion		**1.000 m**
Propeller options					
Scale corr		**None**	Propeller cup		**0.0 mm**
Kt mult	**[Std]**	**1**	Pitch type		**FPP**
Kq mult	**[Std]**	**1**	Cav breakdown	**[Off]**	
Blade t/c		**0**	Shaft angle corr	**[On]**	**0.00 deg**
Roughness		**0.0 mm**	Added angle of run		**0.00 deg**
Engine data					
Engine file		**320kW.eng**	Gear ratio		**2.423**
Rated RPM		**0**	Gear efficiency		**1**
Rated power		**0 kW**	Shaft efficiency		**0.98**
Report ID20110623-1131			HydroComp NavCad 5.42.0122.NC.S838.484		

Powering Check with 9.9M Plug

Symbols and values	
Vel	= Ship speed
PEtotal	= Total effective power
WakeFr	= Taylor wake fraction coefficient
ThrDed	= Thrust deduction coefficient
RelRot	= Relative-rotative efficiency
EngRPM	= Engine RPM
PB/prop	= Brake power per propeller
PropRPM	= Propeller RPM
J	= Advance coefficient
Kt	= Thrust coefficient (for horizontal thrust vector)
Kq	= Torque coefficient
PropEff	= Propeller open-water efficiency
HullEff	= Hull efficiency = (1 - ThrDed) / (1 - WakeFr)
OPC	= Overall propulsive coefficient
Thrust	= Total open-water thrust
Thr/prop	= Open-water thrust per propeller
DelThr	= Total delivered thrust
PropTorq	= Propeller open water torque
PD/prop	= Delivered power per propeller
PS/prop	= Shaft power per propeller
PBtotal	= Total brake power
Sigma	= Cavitation number based on advance velocity
MinP/D	= Minimum P/D ratio to avoid face cavitation
TipSpd	= Linear velocity of the propeller tips
Press	= Average propeller blade pressure
MinBAR	= Minimum recommended expanded blade area ratio
%CavAvg	= Average percent back cavitation
%CavPeak	= Peak percent back cavitation (from shaft angle effects)
PropRn	= Propeller Reynolds number
Kt/J2	= Propeller thrust-speed ratio
Kq/J3	= Propeller torque-speed ratio
Cth	= Propeller thrust loading coefficient
Cp	= Propeller power loading coefficient
Fuel/eng	= Fuel consumption per engine
*	= Propulsive coefficient prediction exceeds speed parameter
**	= Exceeds cavitation criteria
***	= Cavitation breakdown is indicated

Appendix E: Industry Propeller Design Data

```
MARIN software
Client Specific Propeller Design Program  (V2008_2)                page 1
================================================
6  October  2009 09:51:38

General input
-------------
Selection from              : Nozzle propeller non steerable
Project reference           : 13008047
Order number                : 9941
Vessel type                 : Research Vessel
User ID                     : jwvs
Thruster model              : HRP 2111 WM
Propeller number            : 9941

Operational input
-----------------
Mode                        : Design
Ship Speed                  :     10.000   [knots]
Design to                   : Power
Propeller diameter          :     750.00   [mm]
RPM engine                  :    2000.00   [1/min]
Gearbox ratio               :    2.42300   [-]
Gearbox/shaft losses        :      0.900   [-]
Available power (engine)    :      200.0   [kW]
Wakefraction                :      0.850   [-]
Density propeller material  :     7650.0   [kg/m3]
Water density               :     1025.0   [kg/m3]
Shaft immersion             :      2.000   [m]
Speed for break torque      :     10.000   [knots]

Geometrical input
-----------------
r/R hub                     :     0.2000   [-]
Ka-series configuration     : Ka 5-75 Nozzle 19A
Rake angle                  :       0.00   [deg]
Skew angle at hub           :      -3.00   [deg]
Skew cross at r/R           :      0.650   [-]
Skew angle at tip           :      20.00   [deg]

Thickness = input           : Yes

r/R 1 =  0.250     t1 =     36.00 [mm]
r/R 2 =  0.600     t2 =     16.00 [mm]
r/R 3 =  1.000     t3 =      8.00 [mm]

Cambercorrection = input    : Yes

r/R 1 =  0.400     c1 =      1.10
r/R 2 =  0.600     c2 =      1.25
r/R 3 =  0.800     c3 =      1.40

Pitch distribution = input  : Yes

r/R 1 =  0.200     f1 =    0.9000
r/R 2 =  0.500     f2 =    1.0000
r/R 3 =  0.800     f3 =    1.0000
r/R 4 =  1.000     f4 =    0.9500
```

```
MARIN software
B-series       Propeller Design Program  (V2008_2)                  page 2
================================================

Calculation results
-------------------
Propeller diameter design   :        750   [mm]
P/D (nominal)               :      1.060   [-]
No of blades                :          5   [-]
Nozzle type                 :        19A

Tip speed                   :      32.41   [m/s]

Thrust (+nozzle)            :      20.94   [kN]
Propeller power             :     180.00   [kW]
Propeller torque            :     2082.4   [Nm]
Propeller revolution rate   :     825.42   [rpm]

Propeller efficiency        :      0.509   [-]

J                           :      0.424   [-]
Kt (prop+nozzle)            :      0.341   [-]
10Kq                        :      0.452   [-]

Kt (nozzle)                 :      0.097   [-]
Kt/sigma                    :      0.154   [-]
sigma                       :      2.216   [-]

Engine power                :      200.0   [kW]
Engine torque               :      954.93  [Nm]
Engine revolution rate      :     2000.00  [rpm]

Break torque (at propeller) :      -351.6  [Nm]
Break thrust                :     -8092.2  [N]
Break thrust (nozzle)       :     -2430.5  [N]

Volumetric pitch / D        :      1.0215  [-]
Virtual pitch / D           :      1.1652  [-]
Exp. blade area ratio       :      0.7853  [-]

Mass (blades only)          :      33.538  [kg] Mass_tot = 61 kg

GD2  (blades only)          :       6.336  [kgm2]    a
GD2 e.w.  Burrill and Robson:       2.129  [kgm2]
GD2 e.w.  Schwanecke        :       2.799  [kgm2]    c
GD2 e.w.  Kruppa            :       2.327  [kgm2]

J = J_prop + J_hub = 0.25*(a+c)+ 0.088 = 2.4 kgm^2

Max. skew angle             :      24.830  [deg]
Rake mm/m                   :       0.000  [mm/m]
Rake at tip                 :       0.000  [mm]

Fsk value DNV   (june 2008) :    1.136993
Fsk = 1 + ((e0.6 - e1.0)/(D/2))**2.0
e = dist between skew line pos when skew is forward
```

MARIN software

B-series Propeller Design Program (V2008_2) page 3

Print of radial (subset) data

r/R	ch(mm)	pitch(mm)	t(mm)	PMTGL(mm)	LEGL(mm)	TEGL(mm)
0.200	160.6	698.5	40.97	23.207	84.239	76.385
0.250	172.5	717.2	35.99	30.550	96.085	76.392
0.300	183.2	733.5	31.54	36.820	106.439	76.783
0.350	193.7	747.5	27.63	41.721	115.333	78.399
0.400	203.8	759.3	24.24	44.934	122.355	81.401
0.500	222.5	776.1	19.06	44.842	130.034	92.433
0.600	239.4	784.3	16.00	31.610	128.256	111.099
0.700	253.2	784.2	14.00	3.572	115.606	137.600
0.800	263.3	776.1	12.00	-35.797	91.147	172.144
0.850	267.2	769.1	11.00	-58.315	74.475	192.694
0.900	269.5	760.3	10.00	-82.226	54.388	215.099
0.950	269.4	749.7	9.00	-107.747	30.409	238.956
0.975	266.4	743.7	8.50	-122.004	15.979	250.471
1.000	261.2	737.3	8.00	-136.179	0.394	260.831

Stress check according to RHOMSOM beam method
Centrifugal stresses included. Effects due to skew not included

Stresses in [N/mm2]

	Hydrodynamical		Centrifugal		Summation	
r/R	Tensile	Compression	Tensile	Compression	Tensile	Compression
0.200	23.283	24.378	3.909	-0.192	27.192	24.186
0.300	29.341	30.722	4.052	0.417	33.393	31.138
0.400	32.600	34.134	3.866	0.663	36.466	34.798
0.500	33.060	34.616	3.352	0.548	36.413	35.164
0.600	30.722	32.167	2.510	0.071	33.232	32.239

Open water data

J	Kt	Kq	Etao
0.00000	0.58540	0.05195	0.00000
0.05000	0.55417	0.05186	0.08503
0.10000	0.52423	0.05159	0.16172
0.15000	0.49528	0.05114	0.23123
0.20000	0.46703	0.05049	0.29441
0.25000	0.43917	0.04966	0.35185
0.30000	0.41141	0.04864	0.40386
0.35000	0.38345	0.04742	0.45047
0.40000	0.35499	0.04599	0.49141
0.45000	0.32573	0.04435	0.52602
0.50000	0.29537	0.04249	0.55320
0.55000	0.26361	0.04040	0.57118

0.60000	0.23016	0.03807	0.57732
0.65000	0.19471	0.03549	0.56756
0.70000	0.15697	0.03265	0.53564
0.75000	0.11664	0.02953	0.47146
0.80000	0.07342	0.02613	0.35781
0.85000	0.02700	0.02241	0.16298

Static section data

r/R	Icog [mm4]	Sectional area [mm2]	Y to ss [mm]	Y to ps [mm]
0.200	0.444058E+06	0.454447E+04	22.21	-18.77
0.250	0.337866E+06	0.437832E+04	19.84	-16.16
0.300	0.253280E+06	0.415693E+04	17.63	-13.92
0.350	0.186913E+06	0.389652E+04	15.65	-11.98
0.400	0.136943E+06	0.363029E+04	13.91	-10.33
0.500	0.760651E+05	0.315283E+04	11.13	-7.93
0.600	0.490123E+05	0.283535E+04	9.44	-6.56
0.700	0.340259E+05	0.257599E+04	8.32	-5.68
0.800	0.218737E+05	0.225842E+04	7.17	-4.83
0.850	0.170244E+05	0.209445E+04	6.58	-4.42
0.900	0.128990E+05	0.192656E+04	5.98	-4.02
0.950	0.952086E+04	0.175722E+04	5.37	-3.63
0.975	0.803624E+04	0.166738E+04	5.05	-3.45
1.000	0.667455E+04	0.156726E+04	4.73	-3.27

Icog	Sectional moment of inertia with respect to a line through the centre of gravity parallel to the pitch plane
Sectional area	Area of each propeller section
Y to ss/ps	Distance from COG to the outmost point of suction/pressure side

Appendix F: Equipment Data

THREE-PHASE SYNCHRONOUS GENERATOR

MJB 250 LA 4

4 POLES

50 Hz-1500 min^{-1} / 60 Hz-1800 min^{-1}

CONTINUOUS DUTY

AMBIENT TEMPERATURE	40°C					WINDING DATA				
TEMPERATURE RISE	H					Winding code	M0			
INSULATION CLASS	H					Number of leads	12			
POWER FACTOR	0,8					Winding pitch	2/3			
FREQUENCY	Hz	50				60				
VOLTAGE Star series	V	380	400	415	440	380	416	440	460	480
Star parallel		190	200	208	220	190	208	220	230	240
RATING	kVA	220	220	220	210	225	235	245	255	270
	kW	*176*	*176*	*176*	*168*	*180*	*188*	*196*	*204*	*216*
EFFICIENCY (%) @ 0,8 p.f.	4/4	92,8	93,2	93,1	93,2	92,7	93,0	93,3	93,4	93,9
	3/4	93,4	93,6	93,5	93,5	93,7	94,0	94,1	94,2	94,4
	2/4	93,6	93,7	93,6	93,5	94,1	94,3	94,4	94,4	94,4
EFFICIENCY (%) @ 1,0 p.f.	4/4	94,3	94,6	94,5	94,6	94,2	94,4	94,7	94,8	95,2
	3/4	94,8	94,9	94,8	94,8	95,0	95,2	95,3	95,4	95,6
	2/4	95,0	95,0	94,9	94,9	95,4	95,5	95,6	95,6	95,6
SHORT CIRCUIT RATIO		0,36	0,40	0,43	0,51	0,29	0,34	0,36	0,38	0,39
REACTANCES (%)										
Direct axis synchronous	xd	340	305	285	240	415	360	335	320	310
Quadrature axis synchronous	xq	165	150	140	120	205	180	165	160	155
Direct axis transient	x'd	26,6	24,0	22,3	18,9	32,6	28,4	26,5	25,2	24,5
Direct axis subtransient	x"d	12,5	11,3	10,5	8,9	15,4	13,4	12,5	11,9	11,6
Quadrature axis subtransient	x"q	14,0	12,6	11,7	9,9	17,1	14,9	13,9	13,3	12,9
Negative sequence	x_2	13,3	12,0	11,1	9,5	16,3	14,2	13,3	12,6	12,3
Zero sequence	x_0	2,7	2,4	2,2	1,9	3,3	2,8	2,7	2,5	2,5

TIME CONSTANTS [s]

Open circuit (T'do)	1,00	Subtransient (T"d)	0,011
Transient (T'd)	0,095	Armature (Ta)	0,013

MECHANICAL CHARACTERISTICS

D-end bearing/Lubrication	6218 2RS C3 / Prelubricated
N-end bearing/Lubrication	6313 2RS C3 / Prelubricated
Weight (IM B34) [kg]	660
Inertia (J) (IM B34) [kgm^2]	1,890
Overspeed [min^{-1}]	2250
Method of cooling	IC 01
Cooling air required [m^3/s] @ 50/60 Hz	0,42 / 0,52
Degree of protection	IP 23
Type of construction available	B2 - SAE / IM B34
Direction of rotation	CW

OTHER DATA

Phase resistance [Ω] @ 20 °C - Star series	0,021
Overloads	10% for 1 hour
3-phase short circuit current	>= 300% (3 I_n)
Voltage regulation accuracy	+/- 0,5 % (in steady state condition, speed from -2% to +5%, p.f. from 0,8 to 1)
Radio interference	EN 55011 Class B Group 1
Wave form THF	< 2%
Total harmonic content	< 2% (at no load)

STANDARDS

IEC 60034-1; CEI 2-3; BS 4999-5000; VDE 0530; NF 51-100,111; OVE M-10, NEMA MG 1.22.

Appendix G: .m Initialization Files

```
% Diesel Generator Emissions Calculations
% Equations for auxiliary engines
% Regression analysis from data provided in EPA, 1985

% P   Rated power output at generator in KW
% L   Load in % of rated power, from model
% s   Sulphur content of fuel
P = 215;
s = 0.01;

NOx_Coeff = 108.58-(2.47*P)+(0.0136*P^2)-(0.000018*P^3);
NOx_Coeff2=0.000684*P;
CO_Coeff = 20.72-(0.0231*P);
CO_Coeff2 = 0.000345*P;
CO2 = 3200;
VOC = 3.27-(2.16*P)-(0.0144*P^2)+(0.0000203*P^3);
PM = 1.1;
SOx = 20*s;

% Ship Resistance Init File
% Static params
% g                 gravity [m/s^2]
% p_air             density of air [kg/m^3]
% p                 density of seawater [kg/m^3]
% v_sw              kinematic viscosity of seawater @ 15 deg C
g = 9.81;
p_air = 1.2466; % @ 10 degC
p = 1025;
v_sw = 1.18831e-6;
Td =0.004;
Fnom = 60;
Vref = 1;
Vbase = 375.6;
Bmax = 1;
Bmin = -1;
Xs = 0.03;
Ki = 300;
Kp = 0;
Seq1_Only = 0;
Ibase = 177.5;

% Ship static params (from FREE!Ship file)
% Lpp               ship length on waterline [m]
% T                 average moulded draught [m]
% FroudeDenom       denominator in Froude number calc
% P_B               emergence of bow
% A_BT              transverse area of bulb [m^2]
% A_T               transom area [m^2], wetted area very small
% C_B               block coefficient
% C_M               midship section coefficient
% C_stern           afterbody form, 0 for normal U-body
% C_p               prismatic coefficient
```

```
% lcb               longitudinal center of buoyancy [%]
% lambda            average hull roughness
% i_e               angle of waterline at bow w ref to center plane
[deg]
% dell              displacement volume moulded [m^3]
% H_B               position of center of transverse area A_BT [m]
% T_F               draught moulded on forward perpendicular [m]
% B                 breadth on waterline [m]
% S_app             wetted area of appendage [m^2]
% A_PT              projected transverse area above waterline [m^2]
% A_PL              projected lateral area above waterline [m^2]
% C_WP              waterplane area coefficient
% S                 wetted area of hull [m^2]
% C_BTO             bow thrsuter coefficient, 0.003 when BT lies in
% cylindrical part of bulbous bow
% d_T               diameter of bow thruster houseing [m]
%                   standard accepted hull roughness, 150microm
S = 351.85;
i_e = 27;
T_F = 3.27;
H_B = 1.65;
C_B = 0.4045;
Lpp = 36.677;
T = 3.27;
FroudeDenom = sqrt(g*Lpp);
dell = 338.35;
d = -0.9;
A_BT = 1.523;
A_T = 1.67;
C_stern = 0;
lcb = -0.019;
B = 6.974;
C_WP = 0.8738;
C_p = 0.658;
C_M = 0.6148;
S_app = 13.326;
C_BTO = 0.003;
d_T = 0.68;
A_PT = 28.484;
A_PL = 105.055;

% Hull Resistance
% Based on Holtrop & Mennen, 1982 & Holtrop, 1984
% All values of Froude are less than 0.5, thus only 1982 paper valid
(slow
% speed)
%
R_total=R_frictional*(1+k1)+R_wavemaking+R_bulbousbow+R_appendage+R_tra
nsom
% +R_a
% R_frictional = 0.5*p*V^2*C_f*(1+k1)*S
% R_wavemaking, used Rw_a from 1984 for froude < 0.4
% R_w = c_1*c_2*c_5*dell*p*g*exp[m_1*F_n^d+m_4*cos(lambda*Fn^(-2))]
% R_bulbousbow, additional pressure resistance of bulbous bow near
water
% surface
```

```
% R_transom, additional pressure resistance due to transom immersion
% R_a, model-ship correlation resistance = 0.5*V^2*S*C_a
% R_appendage = 0.5*p*V^2*S_app*(1+k2)_eq*C_f
% Reynolds R_n = V*Lpp/v

% Coefficients
% c_13              coefficient, function of stern type
% c_12              coefficient, function of draught-length ratio
% c_4               coefficeint, function of forward draft-length ratio
% c_6               coefficient, function of Froude number
% c_3               coefficient, function of bulbous bow
c_7 = B/Lpp; % eqn for 0.11<(B/Lpp)<0.25
c_3 = (0.56*A_BT^1.5)/(B*T*(0.31*sqrt(A_BT)+T_F-H_B));
c_1 = 2223105*c_7^3.78613*(T/B)^1.07961*(90-i_e)^(-1.37565);
c_2 = exp(-1.89*sqrt(c_3));
c_5 = 1-0.8*A_T/(B*T*C_M);
c_4 = 0.04; % eqn for T_F/Lpp > 0.04
c_14 = 1+0.011*C_stern; % 1984 eqn
c_12 = (T/Lpp)^0.2228446; % eqn for T/Lpp > 0.05
c_16 = 8.07981*C_p-13.8673*C_p^2+6.984388*C_p^3; % eqn for C_p<0.8
c_15 = -1.69385; % eqn for Lpp^3/dell<512

% Other variables
% L_R               length of run [m]
F_NI_multiplier = g*(T_F-H_B-0.25*sqrt(A_BT));
F_NT_multiplier = 2*g*A_T/(B+B*C_WP);
m_1 = 0.0140407*(Lpp/T)-1.75254*dell^(1/3)/Lpp-4.79323*(B/Lpp)-c_16;
m_4_multiplier = c_15*0.4; % 1984 eqn Rw_a for froude < 0.4
k2 = exp(-1.89*sqrt(c_3));
L_R = Lpp*(1-C_p+0.06*C_p*lcb/(4*C_p-1));
P_B = 0.56*sqrt(A_BT)/(T_F-1.5*H_B);
lambda = 1.446*C_p-0.03*Lpp/B; % eqn for Lpp/B <12

% C_a               model ship correlation resistance, uses standard
hull
% roughness of 150 micrometers (use additional formula to increase this
% value)
C_a = 0.006*(Lpp+100)^(-0.16)-
0.00205+0.003*sqrt(Lpp/7.5)*C_B^4*c_2*(0.04-c_4);

% C_F               equivalent flat plate frictional resistance, 1957
ITTC correlation line
% C_F = 0.075/(log(Rn)-2)^2
% FF=(1+k1)         form factor of hull
% FF2 = (1+k2)      appendage resistance factor, sonar dome
% R_F_multiplier    frictional resistance
% R_W_multiplier    wavemaking/wavebreaking resistance
% R_B_multiplier    bulbousbow resistance
% R_Tr_multiplier   pressure resistance due to immersed transom
% R_n_multiplier    Reynolds number multiplier
% R_app_multiplier  appendage resistance
% R_BT_multiplier   bow thruster resistance
% R_A_multiplier    model-ship correlation resistance
% C_V               viscous resistance coefficient
% C_air             air coefficient
```

```
FF2 = 2.7; % sonar dome
R_F_multiplier = 0.5*p*S;
FF =
0.93+0.487118*c_14*(B/Lpp)^1.06806*(T/Lpp)^0.46106*(Lpp/L_R)^0.121563*(
Lpp^3/dell)^0.36486*(1-C_p)^(-0.604247); % 1984 eqn
%C_V = FF*C_F+C_a;
R_W_multiplier = dell*p*g*c_1*c_2*c_5;
R_B_multiplier = 0.11*exp(-3*P_B^(-2))*A_BT^1.5*p*g;
R_Tr_multiplier = 0.5*p*A_T;
R_n_multiplier = Lpp/v_sw;
R_app_multiplier = 0.5*p*S_app*FF2;
R_A_multiplier = 0.5*p*S*C_a;
R_BT_multiplier = pi*p*d_T*C_BTO;
C_air = 0.842856324;
R_air_multiplier = 0.5*p_air*A_PT*C_air;

% Propeller Characteristics
% Propulsive Factors (twin screw), 1982
% D                 propeller diameter [m]
D = 0.75;
% t                 thrust deduction factor
% w                 wake fraction
% w = 0.3095*C_B+10*C_V*C_B-0.23*D/sqrt(B*T);
t = 0.325*C_B-0.1885*D/sqrt(B*T);
w_Multiplier = 0.3095*C_B-0.23*D/sqrt(B*T);

% Wind Resitance (BN>0)
% X_w               transverse wind force [N]
% Y_w               lateral wind force [N]
X_w_multiplier = 0.5*p_air*A_PT;
Y_w_multiplier = 0.5*p_air*A_PL;

% Current Resistance
% Spanish Standard ROM 0.2-90
% F_T_current       lateral/transverse current force [kN]
% F_T_current = F_TC+F_TC_prime
% F_TC              lateral/transverse current force due to pressure
[kN]
% F_TC = C_TC*gamma_w*A_LC*10*sin(alpha)*V_c^2*(1/(2*g))
% F_TC_prime        lateral/transverse current force due to drag [kN]
% F_TC_prime = C_R*gamma_w*10*(1/(2*g))*(sin(alpha))^2*V_c^2
% F_L_current       longitudinal current force [kN]
% F_L_current = F_LC+F_LC_prime
% F_LC              longitudinal current force due to pressure [kN]
% F_LC = C_LC*gamma_w*A_LC_prime*10*(1/(2*g))*V_c^2
% F_LC_prime        longitudinal current force due to drag [kN]
% F_LC_prime = C_R*gamma_w*A_LC_prime*(cos(alpha))^2*V_c^2*10*(1/(2*g))
% A_LC              submerged longitudinal projected area exposed to
% current [m^2]
% A_LC_prime        submerged longitudinal projected wetted area [m^2]
% A_TC              submerged transverse projected area exposed to
current
% [m^2]
% A_TC_prime        submerged transverse projected wetted area [m^2]
% Lpp               length between perpendiculars [m]
```

```
% gamma_w           salt water 1.03 [t/m^3]
% C_TC              transverse current force factor
% C_LC              longitudinal current force factor
% C_R
gamma_w = 1.034;
C_TC = 1;
C_LC = 0.6;
C_R = 0.004;

A_TC_prime = (Lpp+2*T)*B;
A_LC = Lpp*T;
A_TC = B*T;
A_LC_prime = (B+2*T)*Lpp;
F_LC_multiplier = C_LC*gamma_w*A_TC*10*(1/(2*g));
F_LC_prime_multiplier = C_R*gamma_w*A_LC_prime*10*(1/(2*g));
F_TC_multiplier = C_TC*gamma_w*A_LC*10*(1/(2*g));
F_TC_prime_multiplier = C_R*gamma_w*10*A_TC_prime*(1/(2*g));

% Wave Resistance
% Spanish Standard ROM 0.2-90
% F_T_wave          lateral/transverse wave force [kN]
% F_L_wave          longitudinal wave force [kN]
% C_fw              waterplane coefficient
% C_dw              depth coefficient, 1.0 for deep water
% Hs                significant wave height [m]
C_dw = 1;
C_fw = 0.064;
F_T_wave_multiplier = C_dw*gamma_w*10*C_fw;
F_L_wave_multiplier = C_dw*gamma_w*10*C_fw;
```